# UC Riverside
## UC Riverside Electronic Theses and Dissertations

**Title**

In-situ Infrared Spectroscopy Characterization of Liquid-Solid Interfaces: A Study on Chiral Modification of Platinum

**Permalink**

https://escholarship.org/uc/item/4wm365z2

**Author**

Ni, Yufei

**Publication Date**

2018

**Supplemental Material**

https://escholarship.org/uc/item/4wm365z2#supplemental

Peer reviewed|Thesis/dissertation

UNIVERSITY OF CALIFORNIA
RIVERSIDE


In-situ Infrared Spectroscopy Characterization of Liquid-Solid Interfaces: A Study on
Chiral Modification of Platinum


A Dissertation submitted in partial satisfaction
of the requirements for the degree of


Doctor of Philosophy

in

Chemistry

by

Yufei Ni

December 2018


Dissertation Committee:
     Dr. Francisco Zaera, Chairperson
     Dr. Ming Lee Tang
     Dr. Jingsong Zhang

The Dissertation of Yufei Ni is approved:

<br>

_____

<br>

_____

<br>

_____

Committee Chairperson

<br>

University of California, Riverside

# ACKNOWLEDGEMENTS

First and foremost, I want to express my gratitude to my Ph.D. advisor, Professor Francisco Zaera for offering me such an invaluable opportunity to study and conduct research in his lab. He has always been a professional chemist and thoughtful mentor. His passion and profound knowledge in chemistry and science overall deeply impress me. During my five years of directed research, I can't remember how many times I was inspired by his insights into the fundamental nature behind the piles of data and observations. He has also let me realize how important it is to properly organize and present the findings rather just pile them up like a no-brainer will always do. I believe these lessons will benefit me from now on. I can never say enough about my appreciation.

I also want to thank Professor Ming Lee Tang and Professor Jingsong Zhang for participating in my oral exam and final defense as committee member, giving me the chance to further polish my research results.

I'd like to appreciate the professional help from the staff at UCR Analytical Chemistry Instrumentation Facility. To Dr. Jie Zhou for his assistance in performing GC-MS tests and data analysis. To Dr. Dan Borchardt for training me NMR basics as well as helping me out when one of my students stuck an NMR tube inside the magnet in class.

# COPYRIGHT ACKNOWLEDGEMENT

1. Ferri, D.; Bürgi, T. An in Situ Attenuated Total Reflection Infrared Study of a Chiral Catalytic Solid-Liquid Interface: Cinchonidine Adsorption on Pt. J. Am. Chem. Soc. 2001, 123 (48), 12074–12084.

2. Heitbaum, M.; Glorius, F.; Escher, I. Asymmetric Heterogeneous Catalysis. *Angew. Chemie Int. Ed.* **2006**, *45* (29), 4732–4762.

3. Gordon, A. D.; Zaera, F. Adsorption of 1-(1-Naphthyl)Ethylamine from Solution onto Platinum Surfaces: Implications for the Chiral Modification of Heterogeneous Catalysts. *Angew. Chemie Int. Ed.* **2013**, *52* (12), 3453–3456.

4. Liu, J. J. Advanced Electron Microscopy of Metal-Support Interactions in Supported Metal Catalysts. *ChemCatChem* **2011**, *3* (6), 934–948.

# DEDIACTION

*To my Grandmother*

**Yaqin Wang**

*For my earliest education from her*

*To my parents*

**Bo Wang and Zhongming Ni**

*for their love all along*

*To my wife*

**Meijie Shi**

*For her love and support*

ABSTRACT OF THE DISSERTATION


In-situ Infrared Spectroscopy Characterization of Liquid-Solid Interfaces: A Study on
Chiral Modification of Platinum


by


Yufei Ni


Doctor of Philosophy, Graduate Program in Chemistry
University of California, Riverside, December 2018
Dr. Francisco Zaera, Chairperson

Improve the enantioselectivity to obtain chiral product has been the major concern in

pharmaceutical and biochemical engineering. In most cases, separation of racemic product

is extremely time consuming and requires special equipment, thus it usually becomes a less

efficient and economic option than chiral synthesis even though such synthesis often

involves modified noble metal catalyst. In this work, chiral modification of platinum has

been studied to gain better understanding of adsorption mechanism of surface modifiers on

Pt surface as well as it affects the conversion and enantioselectivity of our model reaction—

hydrogenation of activated keto-esters.

Majority of this work has been focused on exploring the factors that may play an important

role in the adsorption of chiral modifier onto a variety of Pt surfaces including

polycrystalline Pt and Pt nanoparticles supported on oxide. Several in-situ FT-IR (Fourier Transform- Infrared) spectroscopy setup has been designed and built based on a Bruker Tensor IR spectrometer. In-situ IR spectroscopy has been proved itself to be overwhelmingly powerful and efficient to study the adsorption geometry of modifiers at solid/liquid interfaces. Pt surface is probed with advanced IR characterization methods such as RAIRS (Reflection-Absorption Infrared Spectroscopy) and Multi-bounce ATR-IR (Attenuated Total Reflection) methods due to their ability to distinguish adsorbed species from dissolved molecules in solution phase.

A series of modifiers are involved in this project, not only limited to the well-studied classic cinchona-alkaloid such as cinchonidine and cinchonine, but also naphthyl-based chiral compounds including (R)- or (S)-(−)-1-(1-naphthyl) ethylamine (NEA), naphthylmethyl amine, and dimethyl naphthyl ethylamine. The adsorption strength of the different modifier molecules was found to be quite different among those compounds, which is illustrated by the fact that quinoline can displace s-NEA from Pt but not vice versa, for instance, and by the observation that when Pt is exposed to a solution containing both quinoline and s-NEA only the quinoline's signature peaks can be detected by ATR-IR spectroscopy. The ordering of the modifiers studied in terms of adsorption strength was found to correlate with their ability to chirally modify the Pt catalyst during the hydrogenation of unsaturated aldehydes.

In addition, adsorption geometry of s-NEA/r-NEA shows that these modifiers adsorb on Pt surfaces through the nitrogen atom of the primary amine moiety not aromatic ring as commonly believed in the past.

Future follow-up work of this project might include: optimizing the IR instrumentation to minimize the interference from polar solvent and efficiently run and monitor hydrogenation reactions using in-situ IR spectroscopy.

# Table of Contents

# List of Figures

xviii

# List of Tables

# Chapter 1 Introduction and Overview

## 1.1 Brief History of Chirality

Chirality, a word derived from 'χειρ'(kheir), which means 'hand' in Greek, describes the property of certain molecules from a very special aspect. 'Chirality' itself was first used as a term for the property of handedness by Lord Kelvin in 1890s[1], which was surprisingly late, long after Louis Pasteur's experimental discoveries made in 1848 where he realized the handedness in molecular structure[2] when he studied the crystallography and optical activity of natural tartaric acid.
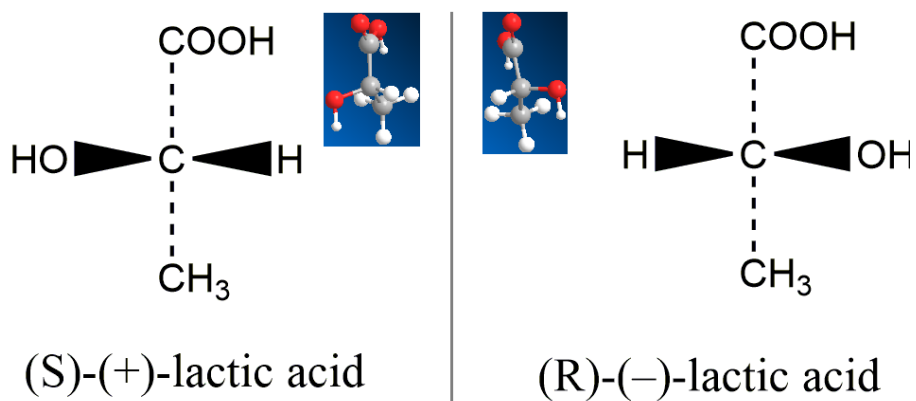


*Figure 1-1 Lactic acid, or 2-Hydroxypropanoic acid, plays an important role in the history of chirality. (S)- (+) lactic acid and (R)- (−)-lactic acid are mirror images of each other; They are not superimposable and known as enantiomers.*

In 1874, French chemist Joseph Achille Le Bel came up with a theory[3] that described the relation between crystal shape and optical activity, which then laid the foundation to modern stereochemistry. Interestingly, Dutch physical chemist van 't Hoff announced a similar hypothesis in the same year and it was later recognized as Le Bel–Van 't Hoff rule. Both of them suggested that the optical isomerism is caused by the tetrahedron structure formed by four different ligands of a carbon center.

Before long, researchers realized that sometimes it could be confusing to distinguish enantiomers by their sense of rotation of polarized light since the sense of rotation is not always a good representation of absolute spatial configuration of atoms. This problem was not solved until the CIP (Cahn-Ingold-Prelog) system was established in 1956[4], where (R)- and (S)- was used as prefixes to indicate the configuration of stereocenter, which we have been using since then.

## 1.2 Asymmetric Heterogenous Catalysis

The central topic of catalysis has been improving conversion and selectivity by optimizing reaction pathway. Asymmetric catalysis has drawn more and more attention as the demand for enantiomerically pure compound keeps surging. Chirality is ubiquitous in the biochemical and pharmaceutical world. In 2000, worldwide sales of chiral drugs in single-enantiomer dosage forms continued growing at an annual rate of more than 13%[5], reaching $133 billion and the figure would hit $200 in 2008 according to the consulting form Technology Catalyst International.

Given its importance in the field of both industrial application as well as chemistry and biochemistry research, there have been many review articles[6–9] covering various chiral catalyst for asymmetric synthesis. Comparing to homogeneous catalyst, ease of separation and recovery, better stability have always been the advantage of heterogeneous catalyst. Typical asymmetric heterogeneous catalysts include: chiral homogeneous ligands immobilized onto a suitable support such as oxides[10] or functionalized polymers[11];protein or peptides based macromolecular chiral catalyst[12] and noble metal catalyst with surface modification[13,14,15]. In this work, heterogenous catalysis enhanced by chiral modifier will be discussed in detail.
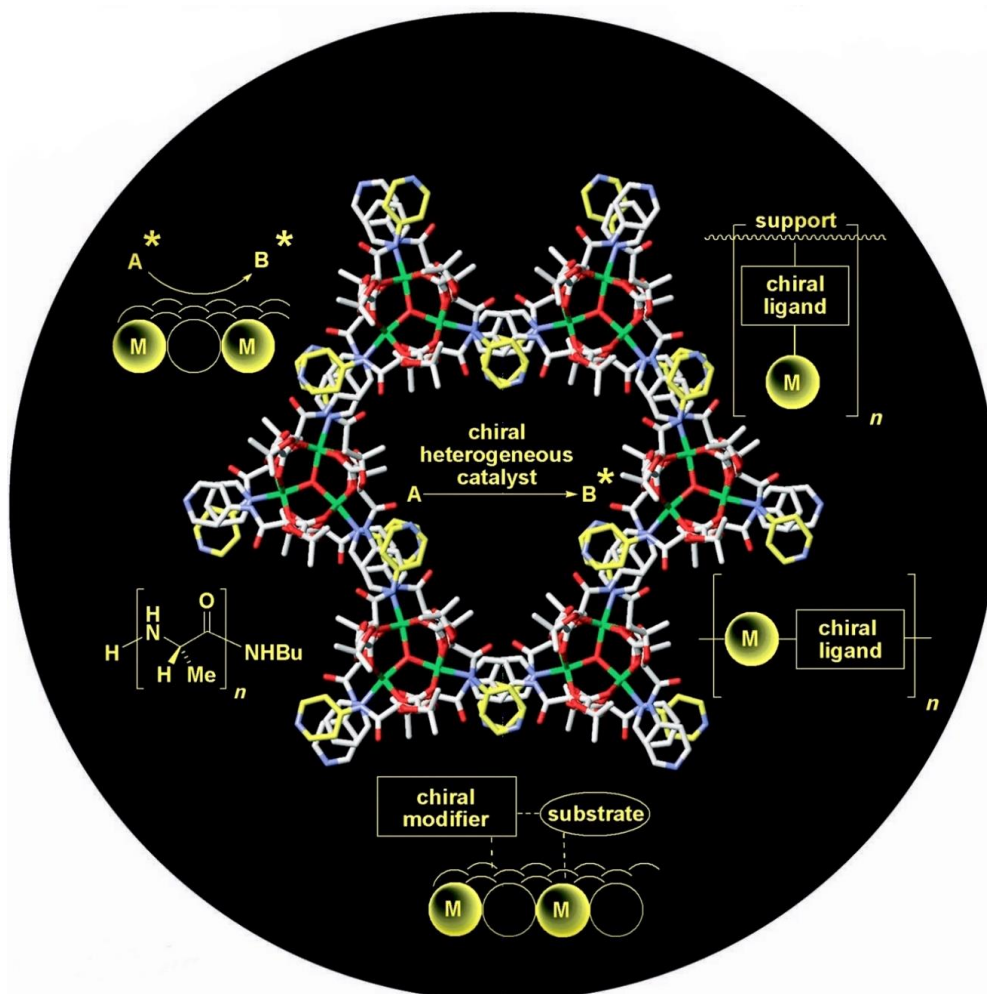
*Figure 1-2 Schematic illustration of some most adopted chiral catalysis systems used for asymmetric synthesis. Adapted with permission from reference 6, Copyright © 2006 by John Wiley Sons, Inc*

## 1.3 Surface Modification of Noble Metal Catalyst

This work will focus on the discussion about hydrogenation of activated C=O bonds in compounds keto-esters (ethyl pyruvate) and ketones (2,2,2-trifluoroacetophenone).
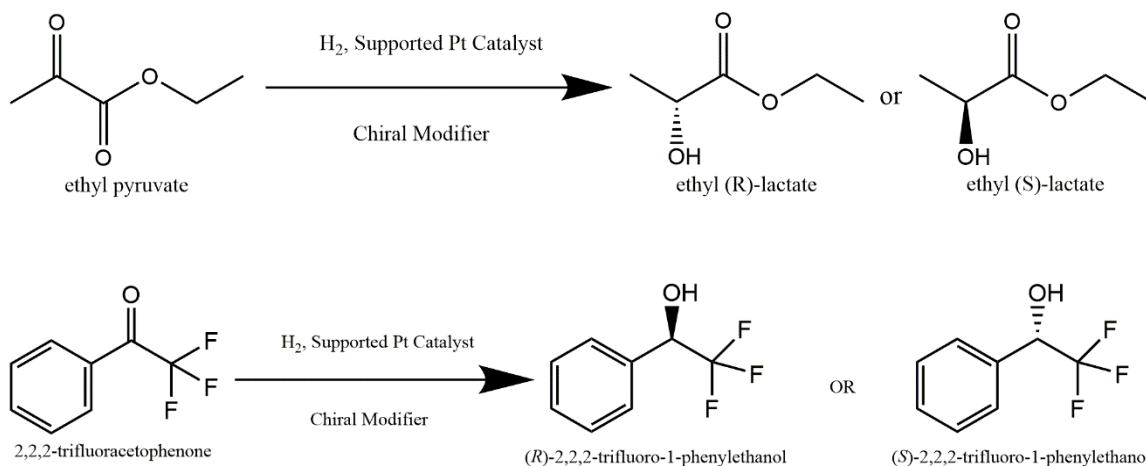
*Figure 1-3 Examples of hydrogenation of C=O bonds in activated keto-ester and ketone. Most studied chiral system used for these reactions is cinchona alkaloid modifiers with which overall enantiomeric excess can reach more than 90% under optimal conditions[16].*

There are many factors to be considered when we design the optimal catalyst-chiral modifier systems and reaction conditions. On the catalyst side, depending on the modifier, particle size of noble metal catalyst, facets exposed (shape of particles) and the support where nanoparticles are loaded. Other factors for tuning reactivity include solvent, $H_2$ pressure as well as other additives[17], which can sometimes change the property of solvent, to improve performance.
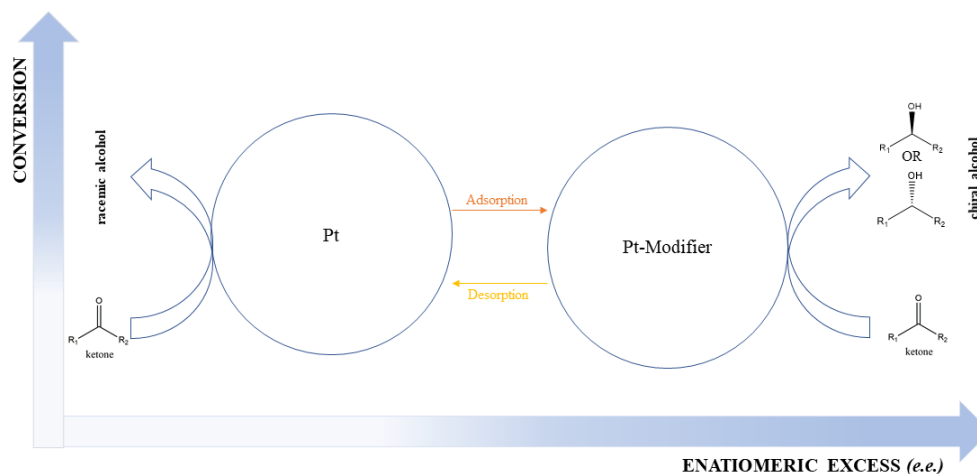
*Figure 1-4 Schematic illustration of surface modification of supported platinum in a catalyzed hydrogenation of ketone. Adsorption equilibrium of modifier on Pt surface is essential for the enantiomeric excess. An extreme example is Pt without modifier, reaction product is a racemic mixture which contains alcohols of both configurations.*

In 1979, cinchona alkaloids were first reported as modifier for asymmetric catalytic reactions by Orito and co-workers[18] in their study on hydrogenation of methyl benzoylformate catalyzed Pt/C modified with cinchonidine. Since then, there have been numerous studies around the topic of cinchonidine modified Pt catalyst. Most researchers believe that the excellent performance of cinchona alkaloids as chiral modifier comes from their molecular structure: the aromatic ring (quinoline ring) serves as an anchor for adsorption onto Pt surface; the bicyclic amine moiety (quinuclidine) interacts with reactant through possible hydrogen bonding. Based on this model, the configuration of cinchonidine on Pt surface has direct impact on the enantiomeric excess (e.e.) of the catalytic reaction.
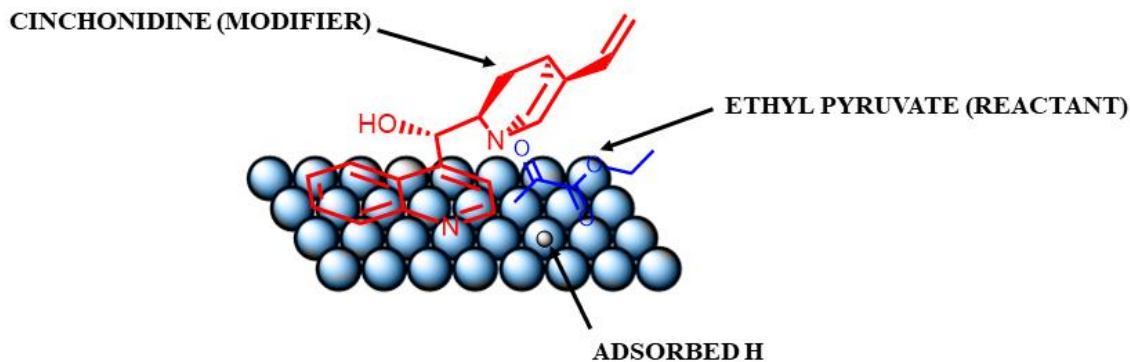
*Figure 1-5 Schematic representation of hydrogenation of ethyl pyruvate occurred on cinchonidine modified platinum surface. Modifier and reactant molecules form a complex structure with a 1:1 ratio. The orientation of reactant molecule is limited by the configuration of modifier molecule and thus only one reaction path is allowed, which end up with a preferred product configuration instead of racemic mixture.*

The confirmation of cinchona alkaloids modifiers can be affected by many factors such as solvent[19,20], temperature[21] and protonation of the amine moiety[22]. Meanwhile, adsorption geometry of cinchonidine and cinchonine is also dependent on the co-adsorption of hydrogen during reaction. This effect of adsorbed hydrogen is first introduced in a DFT study by Hahn and co-workers[23] and confirmed later by Motobayashi et al in an operando ATR-IR spectroscopy study[24]. In this case[25], under low hydrogen coverage or clean surface, cinchona alkaloids modifier molecules adsorb on Pt through quinoline ring near parallel to Pt surface. Under higher hydrogen coverage, the modifiers adsorb on the surface in a tilted manner. Partial hydrogenation of quinoline ring and hydrogen atoms transferred to the vinyl group will destabilize the adsorption of modifier while hydrogen's interaction with N atom of the quinoline ring and amine group leads to stabilization. In protic solvents like

acetic acid, N atom of quinuclidine is protonated and forms a NH⋯O hydrogen bond with the ketone[26].
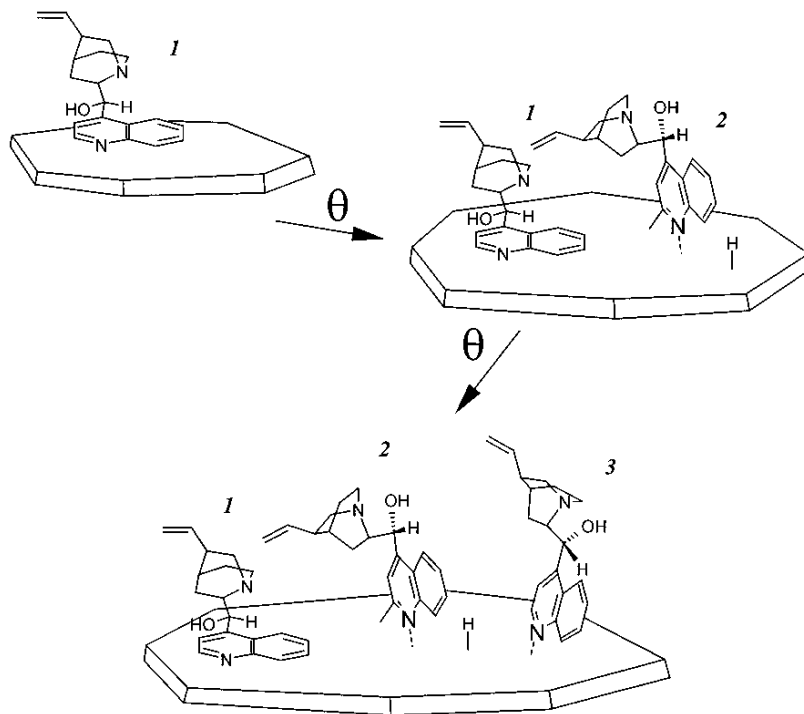


*Figure 1-6 θ detonates the surface coverage. Under low coverage, cinchonidine adsorb onto Pt via its π-system which lead to a near parallel adsorption pattern but not totally flat on the surface. As coverage increases, the space available on Pt becomes limited and thus a tilted orientation of modifier molecules is preferred. Adapted with permission from ref. 25. Copyright (2001) American Chemical Society.*

This work will concentrate more on discussing the adsorption geometry and reaction performance of NEA derived modifiers, which are among the synthetic modifiers developed more recently and features simpler structure compared to cinchona alkaloids while bearing the similar functionalities believed responsible for chiral modification of Pt surface.
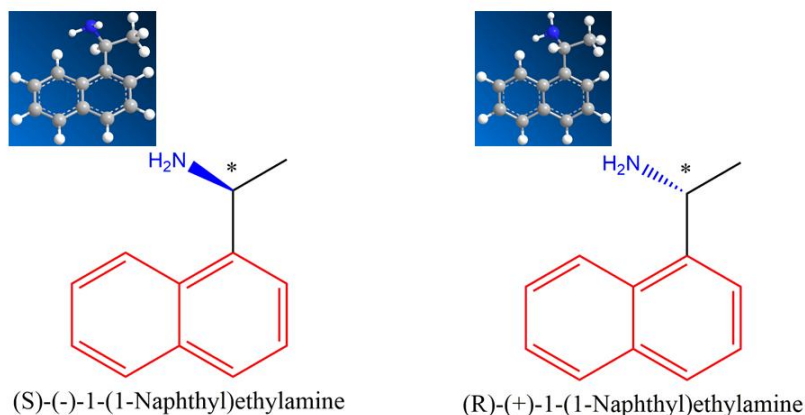


*Figure 1-7 Structural formula of an enantiomeric pair of NEA derived modifiers. They both feature an aromatic ring (naphthyl group, in red) and a primary amine group. Adjacent carbon atom is the chiral center, asterisked as shown above.*

However, unlike cinchona alkaloids, there have been some debates over the adsorption mechanism and geometry of s-NEA modifiers on Pt surface. High resolution STM studies combined with DFT studies[27,28] under UHV conditions by McBreen and co-workers have suggested that the chemisorption of NEA modifies onto Pt (111) is mainly through π-bond which is similar to cinchona alkaloids. In contrast, this work along with results from previous group members[29] have pointed out that these modifiers bond to metal surface through N atom of the amine group, not aromatic ring as commonly believed.

9

The divergent results from these studies might be explained by the significantly different experimental conditions as well as characterization approaches.

The main challenges in studying surface modification and the adsorption mechanism of modifiers under reaction conditions come from several aspects:

a) Adsorption of modifiers is sensitive to experimental conditions such as solvent, support of catalyst, in-situ vs ex-situ and pre-conditioning;

b) Limited selection of modifier and reaction substrate;

c) Distinguish the signal of adsorbed species from dissolved modifiers in the solution phase;

d) Dilemma while choosing the proper solvent: in-situ IR characterization typically requires non-polar solvents to minimize background absorption while reaction and modification conditions are not optimized in such solvents.

The following chapters will cover the in-situ IR apparatus used for probing liquid/solid interfaces, adsorption of a series of cinchona alkaloids and synthetic modifiers on various supported Pt catalysts. In addition, co-adsorption of modifier and reactant will also be discussed in detail.

# Chapter 2 Instrumentation and Catalyst Characterization

## 2.1 In-situ IR Techniques for Probing Liquid/Solid Interfaces

### 2.1.1 Reflection-Absorption Infrared Spectroscopy (RAIRS)

In-situ characterization has always been a powerful tool when it comes to catalysis studies thanks to ability to track how reaction evolves over time and obtain real-time data[30]. Since typical modifiers are small organic molecules, their adsorption geometry then can be identified through their vibrational modes adsorbed on the metal surface which makes Fourier-Transform IR spectroscopy a great option for such studies.[31,32]

The 'selection rule' which helps distinguish absorption of solvent species and adsorbed molecules on Pt surface comes from the difference in absorption factor of the two components of polarized IR beam. In particular, P-polarized IR beam undergoes a 90-degree phase shift at high angel while s-polarized component maintains a shift of around 180 across all angles of incidence. In this case, a thin layer of adsorbate solution trapped in between metal surface and optical element (usually a prism) will absorb some of the p-polarized light (electric filed paralleled to the plane of incidence). By comparison, the E vectors of s-polarized component nearly cancel out each other on metal surface leaving no absorption from the solution layer.
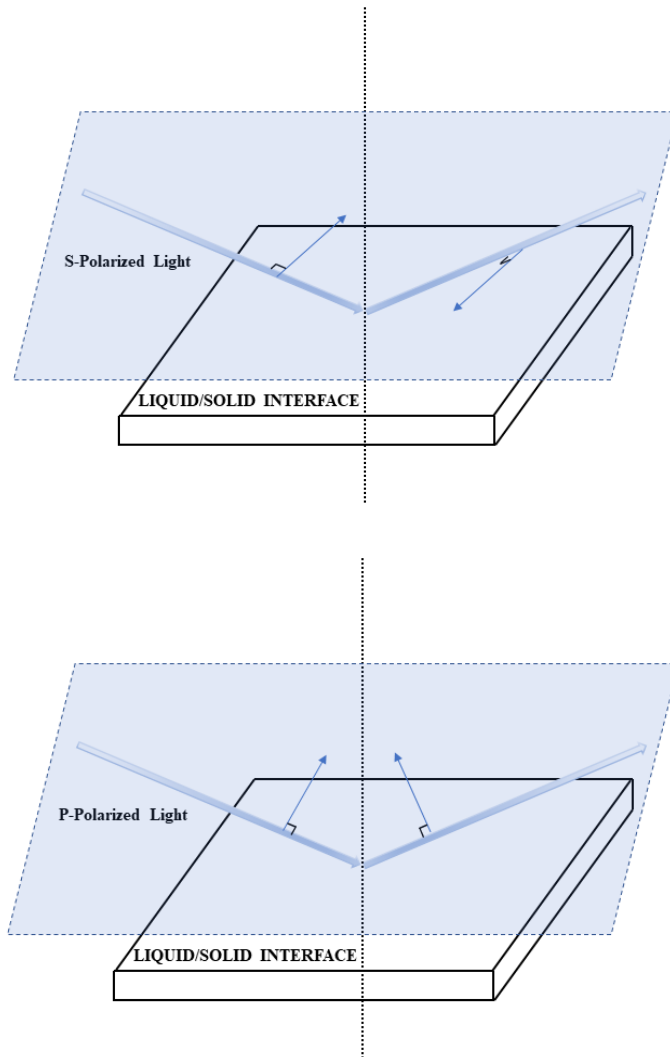
*Figure 2-1 illustration of p-polarized and s- polarized light reflected at liquid/solid interfaces. S-polarized component always undergoes a phase shift of nearly 180 degrees regardless of incident angel(top), which leads to the conclusion that there's no absorption of s-polarized light from the thin layer on liquid/metal interfaces.*

In 1966, the optical behavior of polarized light on metal surface was studied by Greenler[33] where he reached the conclusion that at optimal conditions, the absorption of a thin layer measured by the reflection technique could be 25 times greater than that measured by transmission method at normal incidence. Greenler's work has laid the foundation for reflection techniques that can be applied to surface science studies[34,35].
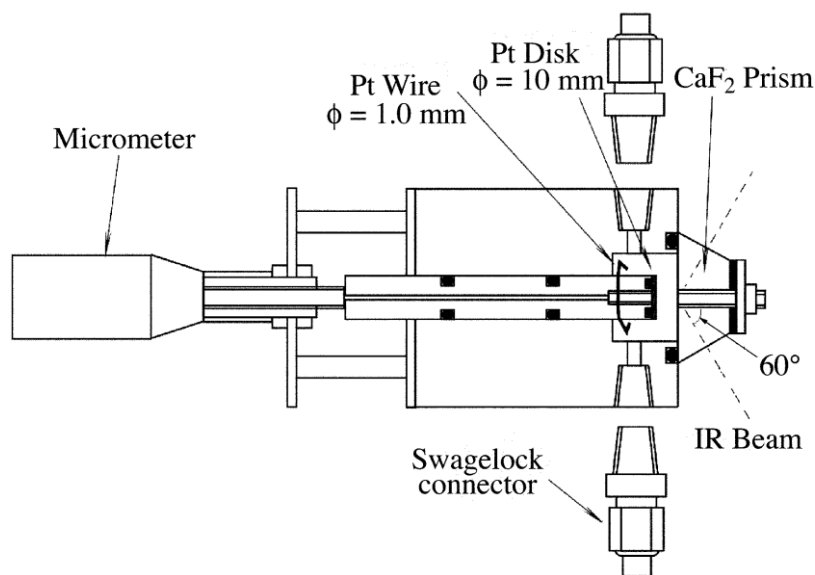


*Figure 2-2 Schematic representation of RAIRS cell for liquid/solid interfaces characterization used in this work. Modifier is prepared as solution and then injected into the cell. Only a small amount of modifier solution is trapped in between the CaF₂ prism and platinum backplate mounted on a Teflon® rod connected with a micrometer screw gauge. The gap between Pt disk and prism can be adjusted by the gauge to for optimal spectrum acquisition. Hydrogen and other gases can be fed through the Swagelok® connector.*

The RAIRS setup in this work was originally designed for Pt polycrystalline disk[36] (10 mm in diameter) and it has successfully revealed the adsorption of cinchona alkaloids[37,38] as well as NEA derived modifiers.
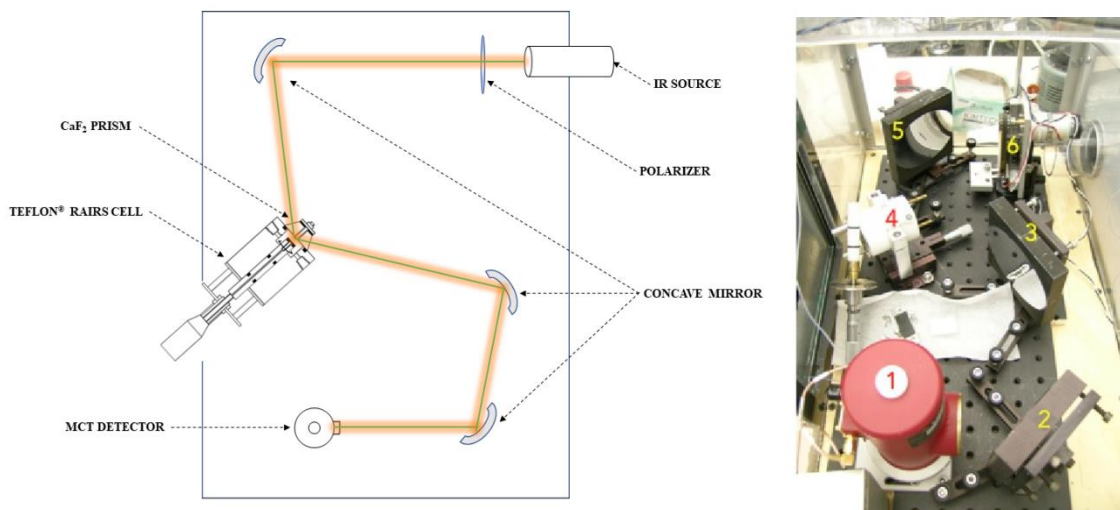
*Figure 2-3 Schematic illustration of the optical compartment of Reflection-Absorption IR Spectroscopy setup (left) and an actual photo taken above the compartment (right, CaF$_2$ prism dissembled from RAIRS cell). As shown in the photo: 1-MCT detector; 2,3,5-concave mirror; 4-Teflon® RAIRS cell; 6-polarizer actuated by a motor;*

IR source is from a Bruker Tensor 27 series FT-IR spectrometer working in external mode. The entire RAIRS setup along with the FT-IR spectrometer is purged with dry air to minimize interference from water vapor. However, this won't help minimize $CO_2$ peaks in the spectra, which can usually be found as two medium-strong peaks at around 2300 to 2400 cm$^{-1}$.

RAIRS apparatus is also connected to a gas handling system which is shared with ATR-IR system. Gas manifold of liquid-solid IR setup includes H$_2$, Ar, CO, O$_2$ while other gases can also be attached for special experiments (such as D$_2$ for studying H-D exchange).
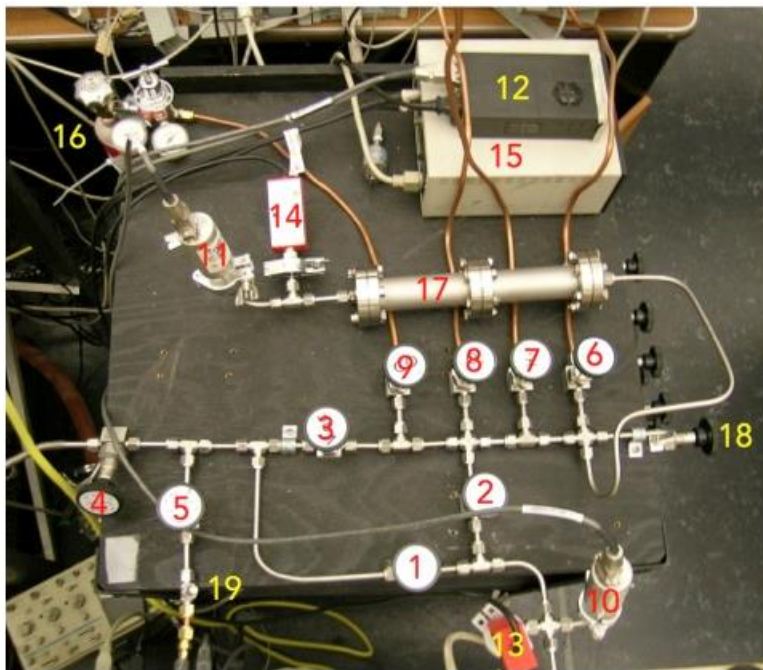
*Figure 2-4 Gas handling system shown in actual picture. 6-9 are valves to the gas cylinders: Ar, $H_2$, $O_2$ and CO. 4 is connected to a mechanic pump to vacuum the gas lines; valve 5 is the gas outlet to the RAIRS optical compartment. Flow rate can be adjusted by 19, a Swagelok metering valve.*

Based on the optical properties of p-polarized and s-polarized IR beam on solid/liquid interface, adsorbates with in thin layer of liquid will preferentially absorb p-polarized IR over s-polarized counterpart.
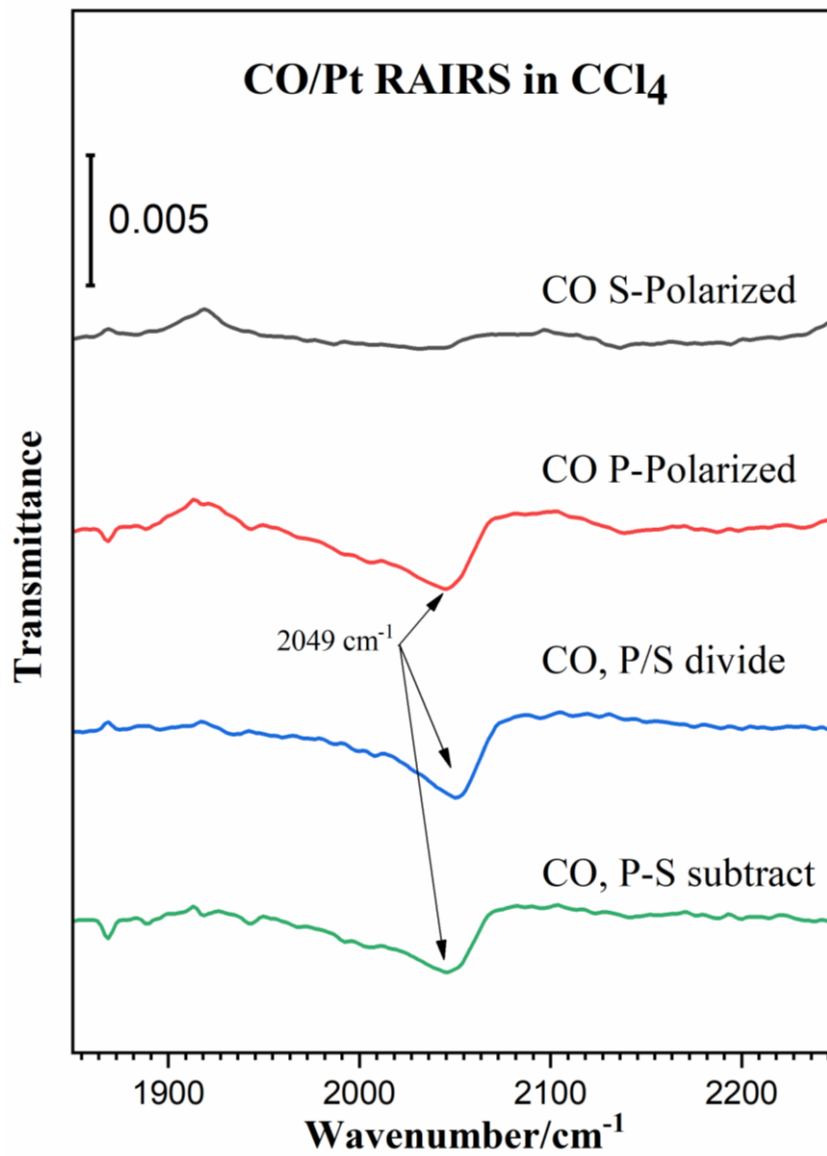
*Figure 2-5 CO adsorption on Pt disk observed in CCl₄ using RAIRS. Pt is in-situ pre-treated with H₂ in CCl₄ and the exposed to CO. Adsorbed CO is detected only by p-polarized IR while free CO shows up in both P and S spectra as a weak bump around 2135 cm⁻¹. Only a narrow range of whole spectrum is selected to show the top-adsorbed CO on Pt surface.*

CO adsorption experiments, or sometimes referred as CO titration quantitively, is a powerful tool to identify different types of active sites on various metal surfaces. However, when it comes to adsorption that occurs on solid/liquid interfaces, FT-IR in transmission mode usually suffers from low S/N ratio and requires extra effort to locate the IR signature peaks of adsorbates from the dissolved species. With the help of reflection absorption techniques, as shown in figure 2-5, CO molecules adsorbed on the top sites of Pt can be identified from free CO after proper data processing (p divided by s or s subtracted from p).
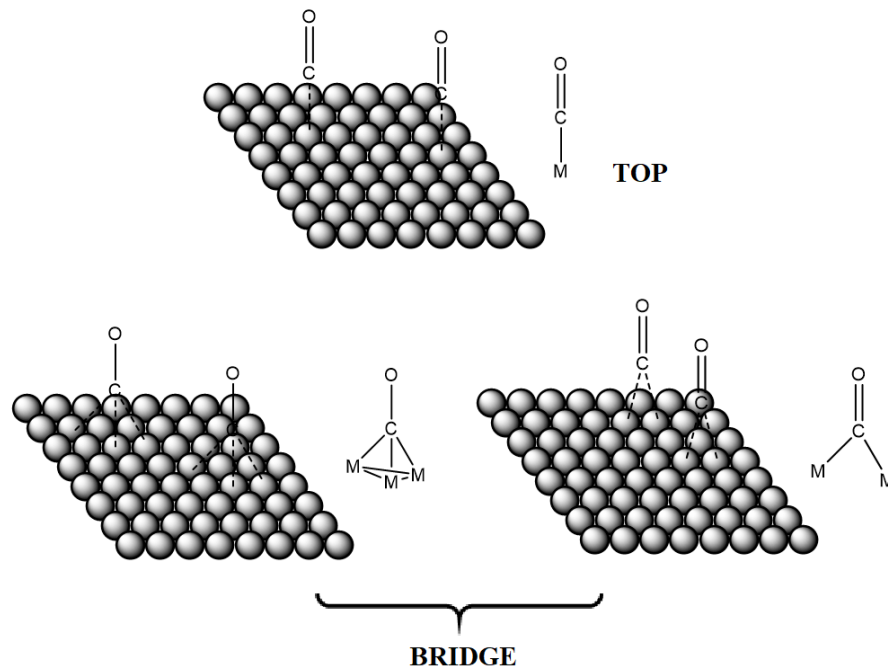


*Figure 2-6 CO adsorebed on metla surfaces via different sites (top, two-fold or three-fold brdge sites).*

In this work, the RAIRS setup, which previously has been designed for experiments with Pt polycrystalline disk, is also utilized to explore the adsorption of modifiers on supported powder catalyst where Pt nanoparticles are loaded onto proper oxide such as $SiO_2$ or $Al_2O_3$.
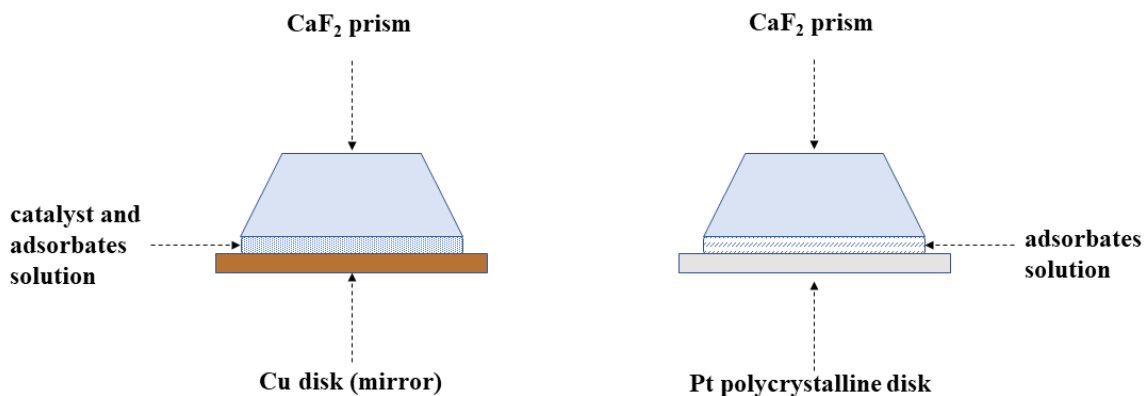


*Figure 2-7 illustration of the thin layer of liquid trapped between CaF$_2$ prism and solid disk. Left: Cu is used as backplate serving as a mirror only, Pt powder catalyst is pressed by the prism and Cu disk along with modifier solution. Right: Pt polycrystalline disk works as a mirror and adsorption interface the same time.*

Unlike the case with Pt polycrystalline disk, for powder catalyst experiments, RAIRS actually operates under transmission mode instead of reflection mode as Pt does. This presumption is later confirmed by experimental data and will be discussed in next few chapters.

*2.1.2 Multibounce Attenuated Total Reflection IR (ATR-IR)*

Attenuated Total Reflection IR spectroscopy is another experimental technique that take advantage of the optical characteristic of IR light being totally reflected on the surface of optical element (usually Ge or other metal). ATR-IR renders it possible to directly analyze the sample without further preparation, which is necessary to study the behavior of catalyst under in-situ or operando conditions[39,40].
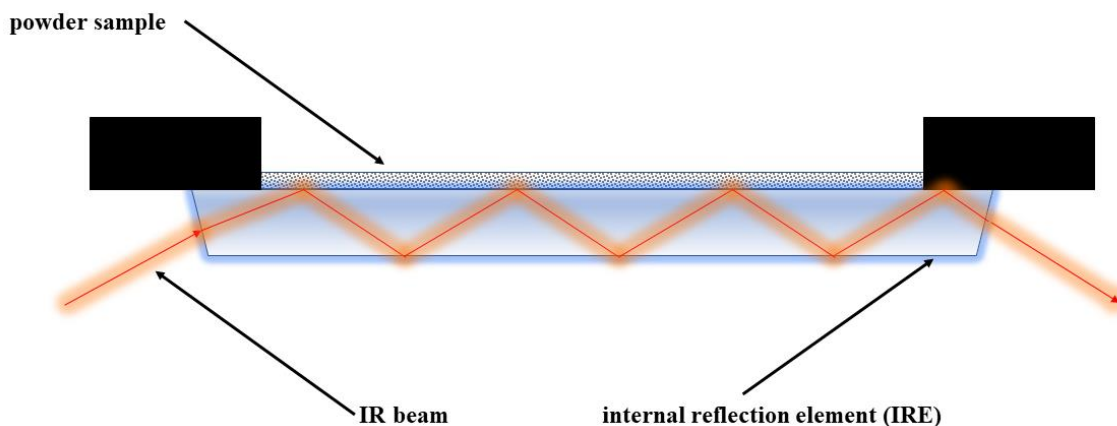


*Figure 2-8 schematic representation of ATR-IR accessory for FT-IR spectrometer.*

ATR assembly shown in figure 2-8 is usually installed in the optical compartment of a commercial spectrometer. IR beam is generated by the spectrometer and then travels inside the internal reflection element (sometimes also referred as ATR crystal) and then collected and processed by the internal detector of spectrometer. Sample is loaded in the form of a thin film evenly dispersed on the IRE surface to achieve optimal signal to noise level. Typically, ATR crystal is made of an IR transparent material which has high refractive

index because the refractive index of ATR crystal needs to be higher than that of the sample above it  so that total reflection will always occur on the interface.

An important aspect of total internal reflection is evanescent wave. Although the 'entire wave' is reflected back into original medium (higher refractive index), part of it still penetrates the second medium with smaller refractive index. The evanescent wave tends to travel along the boundary while it doesn't carry any energy or momentum. It's only the results of boundary conditions. The depth of penetration depends on wavelength as well as the medium that the incident light travels inside, which can be written as:

$$dp = \frac{\lambda_1}{2\pi\sqrt{\sin^2\theta - (n_2 - n_1)^2}}$$

Where dp is the maximum depth that the original incident can penetrate the second medium, which usually decays exponentially as it travels deeper into the medium.

*Table 2-1 Common materials of ATR crystal (Internal Reflection Element, IRE) and selection of their optical properties. Data source: Bruker ATR Application Note AN#79.*

| Material | Spectral Region ($cm^{-1}$) | Refractive index | Depth of penetration at 45°, 10000 $cm^{-1}$ (µm) | Hardness (knoop) |
|---|---|---|---|---|
| ZnSe | 20,000-500 | 2.43 | 1.66 | 130 |
| ZnS | 22,000-750 | 2.25 | 1.54 | 355 |
| Ge | 5000-600 | 4.01 | 0.65 | 550 |
| Si | 10,000-100 | 3.42 | 0.81 | 11150 |
| Diamond | 45,000-10 | 2.40 | 1.66 | 9000 |

In this work, the choice of ATR crystal is Ge from PIKE Technologies. Ge crystal features higher refractive index and thus place less restrictions on the selection of modifier and solvent. Smaller penetration depth of Ge also helps to minimize the interference from the solution layer above catalyst film. The major drawback of Ge as ATR crystal is relatively narrow spectral region. However, it will not place any limits on the modifiers involved in this work since 5000-600 cm$^{-1}$ is wider than the vibrational modes mentioned here (usually 4000-900 cm$^{-1}$)
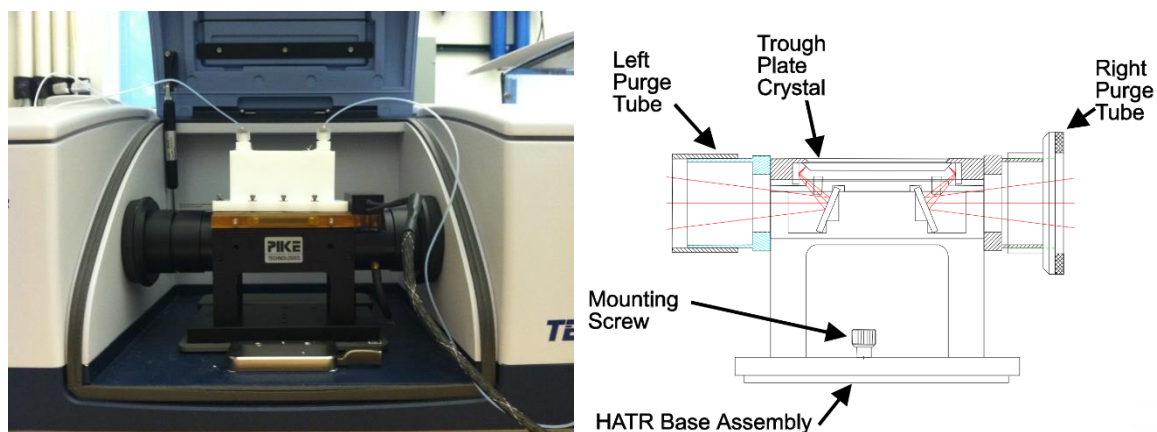


*Figure 2-9 Left: Photo of ATR accessory installed in the compartment of a Bruker Tensor 27 FT-IR spectromeete. Right: Schematic representation of the base assembly with top-mounted ATR crystal.*

ATR-IR setup also shares the gas lines with RAIRS apparatus described in last section to provide in-situ pre-treatment for powder catalyst before adsorption experiments. The volume of ATR cell under Teflon® cover is approximately 10 ml and early experiments follows a static method where modifier solution is injected into the ATR cell and then various gases can be bubbled into/exit the cell via the inlet/outlet. However, due to the lack of solution exchange and proper stirring inside the cell. The concentration will change over exposure time because of consumption from adsorption.
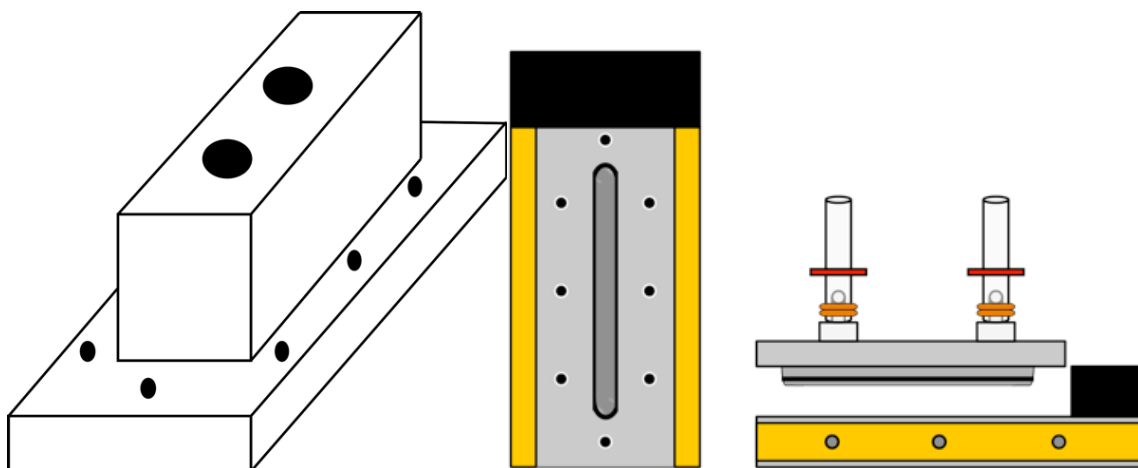


*Figure 2-10 Comparison of Teflon® cover (left) and metal cover with liquid—circulation feature (right) for ATR-IR cell*

To avoid concentration change and possible condensation of modifiers on metal surface, a cell design with smaller volume and ability to circulate solution in the ATR cell is necessary.
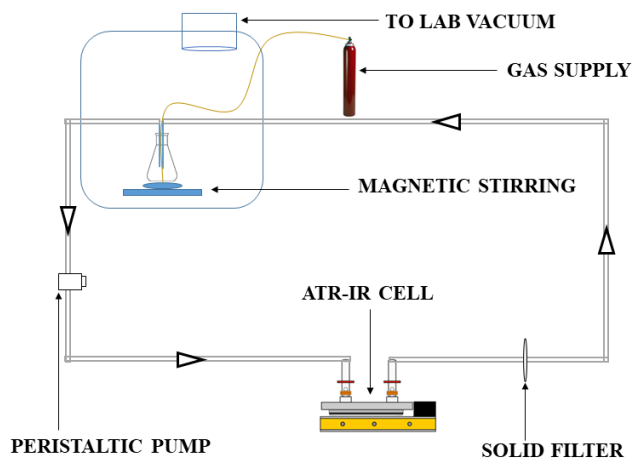
*Figure 2-11 schematic representation of ATR-IR cell and peripheral devices for liquid circulation*

*Table 2-2 Features of gear pump and peristaltic pump for liquid circulation by comparison*

| Features | Gear pump | Peristaltic pump |
|---|---|---|
| Liquid displacement | Fixed volume | Depending on tubing type |
| Pulsation | Minimal to none | Significant |
| Particulate | Can't handle particulates | Yes |
| Viscosity | Lower | Relatively high |
| Pressure | High | low |

Table 2 lists the features of gear pumps and peristaltic pumps for liquid circulation. Since in this work, it's still likely that catalyst powder would end up entering the cycle even with appropriate filtering, a peristaltic pump will work better under such circumstance. Another factor is the possible corrosion caused by organic solvent. For peristatic pumps, solvent is cycled with the tubing, which is a disposable part while in the case of gear pump, internal parts might be damaged by solvent flushing and needs to be replaced at after a certain period.

In a typical ATR-IR experiment setup depicted in figure 2-11, modifier solution or pure solvent can be circulated in the closed-loop system by a peristaltic pump. Solution that exits the ATR cell is filtered to prevent catalyst powder from entering the cycle. Solution can be saturated with various gases for different purposes such as in-situ pre-conditioning of catalyst sample using $H_2$. Though solution is flowed in a closed-loop setup, adsorption of gas phase species can also be examined by bubbling specific gas into the solvent and by flushing the ATR, which theoretically exposes sample to the gas molecules dissolved in solvent, adsorption can be tracked as a function of exposure time.
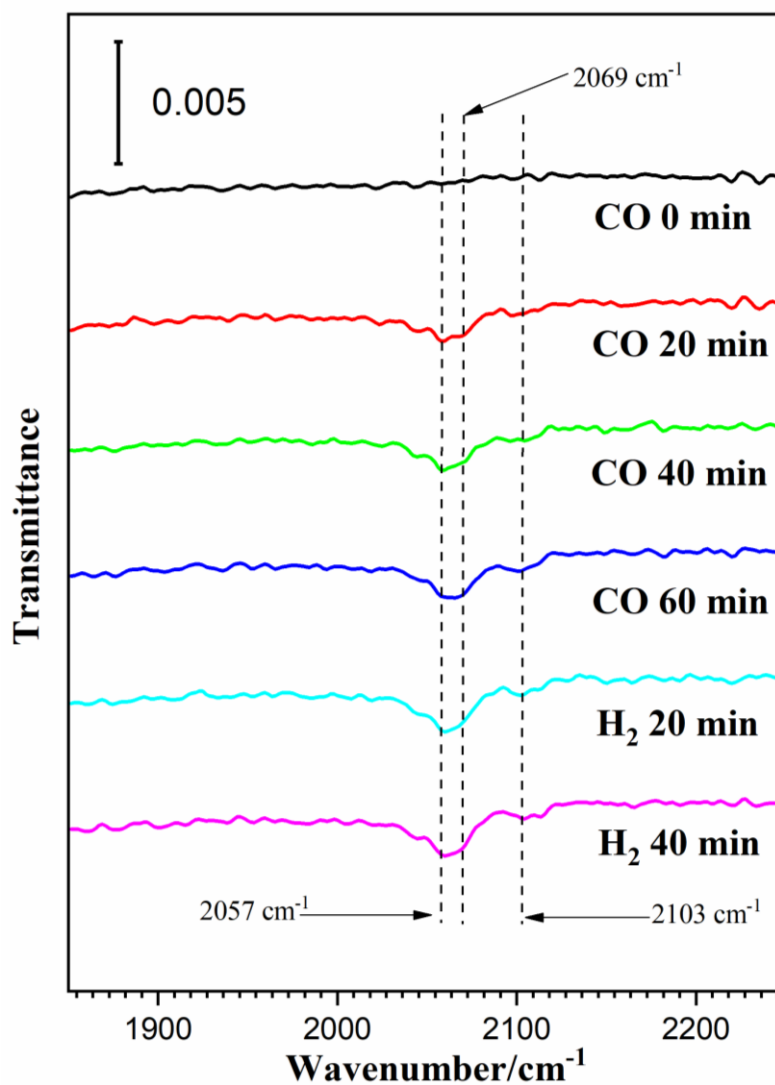
*Figure 2-12 An ATR-IR example of CO adsorption on Pt nanoparticles supported by $Al_2O_3$*

Unlike CO adsorbed on Pt poly crystalline (RAIRS), behavior of CO on supported Pt is more complicated due to more diverse active sites on the surface of Pt nanoparticles. 2057, 2069 and 2103 cm$^{-1}$ are all signature peaks of on-top adsorbed CO considering the fact that CO adsorption can be affected by the size of Pt particles[41] as well as Strong Metal-Support

Interaction (SMSI)[42]. ATR-IR is a versatile tool for studying the adsorption of either modifiers and gas molecules on metal surfaces.

## 2.2 Characterization of Catalyst and Reaction Mixture

A variety of characterization methods have been utilized to explore the properties of Pt-based commercial catalysts from multiple aspects.

### 2.2.1 Transmission electron microscopy (TEM)

Transmission electron microscopy is a powerful tool for examine the shape, size as well as dispersion of platinum nanoparticles on oxide support. Sample is prepared by disperse 2mg of catalyst in approximately 5ml ethanol or other volatile solvent in a vial. Sonicate the mixture until it forms a uniform slurry. Transfer the slurry to a TEM copper gird (Formvar/Carbon on 400 Mesh Copper) dropwise. The sample is ready for analysis after completely dried.

TEM characterization is performed using a FEI Tecnai12 at Central Facility for Advanced Microscopy and Microanalysis (LaB6, High-voltage range 20 to 120 kV). Since estimated average size of Pt particles is 2-3 nm, resolution of the microscopy is already high enough (line resolution: 0.20 nm; point resolution: 0.34 nm).

## 2.2.2 Specific Area—BET Gas Sorption Analysis

Specific area of catalyst, which mainly reflects property of the support, is measured with NOVA 2000e series surface area analyzer manufactured by Quantachrome Instruments in our lab . In general, Brunauer–Emmett–Teller (BET) theory is an extension of Langmuir Theory. It explains the physical adsorption of gas molecules on a solid surface and is the theoretical basis for the measurement of specific area and pore size for porous materials.

To measure specific surface area and pore size of a given Pt based catalyst, 50 mg sample is weighed out and transferred to a 9 mm stem sample cell. Sample is first degassed in vacuum at 160 °C for at least 6 hours. Turn off the heating and wait the sample to cool down to room temperature. And then measure and calculate the mass of catalyst sample before starting actual BET analysis.

## 2.2.3 Evaluation of Reaction Performance

The catalyst is first preconditioned by sequential treatments in Ar at room temperature for 90 min, O2 at 300°C for 120 min, and $H_2$ at 350°C for 120 min; Sample is then cooled down under an $H_2$ atmosphere and transferred to the high-pressure reactor in our lab (Parr 4566) and mixed with selected solvent. Solutions of the modifier and the reactant (EtPy, 98% purity, Sigma–Aldrich) are added with continuous stirring using a magnetic bar. Small aliquots of the solution were taken periodically and analyzed by gas chromatography (Agilent 6809N) using a chiral column (DB-WAX, Agilent).

## 2.2.4 Nuclear Magnetic Resonance (NMR)

NMR has been used to examine the transformation of s-NEA, especially the hydrogens , under reaction condition. A small aliquot solution (in $CCl_4$) is transferred to a 5mm VWR Precision NMR sample tube. A capillary tube filled with $CDCl_3$ is placed in the NMR sample tube as we.

$^1$H NMR experiment is performed on a Bruker Avance NEO 400 2-channel z- axis gradient spectrometer.

## 2.2.5 GC-MS Fragment Analysis

Gas chromatography-mass spectrometry is employed in this work to analyze the product of s-NEA after possible dissociative adsorption on Pt.

The sample dissolved in $CCl_4$ is analyzed on a Waters GCT (2008) high resolution gas chromatography-mass spectrometry equipped with a standard 30 meter, 0.25 micron DB-5 column (Agilent).

## 2.3 A glimpse of Catalyst Properties: Pt/SiO$_2$ and Pt/Al$_2$O$_3$

Both Pt/SiO$_2$ (Sigma Aldrich) and Pt/Al$_2$O$_3$ (Alfa Aesar) catalysts are commercially available and have been pre-reduced before leaving the factory. An additional ex-situ thermal treatment is performed before each test to make sure Pt surface is pristine.
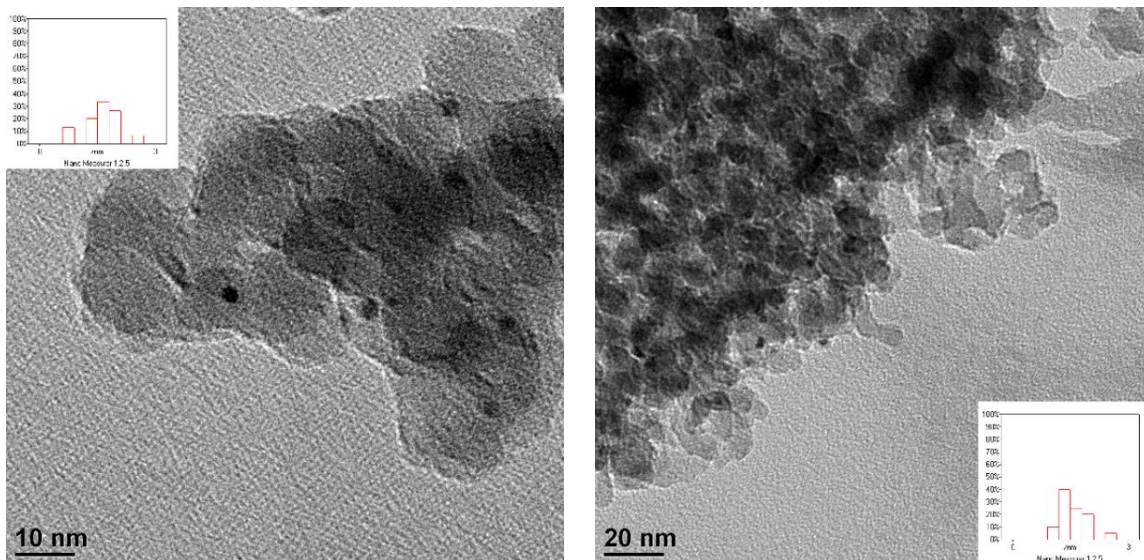
*Figure 2-13 TEM images of 1% Pt/SiO$_2$ before (left) and after (right) ex-situ thermal treatment*
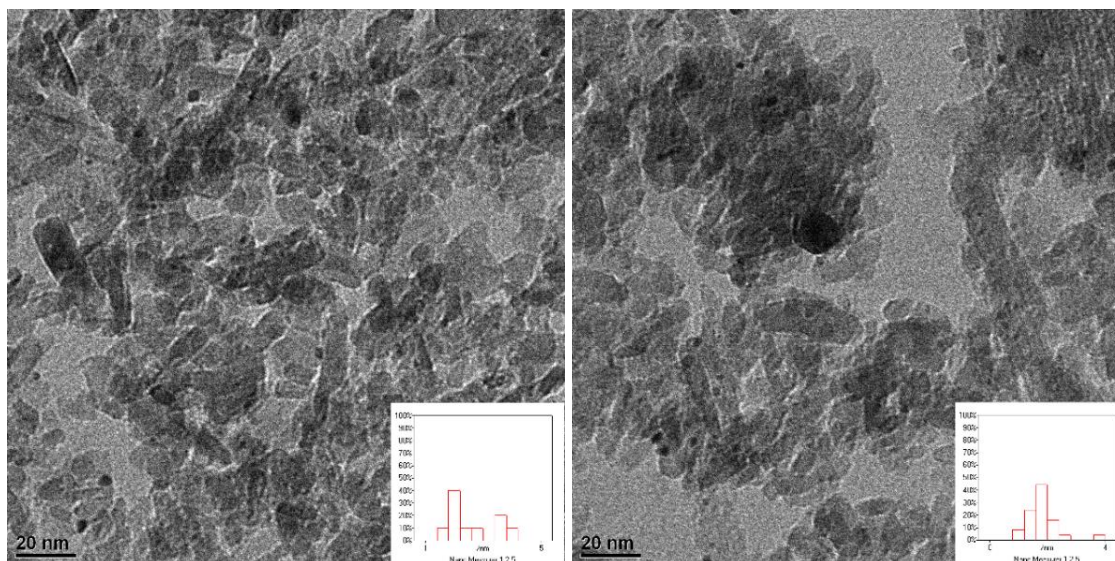


*Figure 2-14 TEM images of 1% Pt/Al$_2$O$_3$ before (left) and after (right) ex-situ thermal treatment*

Pt catalyst is loaded in a quartz tube furnace and purged by Argon at room temperature for 90 minutes and then O$_2$ at 300 C$^\circ$ for another 120 minutes to remove organic impurities on surface and lastly H$_2$ at 350 C$^\circ$ for 120 minutes.

Particle size distribution is measured with 20 selected particles in TEM image. No aggregation has been observed before and after the pre-conditioning. Particle size remains the same with slightly more unified distribution after the thermal treatment.

At the end of last chapter, the effect of particle size on the adsorption process is mentioned and based on the TEM images above, there is no significant difference in particle size between $Pt/SiO_2$ and $Pt/Al_2O_3$ and both are within 2-3 nm in average.

Another important aspect of the platinum catalysts is the support. The specific surface area of $Pt/SiO_2$ and $Pt/Al_2O_3$ has been measured using multi-point method.
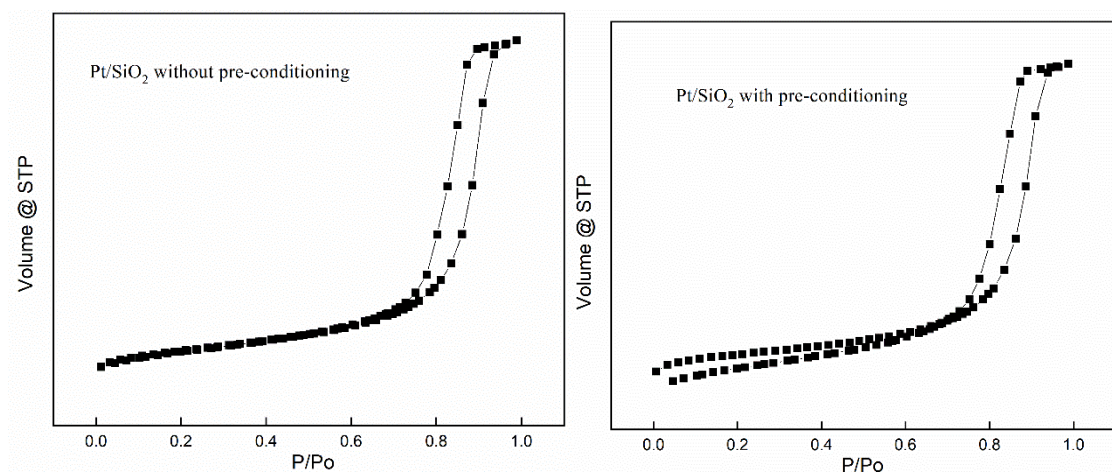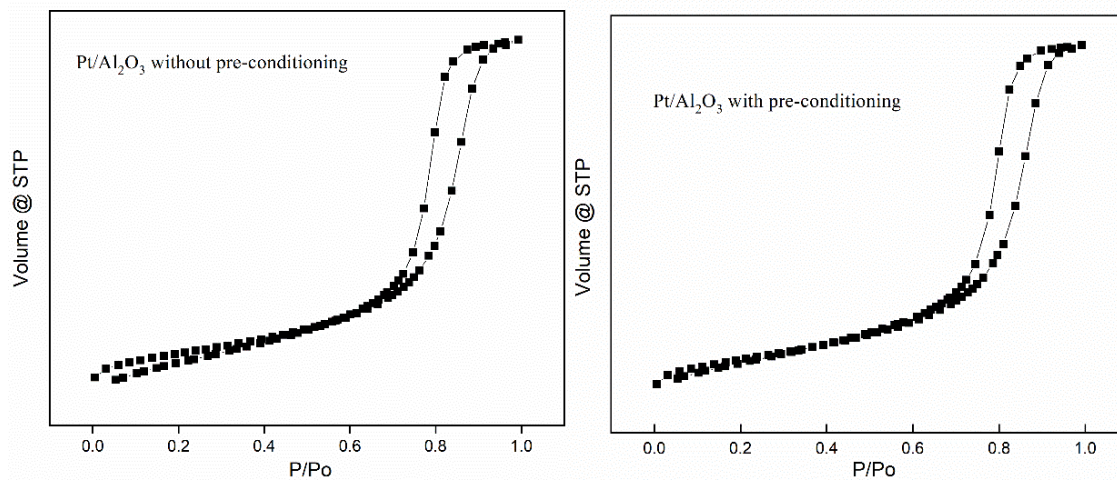
*Figure 2-15 Multi-point measurement in the BET specific area analysis of 1%Pt/SiO₂ (top) and 1% Pt/Al₂O₃ (right) before (left) and after (right) thermal pre-conditioning as described.*

# Chapter 3 First Glimpse of the Adsorption of Surface Modifiers on Pt Surfaces: Prerequisites and Structural Dependence

## 3.1 In-situ Pre-treatment of Pt Catalyst—Influence of Dissolved Gases on the Adsorption of Modifiers

### 3.1.1 Introduction

This section will cover discussion about the influence of gases dissolved in liquid phase. Hydrogen not only serves as the main reactant for hydrogenation reactions, but also is one of the pre-requisites for adsorption of modifier molecules onto Pt surfaces. These results have been observed in the past with poly-crystalline Pt using RAIRS[43]. Most of the observations also applied to Pt nanoparticles in this work despite the vastly different surface conditions of these two forms of Pt.

### 3.1.2 Results and Discussion

In the past, CO adsorption on Pt polycrystalline disk in $CCl_4$ has been reported (ref 43) using RAIRS setup where it was discovered that electro-chemical pre-conditioning is necessary to facilitate the adsorption of modifiers onto Pt surface. Unlike Pt disk, supported Pt nanoparticles require little to none electro-conditioning before adsorption experiments. However, there are still some pre-requisites for Pt particles at the nanometer scale.
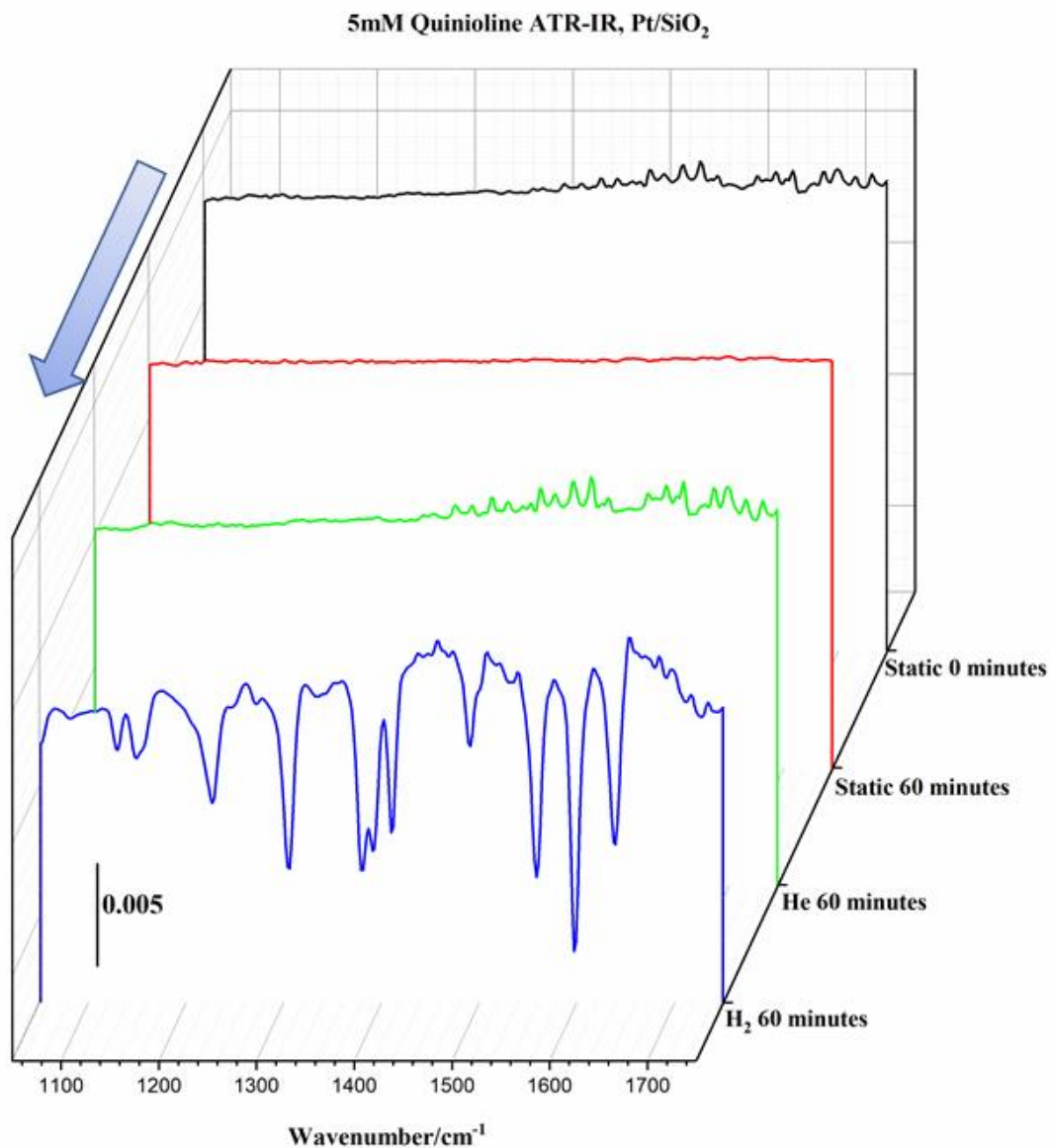
*Figure 3-1 ATR-IR spectra of 1% Pt/SiO₂ exposed to 5mM quinoline CCl₄ solution with bubbling of various gases. Pt catalyst sits in the quinoline solution for 60 minutes followed by 60 minutes of inert gas (Helium) bubbling to make the solution He saturated. In the end, Helium bubbling is switched to H₂ for another 60 minutes. Y-axis is converted and shown in IR transmittance. No solution exchange is involved in this test.*

Figure 3-1 shows the results of quinoline adsorption experiments with 1% Pt/SiO$_2$. Within the first 60 minutes sitting in static quinoline solution (no gas bubbling applied), Pt surface is free from any adsorption per ATR-IR data. In fact, in most previous studies[23,44], regarding either behavior of modifiers or reaction mechanisms, modifier solutions are prepared with a H$_2$ saturated solvent or accompanied by a H$_2$ supply all the time. As a result, the role of H$_2$ as part of the pre-conditioning might be ignored to some extent.



QUINOLINE                              CINCHONIDINE
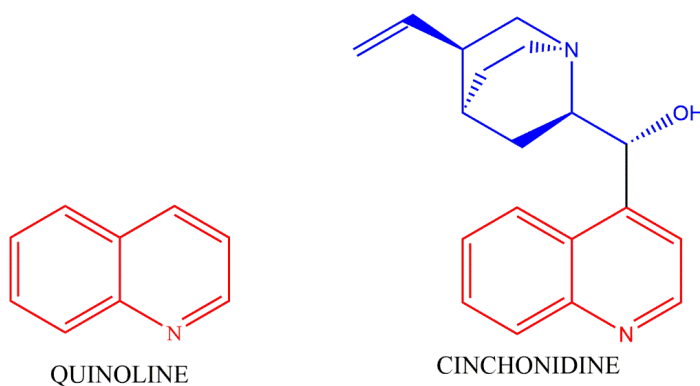
*Figure 3-2 Structural representation of quinoline and cinchonidine*

On the other hand, quinoline, as an important structural component of cinchonidine, is believed to be the anchor of cinchonidine during the adsorption onto Pt surface[25,45]. In addition, due to higher solubility of quinoline in CCl$_4$ compared to cinchonidine and cinchonine, it's usually easier to keep track of the vibration modes of quinoline than that of cinchona alkaloids modifiers using in-situ FT-IR spectroscopy.
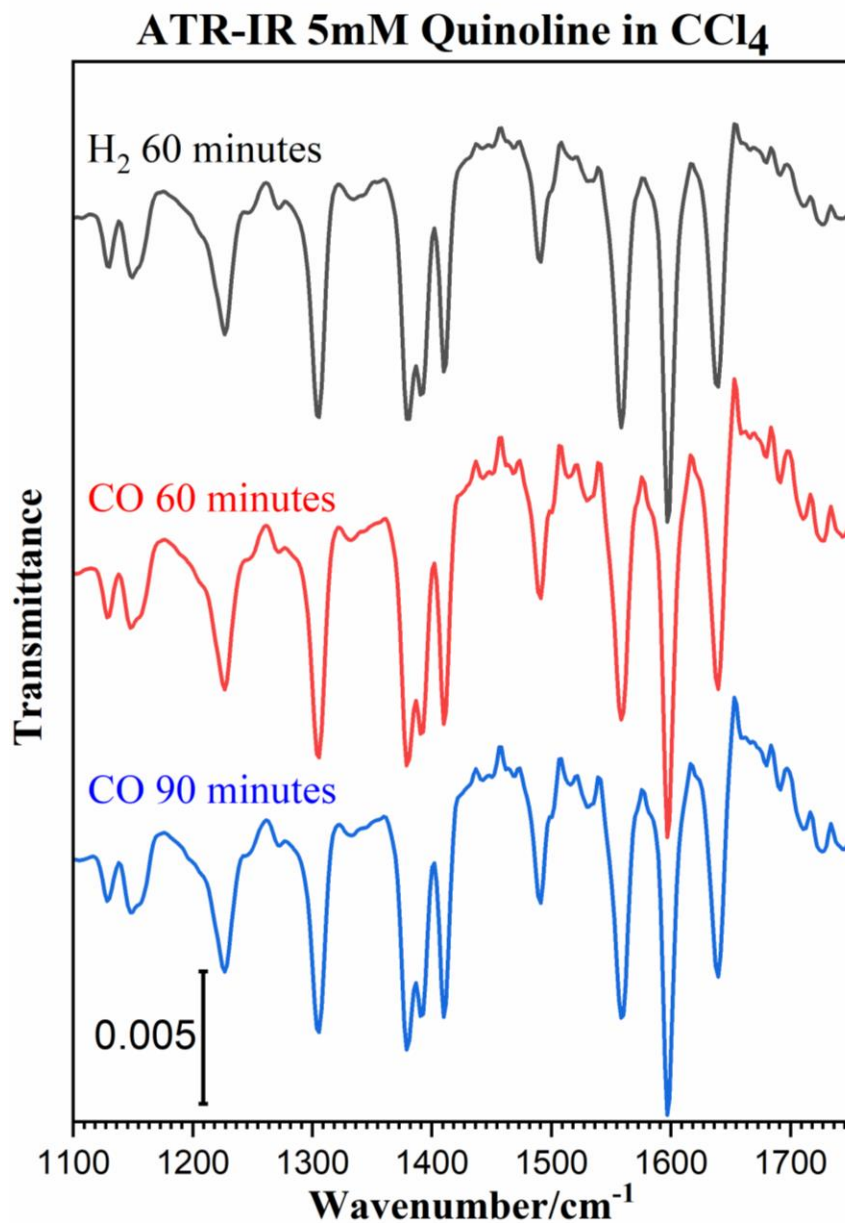
*Figure 3-3 ATR-IR results of 1mM quinoline adsorbed on 1% Pt/SiO$_2$, CO is introduced into the ATR-IR cell after H$_2$ induced adsorption, after which continuous CO bubbling is applied to test its ability to remove adsorbed quinoline from Pt surface.*

Results from figure 3-2 and 3-3 combined suggested that hydrogen pre-conditioning can clean platinum so that quinoline molecules are able to settle on metal surfaces. Inert gas, such as Helium, doesn't favor such a process, which leads to the conclusion that it's not the purging effect of flowing gas that cleans the surface.
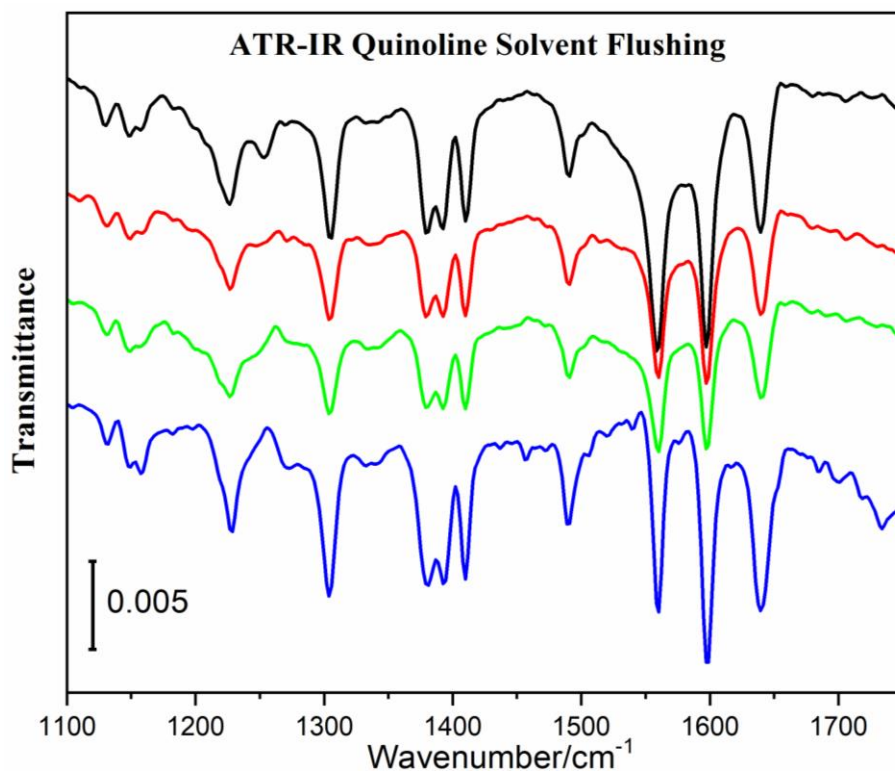


*Figure 3-4 Flushing ATR-IR cell with fresh solvent (CCl₄) to remove adsorbed molecules. Traces from top (black) to bottom (blue) are: before flushing, drain and refill the cell 3 times, 6 times, and leave the catalyst in solvent overnight.*

Meanwhile, exposing Pt surface with quinoline pre-adsorbed to continuous CO will not remove quinoline that has already bonded to Pt even after 90 minutes. This result is in close agreement with the study done by our previous group members using RAIRS and Pt polycrystalline disk[43]. It's generally accepted that hydrogen reduction of catalyst under

high temperature can help to clean metal surfaces and remove contamination and thus improve catalytic performance under reaction conditions[46,47]. However, the Pt/SiO$_2$ catalyst used here is a pre-reduced commercial catalyst and is reduced again at 573K in H$_2$ flow before each experiment yet, the assistance from H$_2$ is still a must for quinoline adsorption.
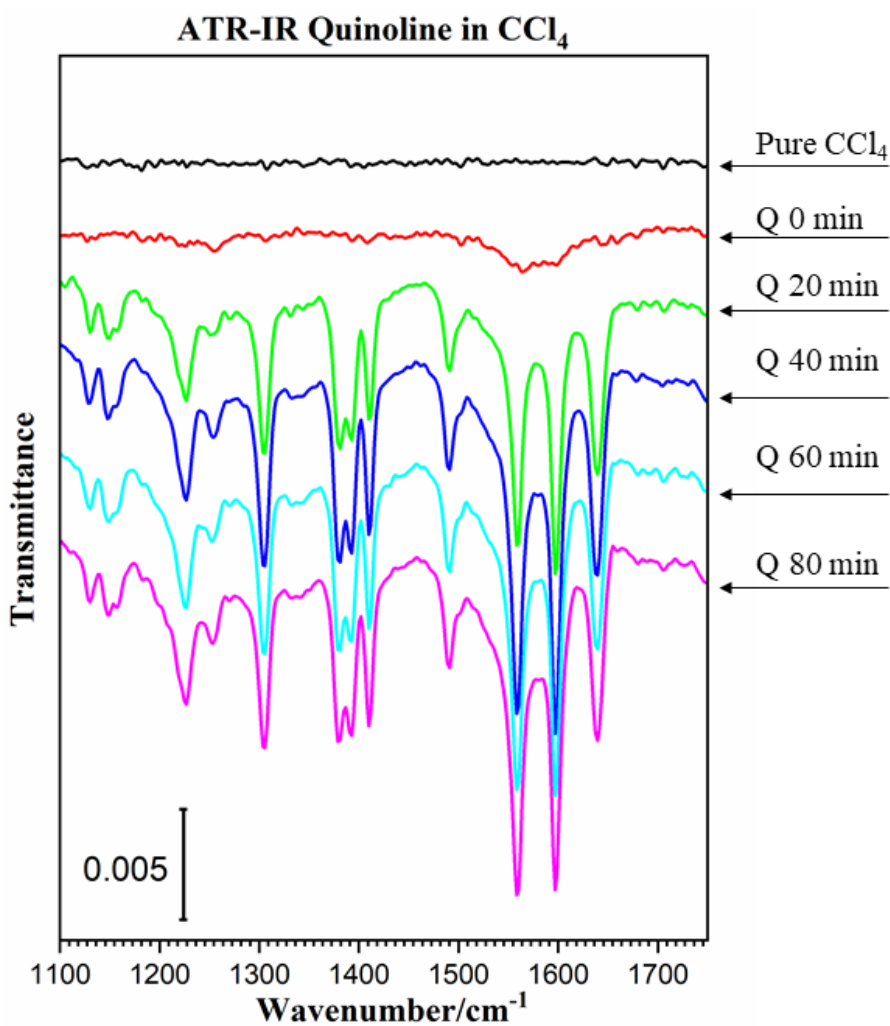


Figure 3-5 ATR-IR spectra of adsorbed quinoline on Pt/SiO$_2$ vs exposure time (with H$_2$ bubbling)

Though CO has been proved to be a strong inhibitor for cinchonidine uptake and can thus delay the adsorption of modifier onto clean Pt surface, once the surface is covered with quinoline, CO is no longer able to remove it even after continuous bubbling which, in other words, a CO-saturated liquid phase. This result suggests that CO and quinoline alone will not block all the active sites on Pt surface and they can bond upon the surface in a relatively independent manner.

Figure 3-4 specifically shows the results from solvent flushing tests after exposing Pt to quinoline solution. Adsorption equilibrium plays an important role in surface modification and hence, will affect its ability to tune selectivity of hydrogenation reactions. When the concentration of a modifier decreases, for example, as a result of solvent flushing, the equilibrium will shift toward the direction to compensate such loss in solution phase, which eventually will lower the amount of modifier adsorbed on Pt. As is shown in the ATR-IR spectra, quinoline is partially removed due to fresh solvent flushing, which is indicated by decrease in IR peak intensity. Nonetheless, this trend doesn't hold up as flushing continues, even after 6 cycles of drain and refill with $CCl_4$ solvent, traces of adsorbed quinoline becomes weaker but still remain. However, this doesn't necessary lead to the conclusion that adsorbed molecules are so stable that they cannot be washed away. In fact, with the help of 'better' solvent in which the specific modifier is more soluble, the adsorption/dissolving equilibrium will adjust itself accordingly. The effects of solvent will be covered in another section in more detail.

To further explore the initial stage of quinoline adsorption, $Pt/SiO_2$ catalyst is immersed in pure $CCl_4$ solvent and followed by quinoline $CCl_4$ solution (Figure 3-5). IR signals of quinoline are monitored over exposure time more closely. Adsorption does not occur immediately (0 min) and it has already reached saturation within the first 20 minutes of contact, which supports the kinetics data[48,49] of hydrogenation reactions where the saturation in liquid phase only takes up to 3 minutes under given conditions.

Similar effect has also been observed with (S)-(−)-1-(1-Naphthyl) ethylamine, one of the most common synthetic model modifiers, with $Al_2O_3$ supported Pt catalyst. Pt catalyst is first loaded with $H_2$-saturated $CCl_4$, which is then replaced with s-NEA along with CO bubbling. The last step goes back to $H_2$ to examine the cleaning effect of $H_2$ on Pt surface.
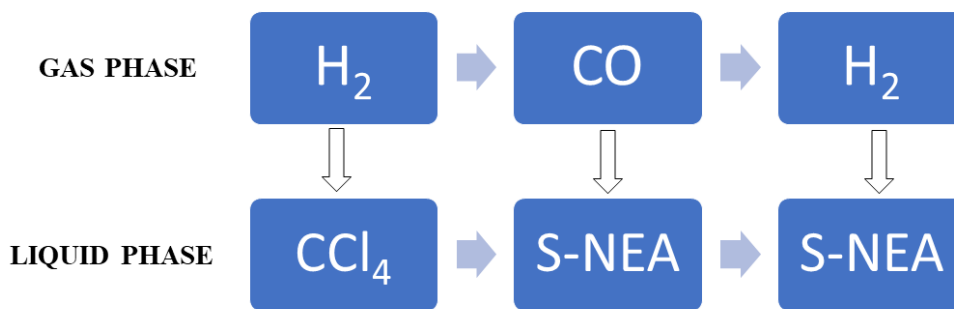


*Figure 3-6 flow chart showing 3 stages during the test of $H_2$ and CO's influence on the adsorption of s-NEA on $Pt/Al_2O_3$ catalyst.*

# Influence of H₂ and CO on s-NEA adsorption
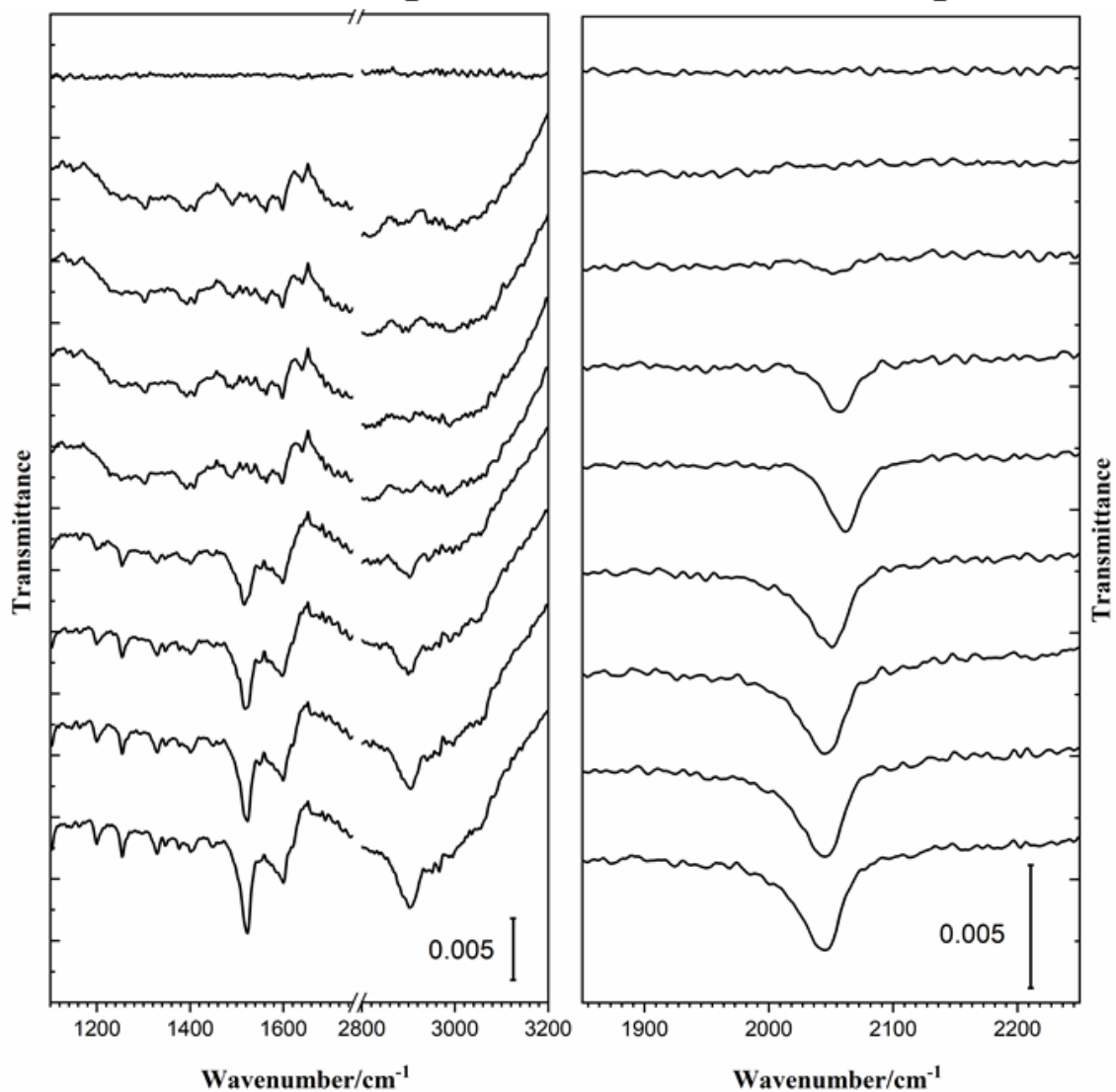


*Figure 3-7 1% Pt/Al₂O₃ catalyst is immersed in fresh CCl₄ solvent that has been saturated with H₂ and then the ATR-IR cell is drained and refilled with 2mM s-NEA CCl₄ solution and (2 traces on top). H₂ supply is then cut off and followed by CO bubbling (3ʳᵈ, 4ᵗʰ,5ᵗʰ trace from top shows 0, 30, 60 minutes of CO bubbling respectively). In the end, gas supply is switched back to H₂ to clean the surface (4 spectra at the bottom, 0, 20, 40, 60 minutes H₂ bubbling).*

H$_2$ promoted adsorption of surface modifiers in hydrogen saturated solvent has been observed with quinoline. In the case of s-NEA, a more comprehensive test has been conducted to further investigate the effects of dissolved gases especially CO in the solution phase.

The IR data of s-NEA are presented in two separate sections, one of which focus on the signals of s-NEA (figure 3-7, left panel) while the other one shows CO stretching (figure 3-7, right panel). It's widely known that frequency (or wavenumber as shown here) of CO vibration mode largely depends on CO coverage on metal surface occupying the same active sites[50,51].

An increasing coverage of Carbon monoxide on Pt surface over time can be identified with the blueshift of IR peak related to CO stretching, it's still not able to remove s-NEA molecules that have already settle on the metal surface. In 60 minutes of CO bubbling, peaks of adsorbed s-NEA stop growing, which is likely because CO does inhibit or at least does not favor interaction between s-NEA and Pt. Once liquid phase is saturated with H$_2$ again, s-NEA coverage will continue to increase. At the same time, CO coverage decreases as more H$_2$ enters liquid phase, which causes the CO peak shift toward the lower wavenumber end of spectrum.

*3.1.3 Conclusions*

In conclusion, s-NEA and quinoline, despite the difference in their molecular structure, their behaviors on Pt surface share several things in common in terms of influence of dissolved gases:

1. Even at room temperature, $H_2$ can enhance the adsorption of modifier which suggests that $H_2$ is not just a reactant in the reaction, it also plays an important role in the process of cleaning and activating metal surface; Though Pt catalyst is already reduced in $H_2$ at high temperature, it's still necessary to perform in-situ $H_2$ pre-condition before each adsorption experiment;

2. In the presence of $H_2$, adsorption of modifiers can quickly reach equilibrium between the solution phase and metal surface. This equilibrium is also the key in surface modification and in other words, tuning the selectivity of hydrogenation reactions;

3. CO has an inhibiting effect on the adsorption of modifier, however, it can't remove molecules that are already on the surface. The experiment results with s-NEA indicate that s-NEA can take over the sites from CO with the help of continuous $H_2$ supply but not vice versa.

## 3.2 Structural Dependence of Adsorption Ability of Organic Molecules—What Makes a Good Modifier

### 3.2.1 Introduction

The mechanism of surface modification and the ability of modifiers to bestow chirality on catalyst has been thoroughly studied and the structure of modifiers can determine their performance in modifying catalyst. In addition, to further expand the selection of modifiers, a profound understanding of the role of each function group of modifier molecules becomes more essential.

Adsorption of cinchona alkaloids modifiers has been well studied for decades and there is less divergence when it comes to the mechanism of surface modification by this type of modifiers. Yet, adsorption geometry of NEA and derivatives is still under debate. This section will start with a brief glance at correlation between structure and adsorption of certain modifiers.

*3.2.2 Results and Discussion*

In the past, in-situ IR studies on cinchona alkaloids have successful revealed the adsorption mechanism of modifiers[45,52]. cinchonidine/cinchonine is anchored to Pt surface via quinoline ring[53,54] while the quinuclidine interacts with the reactant to form a complex with a 1:1 ratio[55]. Adsorption geometry of modifier molecules will change the enantiomeric excess eventually and the proof for such connection can be revealed using in-situ FTIR techniques[56].
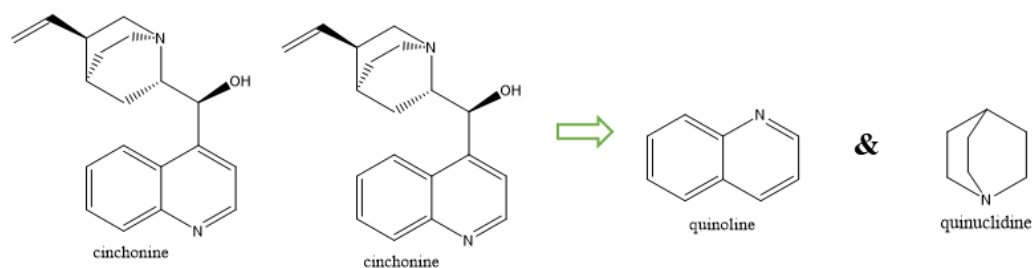


*Figure 3-8 Structure break-down of two types of common cinchona alkaloids modifiers. Despite being pseudo enantiomers of each other, they can lead reactions to product with opposite configuration.*

Nevertheless, there are still several conflicting proposed pathways regarding adsorption geometry of s-NEA and similar synthetic modifiers. They have drawn quite some attention because of their simpler structure over natural compounds as modifiers. Some researchers[57] believer that chemisorption interaction of NEA involves a combination π-bonding of naphthyl ring as well as a dative bonding via amine group[58–60].

On the other hand, however, this work along with precious work[15] in our group has pointed to another route where NEAs adsorb on Pt surface solely through the amine group without contribution from aromatic ring. This result indicates that NEA undergoes a completely different adsorption pattern from cinchona alkaloid modifiers.

## Naphthalene Derivatives
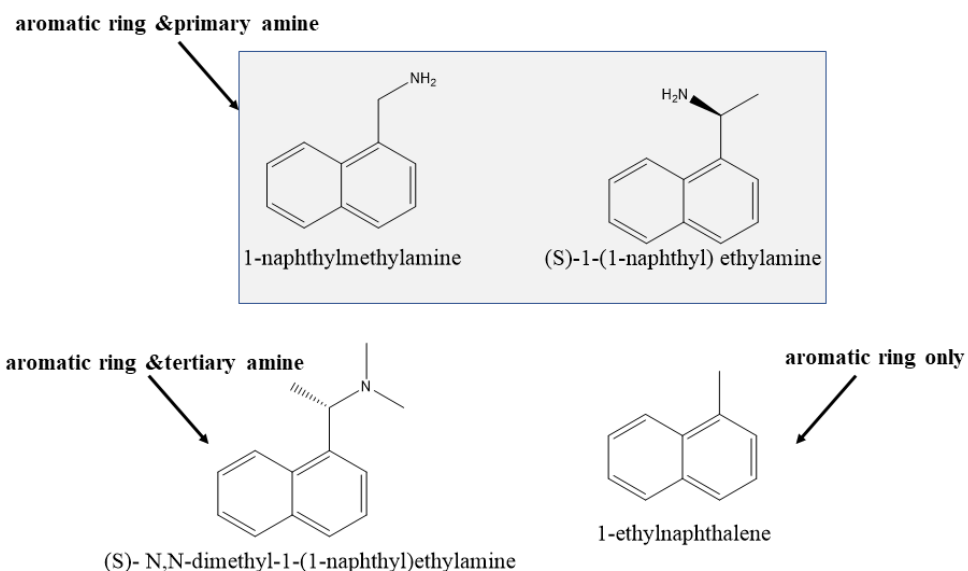


*Figure 3-9 selection of compounds with naphthyl groups to explore the adsorption geometry of NEA modifiers on Pt nanoparticles. All compounds fall in three categories:1. has naphthyl ring and primary amine; 2. aromatic ring but with tertiary amine; 3. Aromatic ring only.*

To investigate the adsorption geometry of naphthyl ethylamine derivatives as synthetic chiral modifiers for platinum catalysts, a series of molecules bearing naphthyl group in their structure have been put in test with 1% Pt/SiO$_2$ commercial catalyst under room temperature (300K).

45

The Pt catalyst is ex-situ reduced in $H_2$ flow at 573K (300 ºC) in a tube furnace followed by in-situ $H_2$ pre-condition at room temperature mentioned in previous section (effect of dissolved gases).
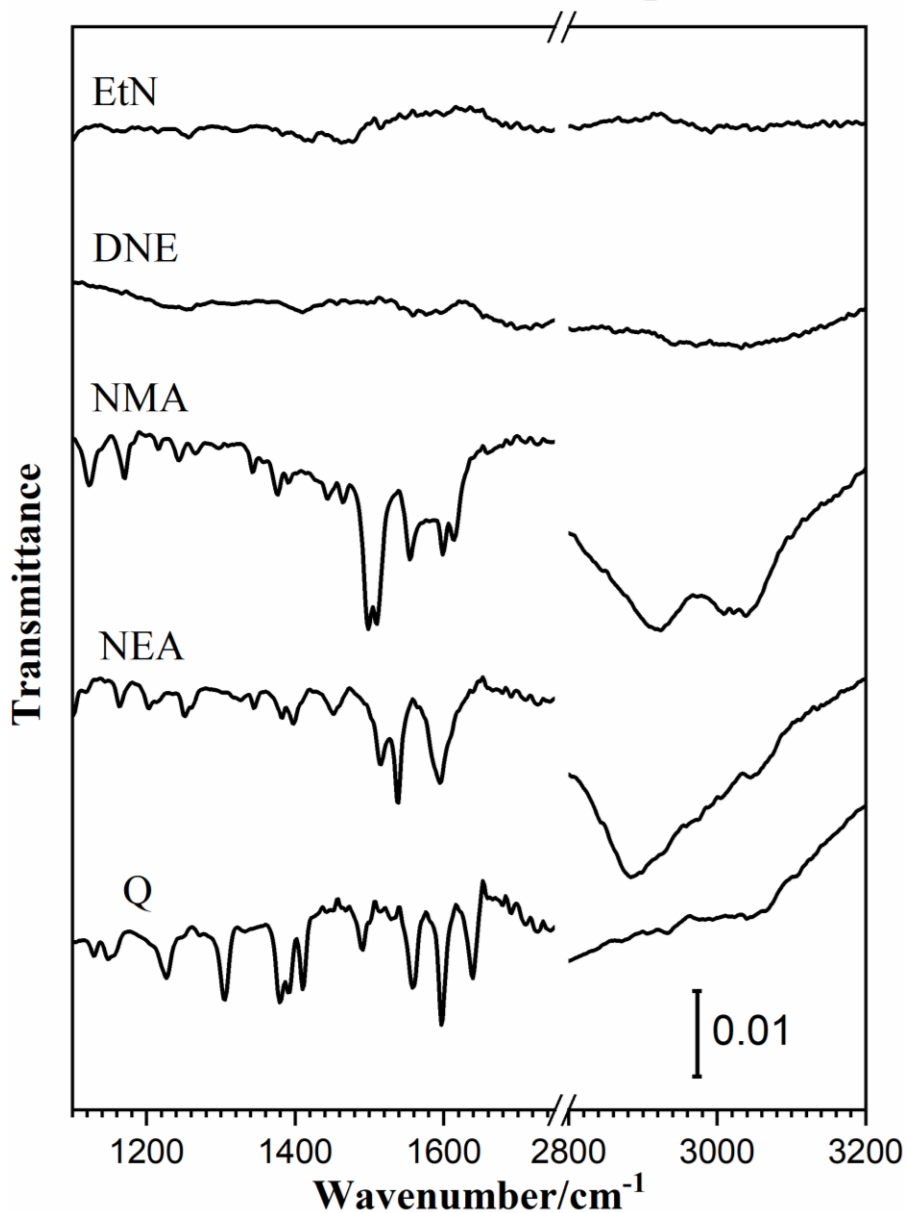
*Figure 3-10 ATR-IR Spectra of 5mM CCl₄ solution of following modifiers: 1-ethylnaphthalene (EtN), (S)- N,N-dimethyl-1-(1-naphthyl)ethylamine (s-DNE), 1-naphthylmethylamine (NMA), (S)-1-(1-naphthyl) ethylamine (s-NEA), quinoline (Q) respectively, with 1% Pt/SiO₂*

Figure 3-10 above shows that two of the derivatives do not show significant uptake, one of which, s-DNE, features a naphthalene ring and tertiary amine group. The other compound, EtN, only has an aromatic ring. The fact that both of them don't adsorb on the surface of Pt/SiO$_2$ suggests that naphthyl group, or in other word, the aromatic system, doesn't contribute to the interaction between modifiers molecules and Pt.
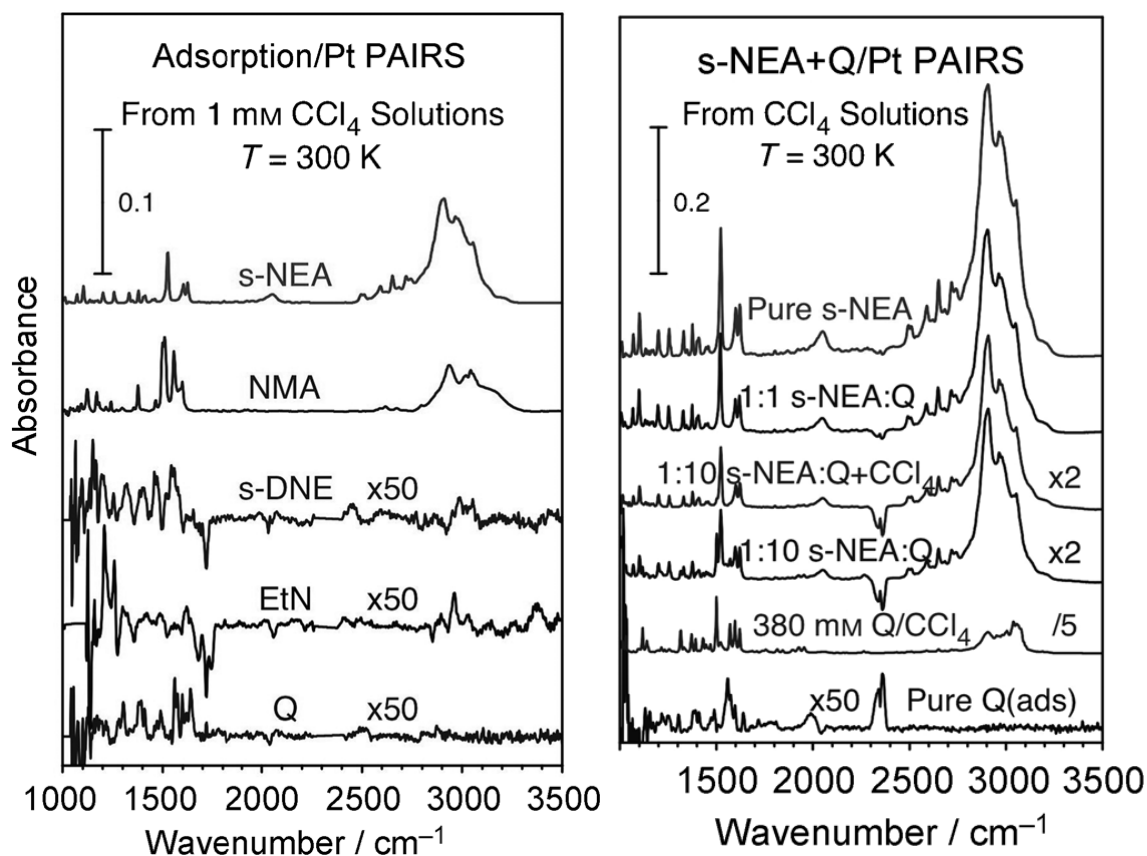


*Figure 3-11 Adsorption of NEA derivatives on Pt polycrystalline disk in CCl$_4$ (left) and co-adsorption of s-NEA and quinoline (Q) using same experiment setup. Adapted with permission from reference 29, Copyright © 2013 by John Wiley Sons, Inc*

The ATR-IR data of NEA derivatives, herein, confirm the observations from previous Pt disk RAIRS experiments only except that, in the case of platinum disk, NEA uptake is much stronger than that of quinoline (figure 3-11), which indicates stronger interaction of NEA-Pt. This result is also confirmed by corresponding co-adsorption test of NEA and quinoline (figure 3-11, right panel). When Pt disk is exposed to a solution that contains both s-NEA and quinoline, quinoline uptake is always overwhelmed by adsorbed NEA even considering that NEA is much less concentrated with Q being largely excessive in solution phase. Such phenomenon in co-adsorption experiments can be explained by the difference in adsorption mechanism of NEA and quinoline, or in other words, cinchona alkaloids. Besides, it might also be a result of weaker uptake of quinoline by nature.

By comparison, adsorption experiment with supported Pt nanoparticles tells a slightly different story. Still, NMA and NEA are the only two compounds with naphthalene ring that can adsorb on Pt surface. Meanwhile, quinoline uptake is on par with NEA and NMA, which contradicts the result from RAIRS data using Pt disk.
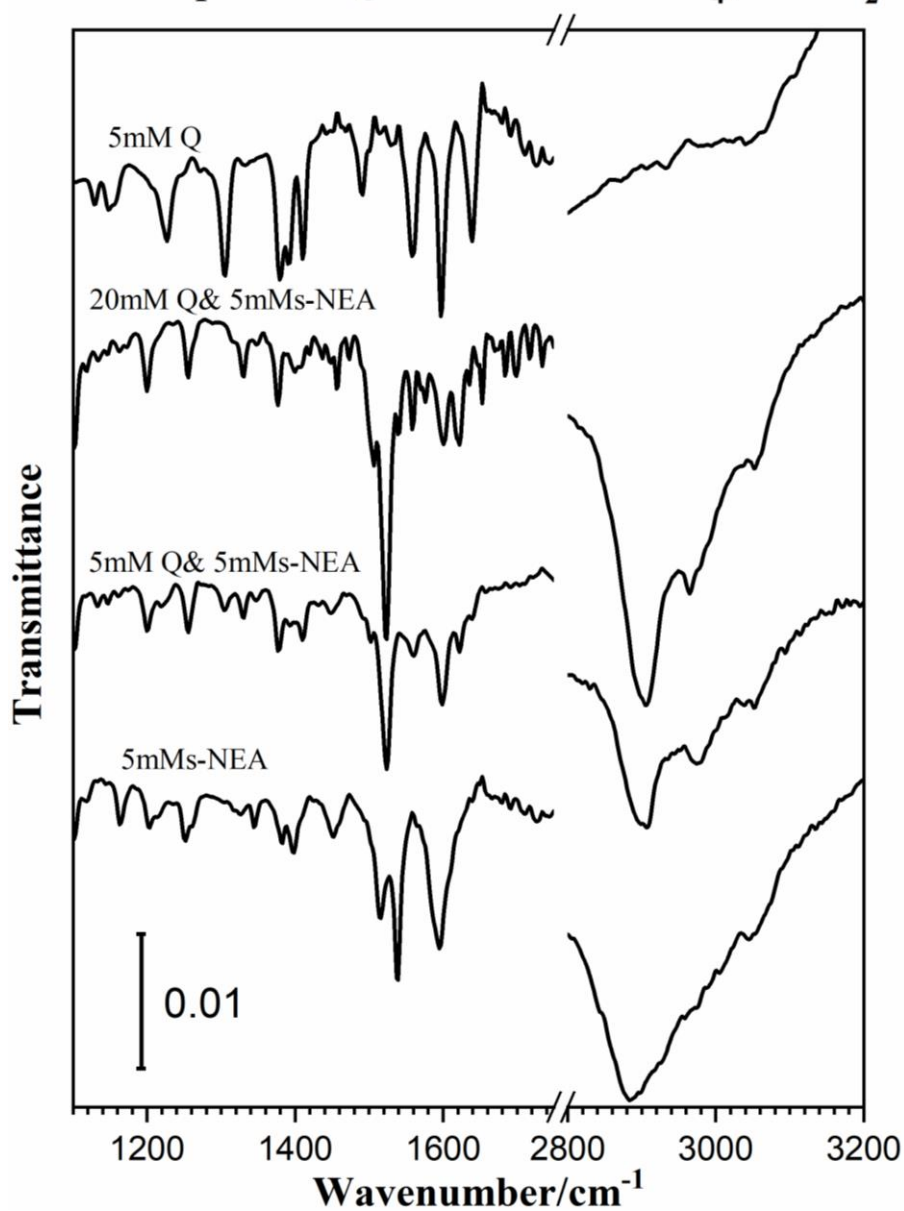
*Figure 3-12 Co-adsorption of NEA and Quinoline (Q) in CCl₄ on SiO₂ supported Pt nanoparticles. Four separate trails have been plotted as shown above (top to bottom): a) 5mM quinoline in CCl₄; b) solution containing 20 mM Q and 5mM s-NEA; c) 5mM Q and s-NEA; d) 5mM s-NEA only.*
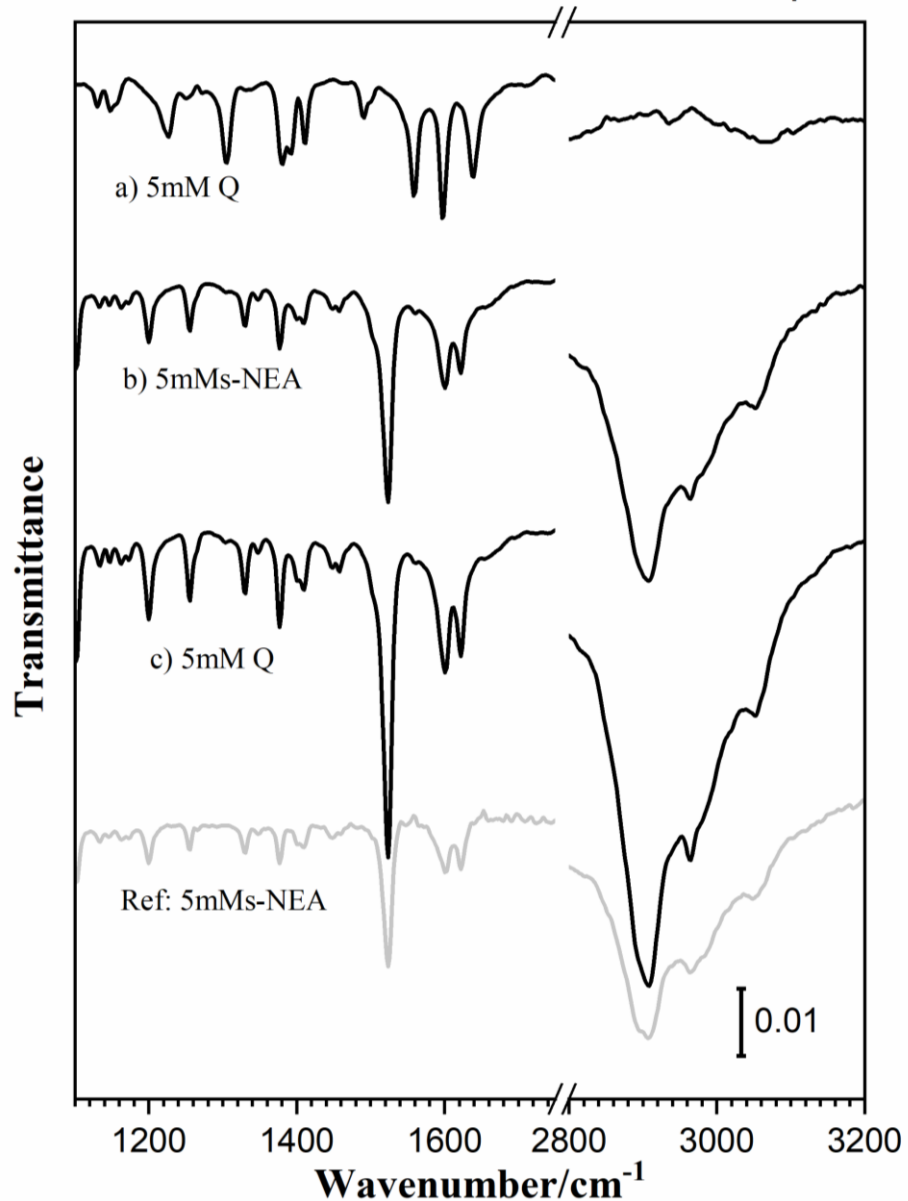
*Figure 3-13 Sequential flushing test of quinoline and NEA with the same concentration (5mM, in CCl₄) using Pt catalyst loaded on a different support: γ-Al₂O₃. Catalyst is first exposed to a) 5mM quinoline in CCl₄; then b) 5mM s-NEA, followed by another c) 5mM quinoline. ATR-IR spectrum of 5mM s-NEA is included at the bottom for reference.*

Co-adsorption of quinoline and s-NEA is closely examined with two set of experiment. First one, as seen in figure 3-12, is a solution that contains both compounds at the same time. When Pt/SiO$_2$ is exposed to an equal molar solution of NEA and quinoline, there are no signs of quinoline signature peaks. Further increasing the molarity of quinoline in CCl$_4$, which forms a 4:1 ratio of quinoline over s-NEA, quinoline uptake starts to take place but overall NEA is still the dominant species on Pt surface, unlike the case with Pt polycrystalline disk, where mixed solution of s-NEA and quinoline always end up with a full uptake of s-NEA even with the presence of a ten-fold excess of quinoline[29]. The absence of competitive adsorption on Pt disk is probably due to the surfeit of active site on the surface of Pt disk.

Upon further examination of co-adsorption of s-NEA and quinoline on Pt/SiO$_2$, quinoline uptake, with s-NEA being 4 times more concentrated, tells an interesting story with some complexities. To begin with, peaks at 1410, 1559 cm$^{-1}$, which represents in-plane deformation and stretching of quinoline ring, remains with excessive amount of s-NEA. At the same time, in-plane C-C stretching of s-NEA adsorbed on Pt/SiO$_2$, shown as two adjacent peaks at 1514 and 1539 cm$^{-1}$ merged into a single peak at 1524 cm$^{-1}$. All the changes in peak positions involve vibration modes of the ring structure itself. Quinoline cam still bond to Pt surface regardless of the concentration of s-NEA. What's more, interaction between s-NEA and Pt seems to become stronger with the help of quinoline on Pt surface. (discussed in chapter 4, comparison of s-NEA on Al$_2$O$_3$ and SiO$_2$ supported Pt).

Then it comes to the sequential flushing experiment. $Pt/Al_2O_3$ in ATR-IR cell is flushed with 5mM quinoline $CCl_4$ solution followed by s-NEA of same concentration. In the end, another quinoline flushing cycle is applied to see whether such process is reversible under comparable conditions.

As shown in figure 3-13, pre-adsorbed quinoline will be removed by s-NEA solution but not the other way around, which is another proof that NEA-Pt interaction is stronger than Q-Pt at solid/liquid interface. However, it's worth noting that competitive adsorption between quinoline and s-NEA does occur to some extent when the there is only a limited number of sites for adsorption on Pt surface.

Again, going back to the intensity difference in quinoline uptake when comparing RAIRS and ATR-IR data, besides the dissimilarity regarding instrumentation, the surface environment of Pt is another factor that needs to be considered. Pt disk in RAIRS experiments has far more active sites than supported Pt nanoparticles such as $Pt/SiO_2$ and $Pt/Al_2O_3$ could possibly have given their low Pt loading (both 1%), which, in turn, higher capacity for adsorption of NEA and Quinoline.

*3.2.3 Conclusion*

This section covers the adsorption of a series of NEA derivatives in $CCl_4$. Two types of commercial catalyst have been used: $Pt/SiO_2$ and $Pt/Al_2O_3$ and both are loaded with 1% Pt nanoparticles with no specific shape.

Among all naphthalene family derivatives, only those with amine and primary group show significant uptake when tested with Pt catalyst, which coincides with RAIRS data. DNE and EtN, neither of which bears primary group, are not able to adsorb on Pt. This could raise doubts about the proposal by other existing work that aromatic ring in NEA derivatives will contribute to the adsorption.

Co-adsorption tests data shows that NEA-Pt interaction is likely to be stronger than Quinoline-Pt, which is also an indication of different adsorption mechanism of these two molecules. In addition, considering the fact that Pt disk has more accessible sites to modifier molecules than supported Pt catalyst does, quinoline-Pt interaction is more sites specific compared to NEA derivatives. Thus, when there is only limited amount of Pt sites on surface, as with the case of Pt/Al$_2$O$_3$ and Pt/SiO$_2$, quinoline and s-NEA uptake are of similar intensity and the number of active sites is becoming the bottle neck. Details on the NEA adsorption geometry on Pt will be discussed in the following chapters.

# Chapter 4 Behavior of NEA and NMA on Pt surfaces in Various Chemical Environments

This section will focus on the discussion about s-NEA adsorbed on various Pt species: Pt/SiO$_2$ and Pt/Al$_2$O$_3$. In most reaction kinetics studies, alumina supported Pt catalyst are used as catalyst for asymmetric hydrogenation[61,62], yet, the performance difference caused by support is more or less ignored in many cases. Since the reactivity is heavily dependent on the modification process, which in other words, the adsorption of chiral modifiers on the surface of catalyst, it is of great importance to examine how the support of catalyst will affect the adsorption geometry directly or indirectly[63–66] because metal-support interaction can have significant impact on the metal and its catalytic performance as a whole[67].

What's more, due to the complicated nature of hydrogenation of C=O catalyzed by chirally modified catalyst, the interaction is not limited to modifier and Pt nano particles, but also involves the modifier, solvent, substrate, support and Pt all together. Thus in-situ FT-IR alone as a characterization tool alone will not be able to provide enough information about the process taking place during surface modification as well as hydrogenation.
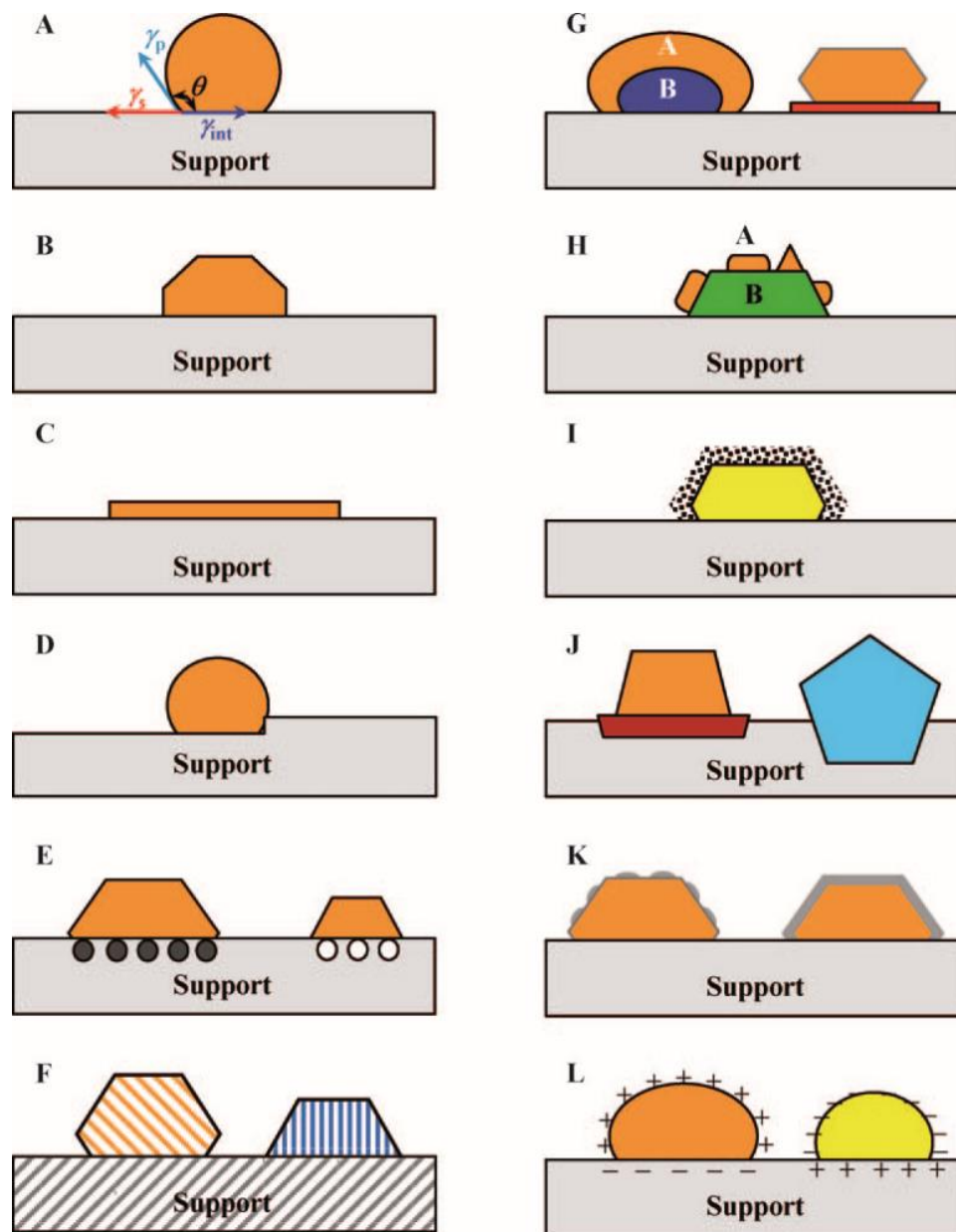
*Figure 4-1 schematic illustration of metal-support interactions. Most commercial catalysts belong to type A, B and C, which are weak, intermediate and strong metal-support interaction respectively, as shown in the figure. Adapted with permission from reference 67, Copyright © 2011 by John Wiley Sons, Inc.*

Different types of metal-support interactions are illustrated in figure 4-1 above. In general,

support in a catalyst can change both physical and chemical properties of metal particles

56

that are loaded on top of them such as dispersion, particle size and oxidation states of the metal. In this chapter, adsorption of modifier molecules on two types of commercial catalyst, $Pt/Al_2O_3$ and $Pt/SiO_2$ will be discussed in detail.

## 4.1 Adsorbed s-NEA on Platinum Surfaces

*4.1.1 Vibration Modes of Adsorbed S-NEA On Pt/SiO2, Pt/Al2O3—Details About IR Peak Assignment*

In last chapter, the pre-requisites for adsorption of surface modifiers on Pt surface has been summarized and at the same time, the structural dependence of these modifier has been discussed with two types of Pt powder catalyst. The results suggest that spectra of adsorbed modifiers can be quite different to those obtained using pure compound.
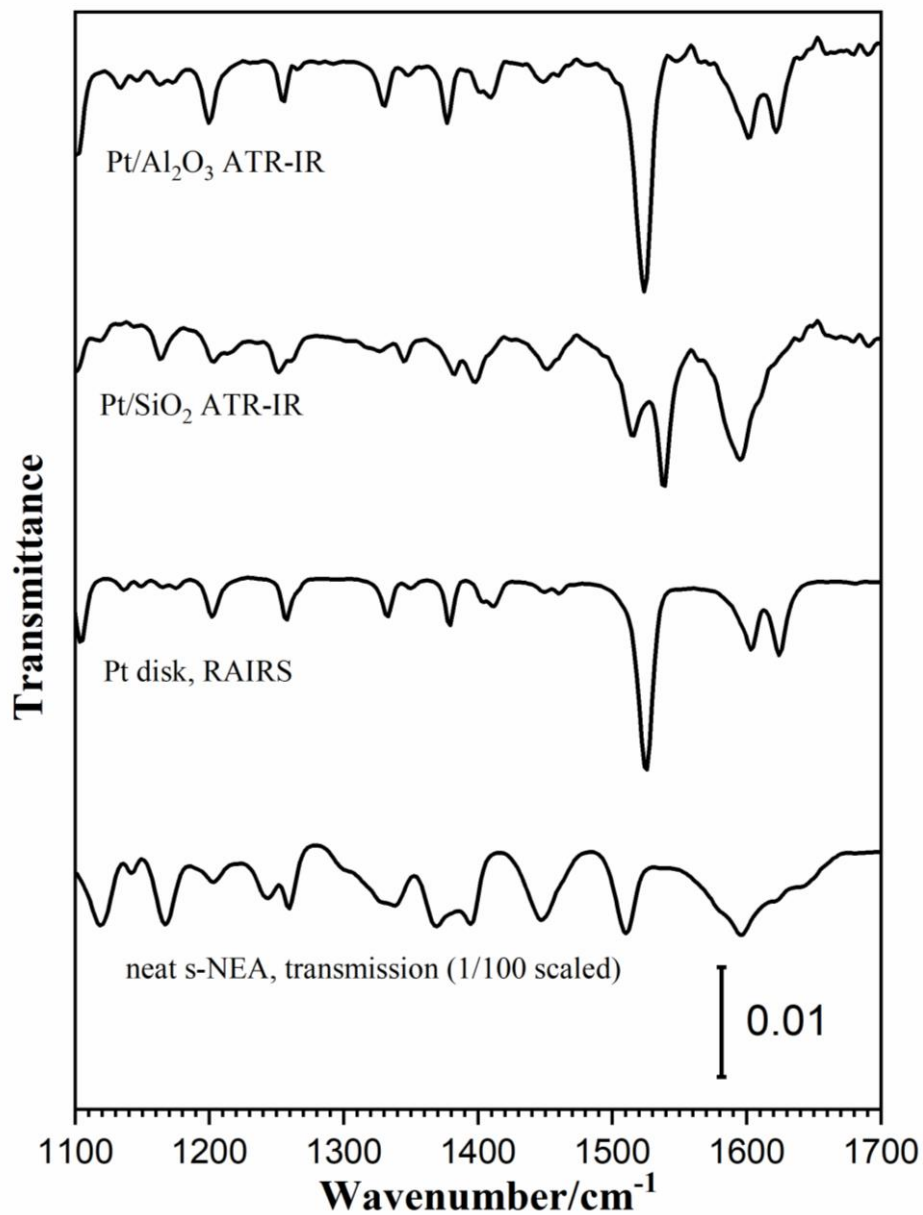
*Figure 4-2 1mM s-NEA adsorbed on various types of Pt surfaces in CCl₄ at room temperature*

To start with, transmission FT-IR spectrum of pure s-NEA (Figure 4-2, bottom trace, 1/100

scaled for better view) in liquid phase include all the possible vibration modes, which set

the baseline when identifying the IR peaks of adsorbed NEA and dissolved species. Due to

the interaction between NEA molecules with catalyst (Pt or support) as well as the effect of solvent, shift of certain peaks are expected accordingly. As a result, such shift of IR peaks can reveal a lot of information regarding the orientation of certain functional group of the modifier during adsorption.

Pt foil data is from a previous study by our group[29] (figure 4-2, $3^{rd}$ trace from top)where adsorption of s-NEA on Pt polycrystalline disk is examined with RAIRS technique. As discussed in previous section, Pt disk, by comparison, has far more active sites that are accessible for modifier molecules. In this case, modifier molecules will possibly display different vibration modes as a result.

*Table 4-1 Assignment of IR peaks for s-NEA species in different chemical environment as illustrated in figure 4-2. Adapted with permission from reference 67, Copyright © 2017 by John Wiley Sons, Inc.*

| mode | Pt/Al$_2$O$_3$ | Pt/SiO$_2$ | Pt foil RAIRS | Liquid |
|---|---|---|---|---|
| $\delta_{oop}(CH)_{ring}$ | 1101 | 1101 | 1103 | |
| $\delta_{ip}(CH)_{ring}$ | | 1119 | | 1119 |
| $\delta_{oop}(CH)_{ring}$ | | 1163 | | 1167 |
| $\delta_{ip}(CH)_{ring}$ | 1200 | 1203, 1217 | 1201 | 1204 |
| $\delta_{ip}(CH)_{ring}$ | 1256 | 1252, 1263 | 1257 | 1240, 1260 |
| $\delta(CH)_{amine}$ | 1331 | 1325, 1344 | 1333 | 1327, 1339 |
| $\delta_{sym}(CH_3)_{amine}$ | 1377 | 1381 | 1379 | 1367 |
| $\nu_{ip}(CC)_{ring,sym}$ | 1400, 1408 | 1398 | 1401, 1412 | 1395 |
| $\delta_{asym}(CH_3)_{amine}$ | 1447, 1458 | 1450, 1461 | 1448, 1460 | 1445 |
| $\nu_{ip}(CC)_{ring}$ | 1524 | 1514, 1539 | 1526 | 1510 |
| $\nu_{ip}(CC)_{ring,sym}$ | 1601,1622 | 1595, 1610 | 1602,1624 | 1595 |

Firstly, the dominant peak of NEA comes in at around 1500 cm$^{-1}$, which represents the in-plane deformation of naphthalene ring along the long molecular axis. Respectively, the

corresponding in-plane deformation along the short axis can be identified at around 1600 $cm^{-1}$. Meanwhile, the relative intensities of these peaks are weaker for $Pt/Al_2O_3$ and platinum foil/disk if compared with those from pure s-NEA, which indicates that vibration of NEA molecules along the long axis is less favored on Pt surface. Interestingly, the behavior of NEA on $SiO_2$-supported platinum resembles that of liquid NEA rather than NEA adsorbed on Pt disk or $Pt/Al_2O_3$. What's more, slight blue shifts have been observed for both NEA on $Pt/Al_2O_3$ and Pt disk possibly due to the interaction with metal or solvent. Again, NEA on $Pt/SiO_2$ stands closer to liquid s-NEA instead of the other two Pt species. However, in addition to the signature peak for long-axis in-plane deformation$^{-1}$, $Pt/SiO_2$ shows an additional peak at 1539 $cm^{-1}$.

Secondly, C-H asymmetric deformation of methyl group of ethylamine moiety, which can be found within 1445-1460 $cm^{-1}$, is less relatively less strong than the corresponding mode. More importantly, the peak at 1330 $cm^{-1}$ representing deformation of C-H bond adjacent to the amine group is clearly visible in the spectra recorded with adsorbed species. This region is mostly related to the vibrations within the ethyl group. Peaks within this region also show the greatest differences in terms of peak position between species adsorbed on Pt surfaces and the less disturbed neat NEA.

*4.1.2 Adsorption Geometry of s-NEA on various Pt surfaces*

Based on the vibration modes inferred from ATR-IR data, the adsorption of NEA on Pt on a surfaces is in close agreement with a model that when adsorbing on a surface from liquid

or solution phase, NEA molecules tend to bond to the metal surface through the nitrogen group atom of the primary amine moiety and all the substituents, including naphthyl and methyl group connected to the neighbor chiral carbon, pointing away from the adsorption interface.

It's also likely that the adsorption of NEA on Pt catalyst requires breaking one of the N-H bond of amine group, which also help to explain why s-DNE shows a minimal uptake, probably due to a lack of hydrogen in its tertiary amine moiety. Such dissociative adsorption might also be the reason for the observation that some of the IR peaks representing deformation mode of the C-H bonds in the naphthalene ring are seen at lower wavenumbers. Dehydrogenation of amine group is also viable according to published IR data under UHV conditions[68] regarding thermal decomposition of N-methylaniline on Pt (111) face where they've reported that when amine group undergoes dehydrogenation process, the strong peak for the ring deformation mode shifts toward higher frequencies.

To further examine the possibility, other characterization methods are necessary to identify the dehydrogenation products of the surface modifier. H-D exchange test with NMR spectroscopy can be a feasible option. However, considering the fast and reversible H-D exchange of the hydrogen in primary amine group, it can be extremely challenging to separate and capture the dehydrogenation product from the reaction mixture containing modifier and excessive amount of reactant. Recent data on this part will be discussed later at the end of the dissertation (chapter 7).

Meanwhile, there are still many different voices when it comes to the adsorption process of NEA modifiers on metal surfaces. Baiker and co-workers[26,69,70] have performed series ATR-IR experiment under operando reaction setup[71]. However, hydrogenation reactions prefer solvents with higher polarity than $CCl_4$, which is a common solvent for IR studies because of its low IR uptake. They suggest a different adsorption geometry for NEA because they observed peak broadening of the vibration modes representing naphthyl group, which they then attribute to the interaction between aromatic ring and Pt surface. Yet, ATR-IR, unlike RAIRS with polarized IR beam, is not intrinsically a surface sensitive despite that evanescent wave can minimize the interference from solution phase above the catalyst film loaded onto the ATR crystal. As a result, these broadening could possibly come from dissolved NEA rather than adsorbed modifier species on Pt surface. Additionally, because NEA is more soluble in toluene than in $CCl_4$, it's harder to establish an equilibrium that favors adsorbed molecules more. So, observing steadily anchored NEA on Pt in toluene can be trickier and might need extra care than tests performed in $CCl_4$. Solvent effects on adsorption will be discussed in following section.

McBreen[57] and co-workers also come up with a proposal that NEA adsorption is a combination of naphthyl-Pt interaction and dative bonding between nitrogen of amine group and platinum. They combined high resolution STM and DFT theoretical[72] methods to explore the behavior of NEA molecules on the surface of platinum single crystal. They are also able to use time-lapsed scanning tunneling microscopy (STM) to identify two

modes of transformation between stereochemical states and prochiral compounds can take several complexation geometries during the life time of a complex.

The contracting results of McBreen's study and this work is possibly caused by the fact that they were using Pt under UHV conditions and behavior of NEA under UHV varies significantly from in-solvent counterpart. Typically, molecules in UHV environment is least disturbed compared to those in liquid phase due to extra interaction with solvent.
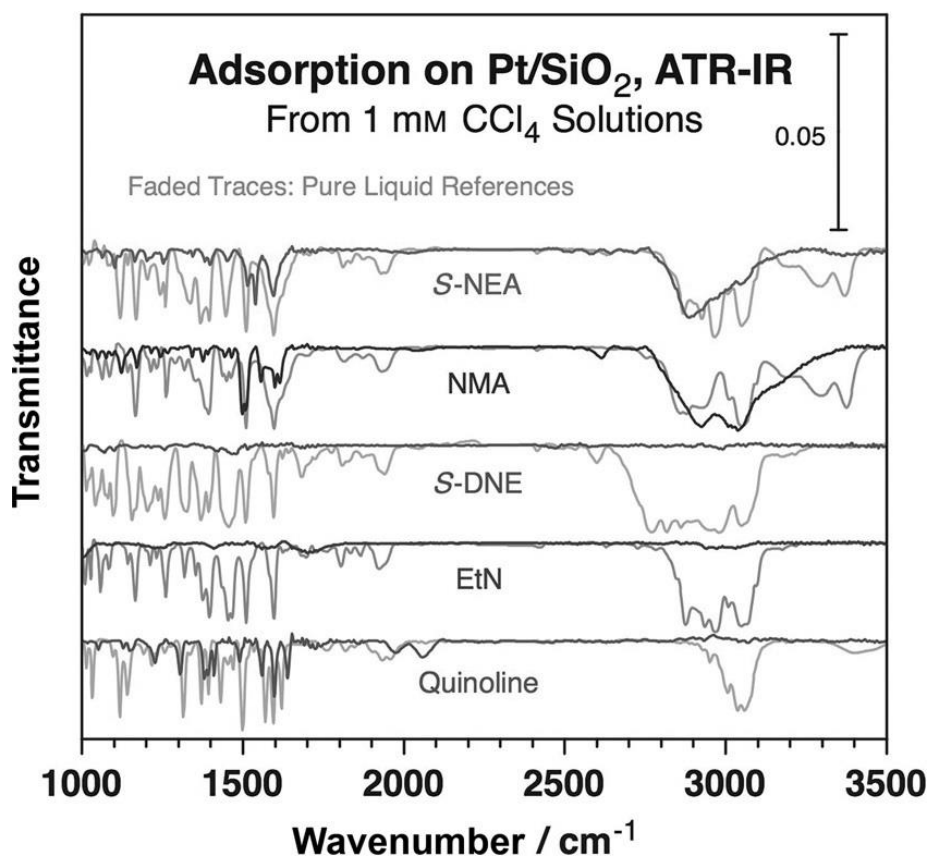


*Figure 4-3 ATR-IR absorption spectra for selected modifiers adsorbed from 1 mm CCl4 solutions onto a commercial 1 wt.% Pt/SiO₂ catalyst. The spectra of the pure compounds are provided as faded lines for reference.*

Besides s-NEA, the behavior of other molecules when adsorbed on Pt surfaces is dramatically different from free molecules of pure compounds. As is suggested by the comparison in figure 4-3 above, the change of vibration modes is reflected by shift of corresponding signature peaks.

### 4.2 NMA adsorbed on various Pt surfaces

Naphthyl methylamine (NMA) is another compound that shows significant uptake in adsorption experiments using Pt powder catalysts and polycrystalline disk. It's the methyl group connected to the carbon adjacent to $NH_2$ that sets these two compounds apart. Such difference is expected to show up in corresponding IR spectra.

## NMA in CCl$_4$, various Pt surfaces
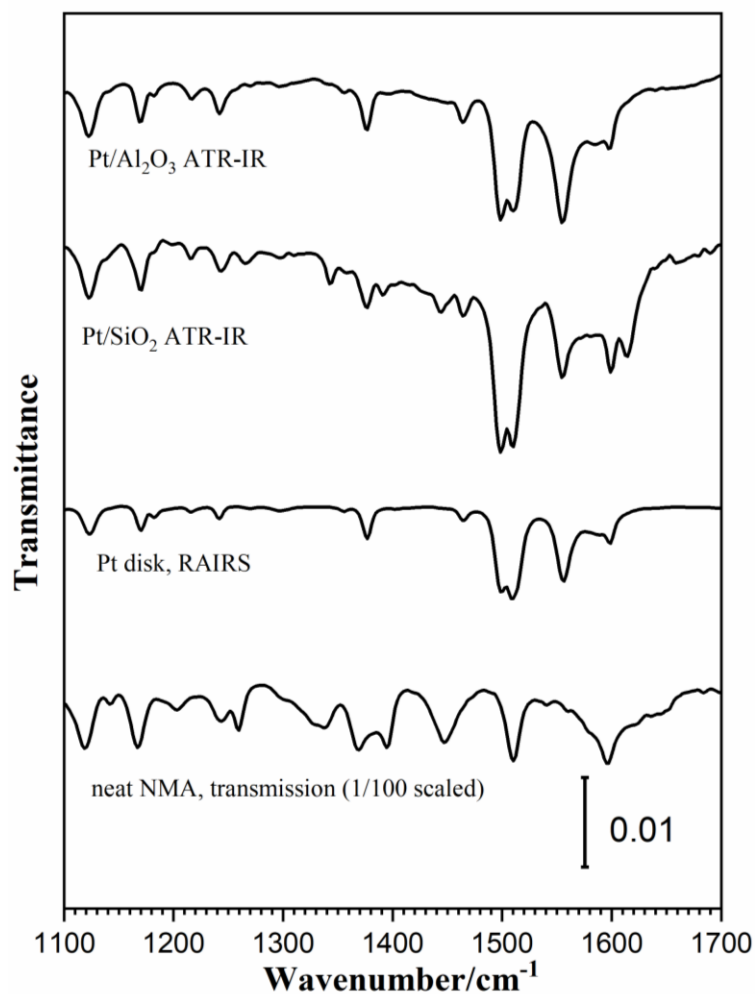


*Figure 4-4 1mM NMA adsorbed on various types of Pt surfaces in CCl$_4$ at room temperature.*

*Table 4-2 Assignment of ATR-IR peaks for NMA under different conditions.*

| mode | Pt/Al$_2$O$_3$ | Pt/SiO$_2$ | Pt foil RAIRS | Liquid |
|---|---|---|---|---|
| $\delta_{ip}$(CH)$_{ring}$ | 1122 | 1122 | 1122 | 1118 |
| $\delta_{oop}$(CH)$_{ring}$ | 1168, 1181 | 1170, 1182 | 1170,1182 | 1167 |
| $\delta_{ip}$(CH)$_{ring}$ | 1217 | 1215 | 1215 | 1203 |
| $\delta_{ip}$(CH)$_{ring}$ | 1242 | 1244,1265 | 1240 | 1244, 1259 |
| $\delta$(CH)$_{amine}$ | | 1342 | | 1327, 1339 |
| $\delta_{sym}$(CH$_3$)$_{amine}$ | 1377 | 1377 | | 1369 |

| $\nu_{ip}(CC)_{ring,sym}$ | | 1390 | | 1394 |
|---|---|---|---|---|
| $\delta_{asym}(CH_2)$ | 1463 | 1444, 1463 | 1464 | 1447 |
| $\nu_{ip}(CC)_{ring}$ | 1497, 1510 | 1498, 1510 | 1498, 1508 | 1510 |
| $\nu_{ip}(CC)_{ring}$ | 1555 | 1554 | 1556 | 1539 |
| $\nu_{ip}(CC)_{ring,sym}$ | 1599 | 1598,1614 | 1599 | 1597 |

Just like the case with s-NEA, NMA adsorbed on various platinum (figure 4-4) surfaces shows largely different vibration modes, which can be reflected clearly by their IR uptake.

To start with, since there is no methyl in the amine moiety of NMA, unlike NEA, as a result, the corresponding IR peaks within 1445-1460 $cm^{-1}$ do change slightly compared to those for NEA. What's more, the split of these peaks in solution phase observed with NEA is also detected here using NMA $CCl_4$ solution with an additional peak seen at a higher wave number, around 1460 $cm^{-1}$. Pure liquid (figure 4-4, bottom trace) only features a single peak at 1447 $cm^{-1}$ while this peak will shift toward the higher frequency end at 1464 $cm^{-1}$ for $Pt/Al_2O_3$ (figure 4-4, 1st trace on top) and Pt polycrystalline disk (figure 4-4, 2nd from bottom). On the other hand, silica supported platinum incorporates both peaks at 1444 and 1463 $cm^{-1}$ respectively. Typically, optical spectroscopy including FT-IR can be used to investigate[73,74] the energy/state distribution of certain compounds under appropriate experimental conditions. The transition as described above from 1447 to 1463 $cm^{-1}$, namely from NMA pure compound, to silica supported Pt nano particles then all the way to platinum on alumina and platinum polycrystalline foil. Similar transition can be found in the in-plane C-C stretching modes of NEA in the range of 1510 to 1540 $cm^{-1}$ as well as the 1595 to 1610 $cm^{-1}$.

## 4.3 Conclusion

ATR-IR results in this section reveal more details on the adsorption geometry of NEA derivatives on series of different Pt surfaces. These data also provide solid evidence for an adsorption geometry that is to some extent, in contrast to some proposed adsorption mechanism. This work indicates an adsorption process that involves the nitrogen of the primary amine group as a possible center and no evidence of contribution from the aromatic ring moiety is found in the ATR-IR tests reported in this work.

A key step taking place during adsorption of NEA modifiers is also suggested, which is the dehydrogenation of primary amine on platinum surface. This can help explain why molecules with tertiary amine (EtN) does not shown significant uptake in adsorption experiment.

Though platinum itself plays an important role and there are many other factors that need to take into account such as the facet exposed (single crystal Pt) or the particle size and specific shape (Pt nano particles), when it comes to Pt catalysts, which are widely used in actual hydrogenation reaction, support is not necessarily just a spectator or a framework that only helps better disperse platinum particles for better catalytic efficiency.

As is shown in ATR-IR experiments, the support does change the interaction between NEA derivatives and platinum surface. Overall, some of the vibration modes representing amine and ring structure shows clear transition when tested with different Pt surfaces. Corresponding signature peaks will shift towards the direction with higher frequency if going from pure modifier to $Pt/SiO_2$, then $Pt/Al_2O_3$ and Platinum polycrystalline disk. Pure compound and Pt foil sit on the two ends of the scale. Pure compound shows the behavior of least disturbed molecules with minimal to no interaction with solid surfaces. To the contrary, platinum polycrystalline disk features the highest number of active sites which, in other terms, shows the strongest interaction between modifier and metal.

The two commercial powder platinum catalysts—$Pt/SiO_2$ and $Pt/Al_2O_3$, although they are both loaded with 1% wt. of spherical platinum nano particles with no specific shape or facet exposed, the strength of modifier-metal interaction observed with these two catalysts is not even close. $Pt/Al_2O_3$ shares more in common with platinum polycrystalline disk while the silica supported catalyst is more of a 'transition' in between liquid and Pt foil. This might indicate a weaker adsorption on the surface of $Pt/SiO_2$ compared to the other two types of platinum species.

The origin of the different property of two supports is still not clear based on current data. This work can provide some preliminary data for future research where synthesized catalysts can be used instead of commercial ones to have better control over the support because the oxide support in commercial catalysts may vary from batch to batch and this

can be a problem to compare the property of support before and after Pt loading. Future exploration of the support effect can start with the following aspect:

1. Acidity of the support[75,76]. The acidity of support is likely to change the metal-support interaction and thus, the adsorption of modifiers. In most studies, no matter what type of modifier is being studied, $Pt/Al_2O_3$ seems to be the preferred option in most cases. The observation in this section may help explain such preference when it comes to the choice of support.

2. Physisorption of the support. Because ATR-IR is not a surface sensitive IR technique, it cannot eliminate the contribution of physical adsorbed molecules on solid surfaces, especially on the support. Though in this work, we find out the contribution from support is negligible. Again, the tests are carried out using commercial oxides samples without Pt loading, which may not reflect the exact properties of the support used when manufacturing the commercial Pt catalyst.

3. The correlation of solvent effect and support effect. Both impact on adsorption of modifiers and acidity again, is a key factor for both solvent and support selection.

# Chapter 5  Effect of Modifier Concentration and Solvent

## 5.1 Introduction

Adsorption of NEA or any other molecules, in most cases, is coverage sensitive. It's been discovered in the past that adsorption geometry of cinchona alkaloids will change from 'flat on surface' to a 'tilted mode'. In solution phase, coverage is directed related to concentration and solubility in specific solvent, which will have effects on the equilibrium between adsorbed/dissolved modifier molecules. In this chapter, 1% $Pt/Al_2O_3$ is used as a model catalyst to further explore the external factors—concentration and choice of solvent.

Solvent has a critical impact on the adsorption process occurring on the platinum surface as well as the hydrogenation reaction. To optimize the surface modification in order to improve the selectivity, special attention is a pre-requisite when choosing the right solvent, which doesn't necessarily translate into which specific solvent is all-around the best. Each modifier and reactant pair may have their most suitable solvent for best reaction performance.

The reason is straight forward—the solvent used in asymmetric synthesis is involved in two major equilibriums, one of which is the adsorption-desorption of reactant or substrate on the surface. The other one is a similar equilibrium that forms a reaction complex that consists of reactant and modifier on platinum surface.

This section will start with NEA adsorbed on $Pt/Al_2O_3$ in $CCl_4$. Pt powder catalyst will be exposed to NEA $CCl_4$ solutions of various concentration to investigate the concentration effect on adsorption geometry. This can be used to simulate the case where NEA is dissolved in a solvent in which it has different solubility and thus, the surface coverage of NEA might vary accordingly.

From there, solvent experiments will be conducted in two ways. The first one is exposing $Al_2O_3$ supported Pt catalyst to NEA dissolved in different solvent. Toluene and ethanol have been tested because they show best performance in hydrogenation reactions[14]. However, the problem with polar solvents in IR experiment is their relatively high IR absorption which will usually end up with strong solvent peaks that can override the weak signals of adsorbed modifiers.

There is another work-around to test the solvent effect on adsorption of modifiers. Pt is first exposed to modifier in $CCl_4$ and then the ATR-IR cell is flushed with other solvent trying to wash away adsorbed species. And then the cell is filled with $CCl_4$ again to avoid large amount of polar solvent left.

## 5.2 Results and Discussion

### 5.2.1 Concentration of Modifier

The studies of adsorption geometry of cinchonidine on Pt have proposed a concentration dependent route where under low coverage, the quinoline ring of cinchonidine is parallel to metal surface and the entire molecule is flat. When concentration increases, there's not enough space to accommodate cinchonidine molecules anymore and as a result, the molecules will become tilted forming a certain angel with the metal surface[16,77,78].

In last section, it has been suggested that NEA derivatives are likely to adsorb on Pt surface via Pt-N interaction instead of platinum and aromatic ring. The model for cinchonidine may not fit NEA due to their different interaction with metal surface considering the fact that naphthyl group is pointing away from the surface, not parallel anchored as cinchonidine at lower concentration.
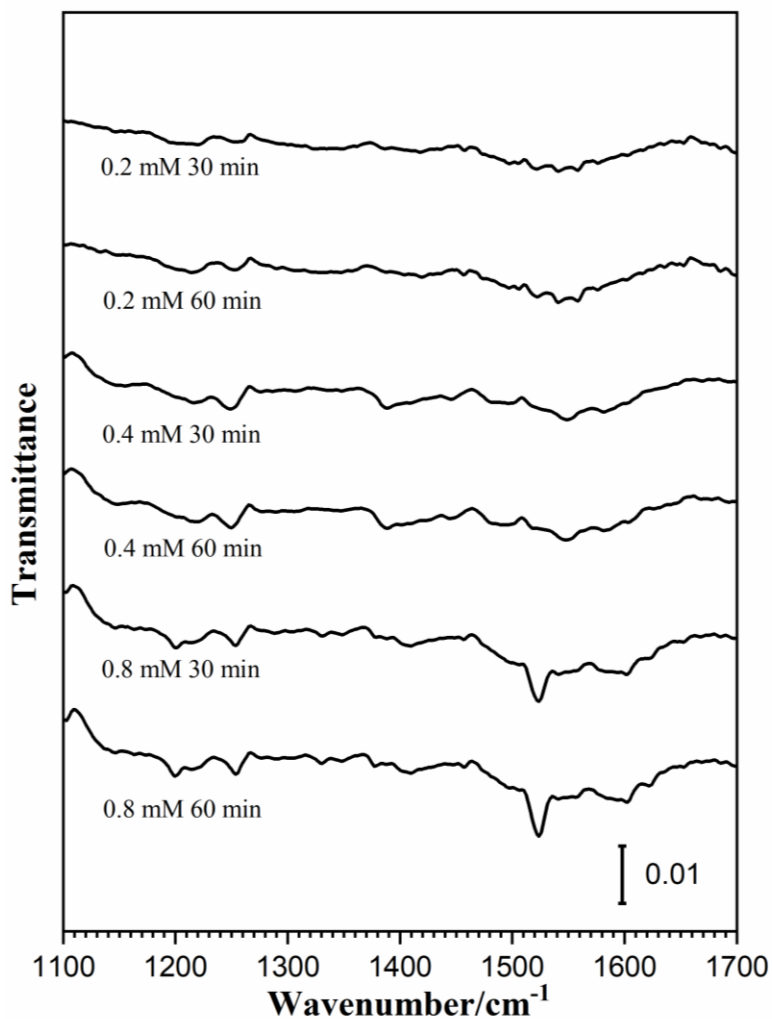
*Figure 5-1  ATR-IR spectra of 1% Pt/Al₂O₃ exposed to s-NEA CCl₄ solution of various concentration.*

Figure 5-1 shows the concentration dependence of adsorption geometry of NEA in CCl4, starting from 0.2 mM (1st and 2nd trace on top) and increased up to 0.8 mM (last two traces on the bottom of figure 5-1). 1% Pt/Al₂O₃ is exposed to each concentration for 60 minutes until  adsorption reaches equilibrium or saturation.

Table 5-1 Peak assignment of ATR-IR spectra of 0.2mM, 0.4mM and 0.8mM s-NEA, 1% Pt/Al₂O₃ in CCl₄. Adsorption is already at equilibrium in the first 30 minutes of exposure. Peak is picked combining both 30-minute and 60-minute spectra in order to better identify the weak peak representing adsorbed species.

| mode | 0.2mM | 0.4mM | 0.8mM | 1mM(ref) |
|---|---|---|---|---|
| $\delta_{oop}(CH)_{ring}$ | | | | 1101 |
| $\delta_{ip}(CH)_{ring}$ | | | | |
| $\delta_{oop}(CH)_{ring}$ | | | | |
| $\delta_{ip}(CH)_{ring}$ | 1216 | 1216 | 1200 | 1200 |
| $\delta_{ip}(CH)_{ring}$ | 1252-1254 | 1254 | 1256 | 1256 |
| $\delta(CH)_{amine}$ | | | 1330 | 1331 |
| $\delta_{sym}(CH_3)_{amine}$ | | 1386 | 1378 | 1377 |
| $\nu_{ip}(CC)_{ring,sym}$ | | | 1400,1407 | 1400, 1408 |
| $\delta_{asym}(CH_3)_{amine}$ | 1458 | 1447 | 1447, 1458 | 1447, 1458 |
| $\nu_{ip}(CC)_{ring}$ | | | 1523 | 1524 |
| $\nu_{ip}(CC)_{ring,sym}$ | | 1604 | 1601,1622 | 1601,1622 |

As mentioned in previous sections, ATR-IR can minimize interference from solution phase but it's not a surface sensitive characterization method. In this case, some of the peaks may not come from adsorbed species on metal surface. They could be molecules physically adsorbed on metal or support and impurities in solvent can also add some difficulties for identifying the peaks for modifier molecules.

The best solution to this problem is compare the ATR-IR spectra with existing transmission IR and RAIRS spectra to locate where these signature peaks should be. In addition, the peaks of adsorbates are usually stronger than weakly adsorbed impurities, so it's not usually an issue to distinguish them. However, when the concentration goes lower, some of the signal/noise level might become lower as well, as seen in the 0.2 and 0.4 mM NEA traces in figure 5-1. Some of the peaks from these traces are hard to assign with confidence.

But there is still useful information out of the low-concentrations s-NEA experiments. Two vibration modes of adsorbed s-NEA have been highlighted in table 5-1, which are the most distinguishable peaks across all concentrations.

First of all, the peak near 1200~1220 cm$^{-1}$, which is form in-plane deformation of the C-H bonds of aromatic ring, shows up at a higher frequency in the spectra representing the two experiments with lower concentration of s-NEA solutions at around 1216 cm$^{-1}$. By comparison, the same vibration mode of pure s-NEA can be found at 1203 cm$^{-1}$ and Pt/SiO$_2$ has a split peak at exactly 1217 cm$^{-1}$. Nonetheless, the 1216 peak found in spectra for 0.2 and 0.4 mM s-NEA is a rather broad weak peak ranging from 1203 to 1216 cm$^{-1}$. Peak broadening is often related to the change taking place in adsorption layer[79] and the width of peaks or full width at half maximum (FWHM) can represent the degree of conformation of vibration modes. To sum up, the deformation of naphthyl moiety of less concentrated s-NEA in CCl$_4$ is resembles the free NEA molecules in liquid phase when compared with NEA solution of 1mM or higher concentrations. This observation suggests that as concentration increases, the in-plane deformation of aromatic ring is affected the most. These findings provide further evidence for the proposed adsorption model that s-NEA and derivatives are bonded to Pt surface through the nitrogen atom rather than the ring structure as cinchona alkaloids modifiers.

The transition of s-NEA from 'pure compound-like' to 'fully adsorbed' is nearly finished at 0.8 mM though the asymmetric deformation of $CH_3$ at 1447 $cm^{-1}$ is still a broad weak peak. Spectra for 0.2 mM s-NEA are missing most of the deformation of C-H on the ring. However, the absence of certain peaks doesn't necessarily lead to any conclusion regarding the adsorption geometry since some of the vibration modes might be relatively weak and thus not visible at lower concentrations. In other words, the more decisive factor is the position of a given peak, which is directed related to the Pt-modifier interaction. It's worth noting that the missing peaks are not always due to forbidden vibration modes on the surface and it can be caused by low concentration and other interference too.

Yet, the peak for in-plane C-C stretch is the strongest peak in 1100-1700 $cm^{-1}$ range, it does not show up until the concentration reaches 0.8 mM, which is considerable late. Between 0.4 mM and 0.8 mM. there is a dramatic change in intensity at this frequency, which possibly suggests the in-plane C-C stretching of the aromatic ring is hindered when the s-NEA concentration is low. This discovery is a complement to our model for s-NEA adsorption—it's likely that aromatic ring of s-NEA might participate in the adsorption process, but only when the surface coverage is low enough.

**2mM s-NEA in CCl$_4$, Pt/Al$_2$O$_3$**

0min

20 min

40 min

60 min

100 min

CCl$_4$ 0 min

CCl$_4$ 20 min

0.01

**Transmittance**

**Wavenumber/cm$^{-1}$**

1100 1200 1300 1400 1500 1600 1700
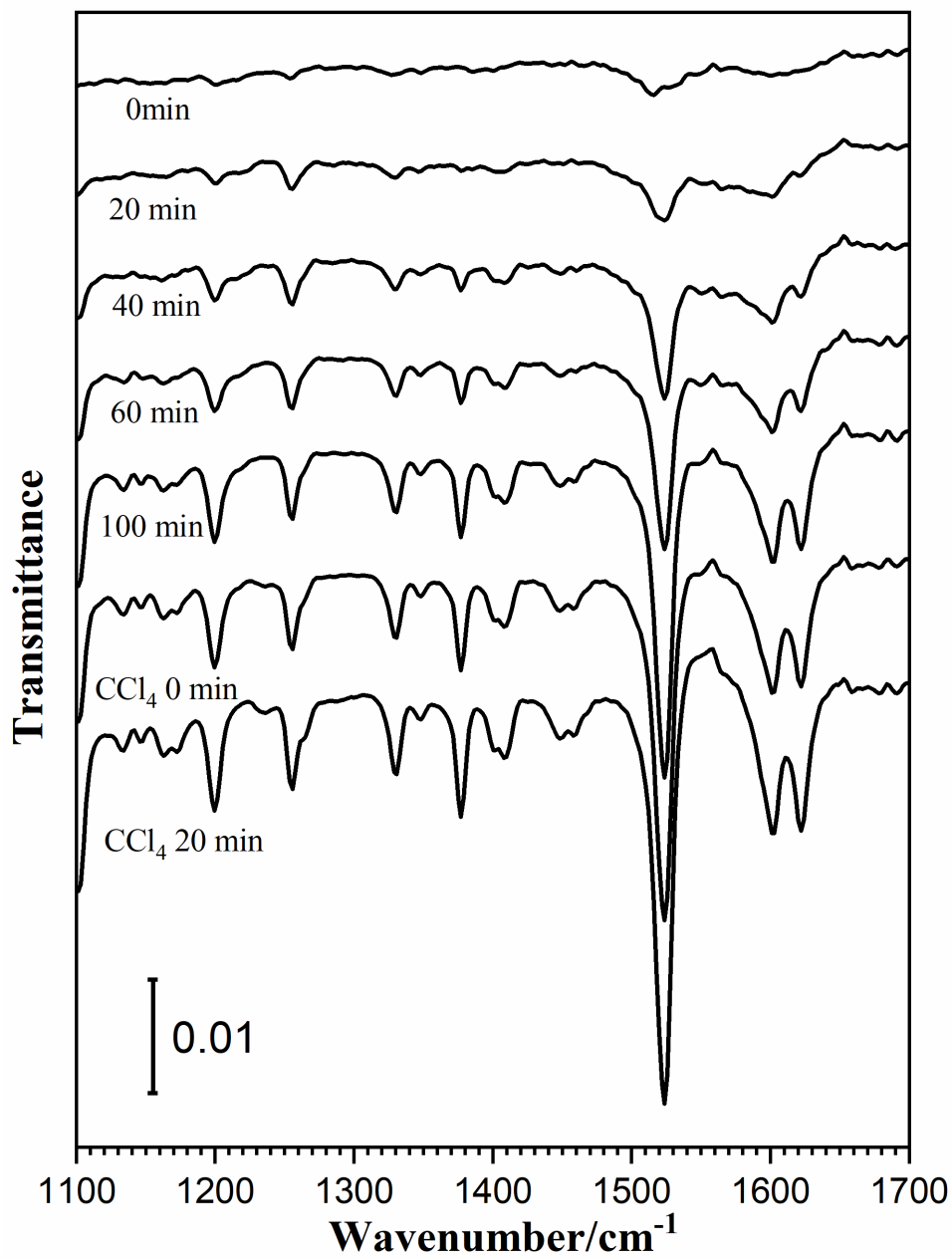
*Figure 5-2 CCl$_4$ flushing experiment of s-NEA adsorbed on Pt/Al$_2$O$_3$ using ATR-IR setup is shown above. Commercial platinum catalyst is exposed to s-NEA in at a higher concentration (2mM) to have a clearer view of solvent flushing.*

*5.2.2 Solvent Effect*

Tests on solvent effect start with dissolving s-NEA in different solvents. First up is the original $CCl_4$ solvent. Pt surface is exposed to 2mM s-NEA $CCl_4$ solution (figure 5-2) that is more concentrated than the one typically used for adsorption tests (1mM).

Ideally, solvent flushing is expected to remove adsorbates from surface or at least shift the adsorption equilibrium between solution phase and solid surface to the direction that favors desorption of modifier since there will be a much lower amount of modifier molecules after solvent flushing.

Quite to the contrary, results as shown in figure 5-2 is clearly telling a different story. First of all, it does take more time to reach adsorption equilibrium for more concentrated s-NEA solution, which is about 60 to 100 minutes. Especially compared to 0.2-0.4 mM solution, which has already become saturated in first 30 minutes of exposure.

The bottom two traces in figure 5-2 present the ATR-IR spectra of $CCl_4$ flushing following 2mM s-NEA adsorption experiment. It can be clearly seen that fresh solvent flushing does not remove adsorbed s-NEA form surface at all, which is possibly because of the s-NEA itself is not quite soluble in $CCl_4$ and thus, Pt-NEA interaction wins the competition against modifier-solvent in this case.
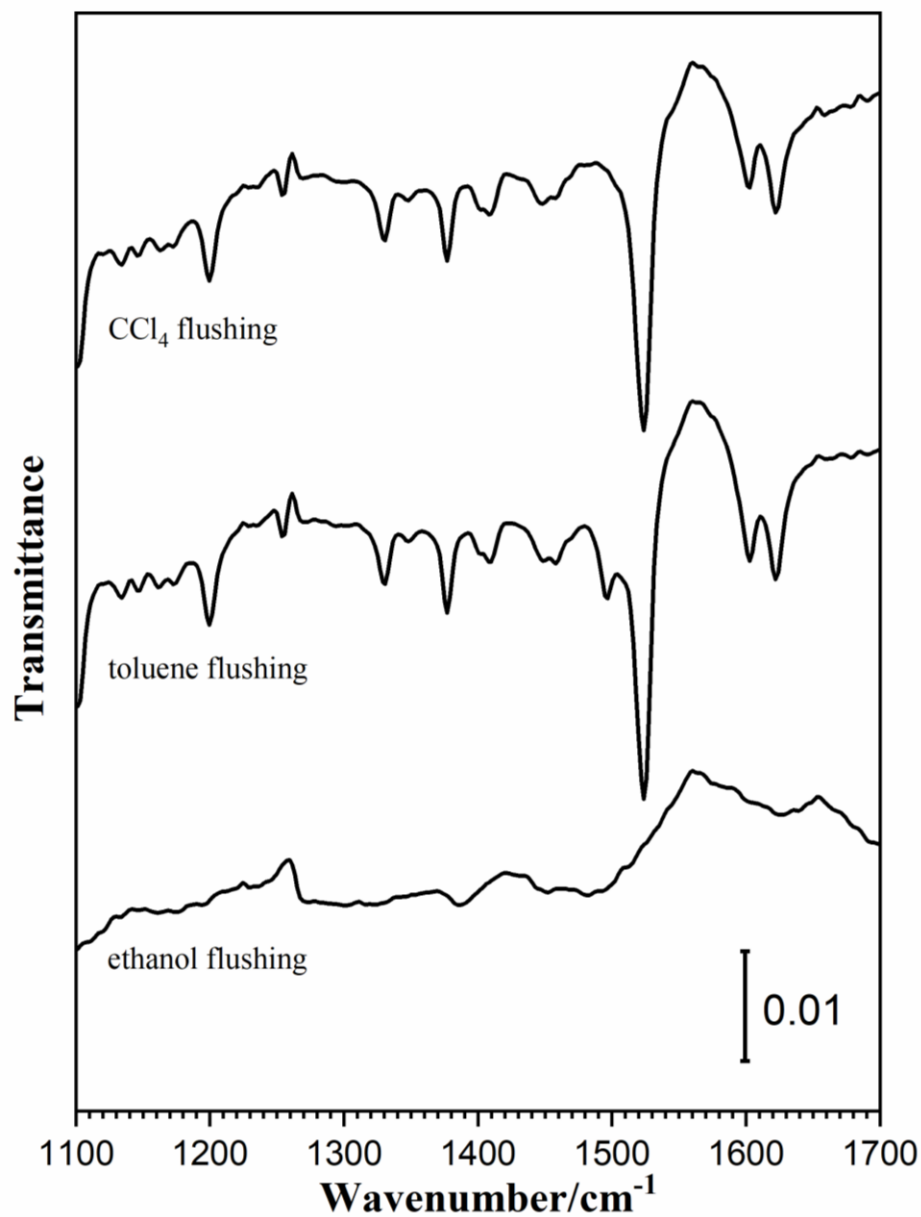
*Figure 5-3 Solvent flushing tests using CCl₄ (top), toluene (middle) and ethanol (bottom). 1% Pt is exposed to a 5mM s-NEA CCl₄ solution first and then flushed by a specific solvent. Then the catalyst sample is flushed with CCl₄ again to remove the previous solvent.*

Figure 5-3 shows the results of solvent flushing experiment of s-NEA with Pt/Al$_2$O$_3$. Since the background spectrum is taken with CCl$_4$, so the ATR-IR cell needs to be flushed with CCl$_4$ again to remove the residue of previous solvent (toluene or ethanol) so that they won't show up in the final spectrum. Still, because of the strong interference of hydroxyl group of ethanol, the spectrum for ethanol flushing test has the worst baseline or signal to noise level among the three solvents.

The measurement of solubility of s-NEA, a liquid compound, requires special equipment but based on a previous published study[20] by our group regarding the role of solvent in the adsorption-desorption of cinchona alkaloids modifiers, in general, it should comply with the 'like dissolves like' principle. Considering the polar nature of s-NEA, the solubility will follow the increasing order of CCl$_4$, toluene, ethanol.

As a result, higher solubility usually is the result of strong solute-solvent interaction[80]. In theory, s-NEA will form stronger solvent-modifier interaction in ethanol than in the other two solvents. It can be clearly seen in figure 5-3 that only ethanol can remove s-NEA molecules that are already bonded to Pt surface while toluene cannot.

Last but not the least, conclusions drawn in this section are all based on the presumption that CCl$_4$ will not wash away anything from the surface otherwise we can't tell that it's either CCl$_4$ used in the back-flushing or the actual solvent is doing the job. And this presumption has already been verified in figure 5-2.

**5mM s-NEA in selected solvent, Pt/Al$_2$O$_3$**

5mM s-NEA CCl$_4$ (1/5 Scaled)

5mM s-NEA toluene

0.01

Transmittance

Wavenumber/cm$^{-1}$
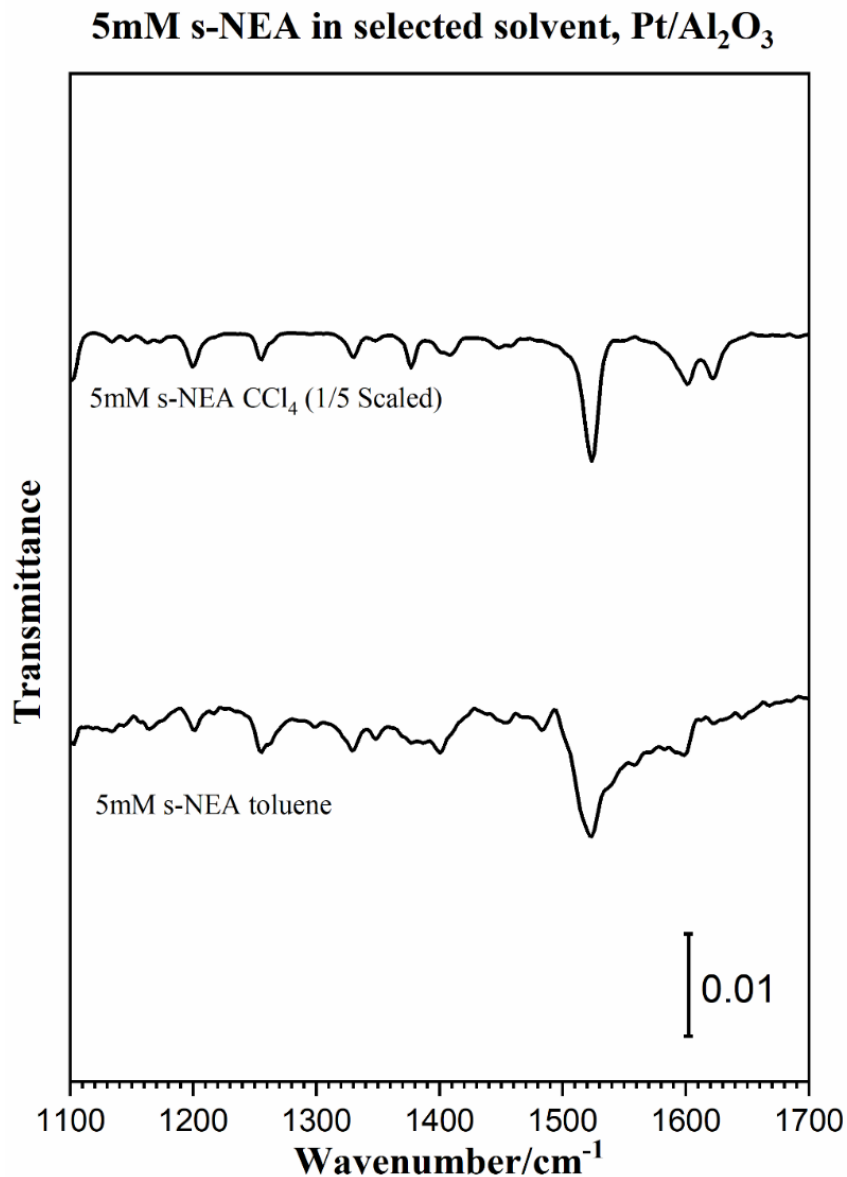
*Figure 5-4 A comparison of ATR-IR spectrum obtained using 5mM s-NEA toluene solution (bottom) and CCl$_4$ solution (top). CCl$_4$ spectrum is scaled to 1/5$^{th}$ of its original intensity. Unlike solvent flushing tests in figure 5-3 that involves two solvents in a single test, this figure here illustrates the case with only one solvent each time.*

Additionally, there is another way to study the modifier-solvent interaction, which is

dissolving the modifier in a certain solvent instead of CCl$_4$, as is seen in figure 5-4. Though

this method is more straightforward than the last one mentioned above (shown in figure 5-3). The implementation will be extremely hard using current ATR-IR setup due to severe interference from solvent uptake. Toluene is a better solvent for s-NEA in terms solubility and even at the same concentration, such advantage over $CCl_4$ will move the equilibrium to the direction with more dissolved modifier molecules. Comparing s-NEA dissolved in toluene and in $CCl_4$, there is no major difference in peak position which suggests that adsorption geometry in these two solvents is not dramatically different.
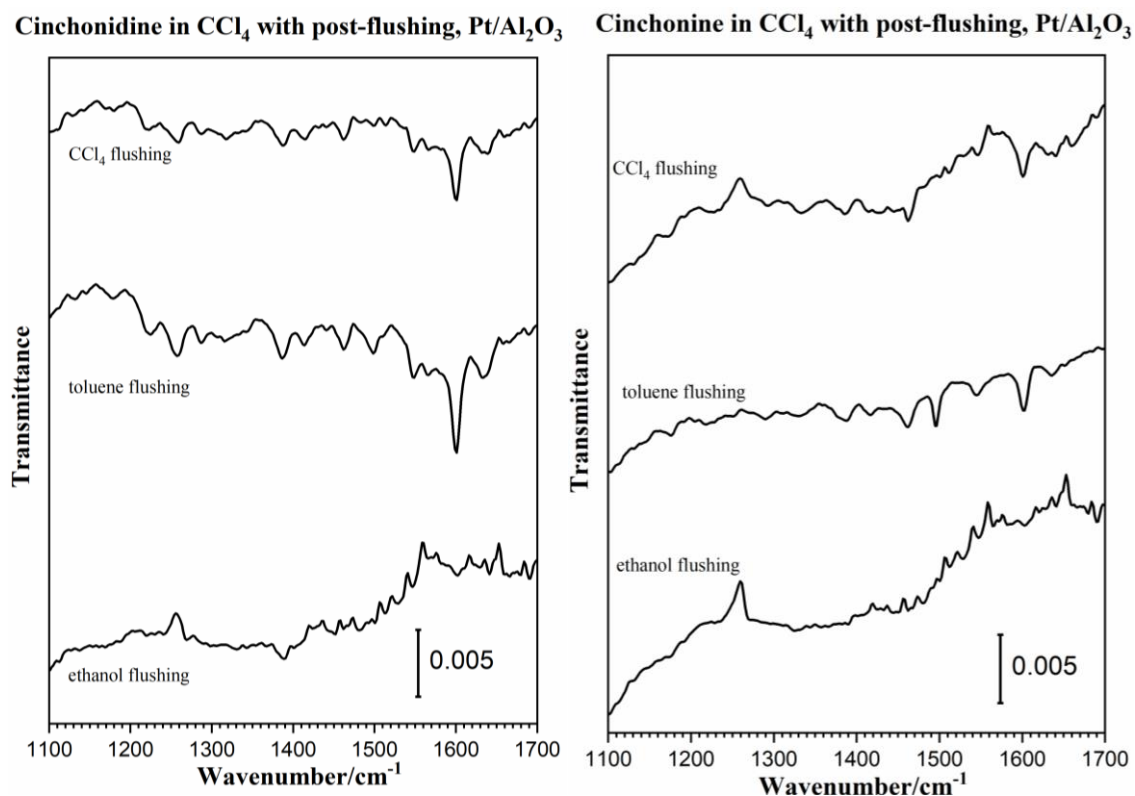


*Figure 5-5 ATR-IR spectra of saturated CD and CN flushed $CCl_4$ solution flushing tests.*

In spite of the difference in adsorption geometry, s-NEA and cinchona alkaloids modifiers behave similarly when flushed with selected solvents. Both of them are polar molecules

and hence, they tend to form stronger interaction with solvent that has higher polarity. Ethanol, the most polar solvent among the three, can easily remove adsorbed cinchonidine or cinchonine completely, yet toluene, which is slightly less polar, cannot do the trick. Similar findings have been published by our group members in the past using RAIRS apparatus with Pt polycrystalline disk. Herein, figure 5-5 indicates that even when there are far less fewer active sites on the surface of Pt catalyst than on Pt disk, the order of flushing power of solvents still comply with the observation made in RAIRS experiments.

## 5.3 Conclusion

The adsorption of NEA and NMA has been closely examined in this chapter. When adsorbed on different types of platinum surfaces, their behavior varies because of the difference in modifier-metal interaction.

Vibration modes of adsorbed NEA reported in this work suggested a possible adsorption model for NEA derivatives that when adsorbing from solution, the modifier molecule bonds through the nitrogen atom in the amine moiety and has all other function groups connected to the chiral center pointing away from the surface. This might be confused with tilted adsorption but can be distinguished by the C-H deformation of the aromatic ring.

A quick comparison of NEA and NMA adsorbed on Pt/Al$_2$O$_3$, Pt/SiO$_2$ and PT poly crystalline disk reveals the order of interaction strength between modifier and metal surface. Pt nanoparticles supported by SiO$_2$ shows weaker bonding with modifiers if compared to the other two Pt species, yet, it's still obviously not the same as pure NEA or NMA

compound without any external perturbation. Although it's been reported that the particle size can have impact[81,82] on the adsorption of modifier and furthermore, the catalytic performance, this possibility is ruled out after TEM characterization of the catalysts, which will be covered in the next chapter. The most probable factor that sets these Pt catalysts apart is the support-metal interaction. Unfortunately, this hypothesis cannot be easily verified with IR or in-situ characterization tools in solution.

Concentration is another key factor that can dramatically change the adsorption process. Adsorption geometry of cinchona alkaloids modifiers is dependent on the concentration, or put in another way, surface coverage. NEA is no exception. At extremely low concentration, the in-plane stretching of C-C bond of aromatic ring is not visible in corresponding ATR-IR spectrum, which might be an indication of naphthyl-Pt interaction in this scenario. Nonetheless, it does suggest the concentration-dependent nature of NEA adsorption.

Last but not the least, dramatic solvent effects on the adsorption of NEA derivative and cinchona alkaloids are observed in this work using in-situ ATR-IR experiments. Two types of tests have been put into practice. One is using $CCl_4$ to dissolve modifier in the first place and then flush the adsorbed species with specific solvent to investigate the ability of that given solvent to remove adsorbate from Pt surface. Both background and final sample spectrum after solvent flushing s are recorded in $CCl_4$ to avoid solvent peaks. The second test is direct adsorption experiment, where the modifier is dissolved in a single solvent and no $CCl_4$ is used unless noted.

As most modifiers are polar molecules, non-polar solvents such as $CCl_4$ will not remove modifiers molecules that have already bonded to the metal surface. As for polar solvent like ethanol, it can wash away s-NEA and cinchonidine/cinchonine easily.

However, the solvent flushing experiments above cannot distinguish $CCl_4$ and toluene since both are not able to get rid of the adsorbates with flushing cycles. $Pt/Al_2O_3$ is then exposed to 5mM s-NEA solution prepared with $CCl_4$ and toluene respectively. The results show that s-NEA uptake in $CCl_4$ is 5 times as strong as that in toluene despite even with the same concentration.

In conclusion, solubility has a direct effect on the adsorption equilibrium and eventually affect the catalytic performance. It's of great important to choose the solvent wisely for asymmetric hydrogenation reactions based on the selection of modifier as well as substrate to achieve optimal conversion and enantioselectivity.

# Chapter 6 Factors Influencing Chiral Modification in Hydrogenation of Ketoesters—A Combined IR and Reaction Study

Reaction data in this chapter is a complement to the results from in-situ ATR-IR studies. Reaction conditions have not yet been optimized to best conditions to achieve best reactivity. Nevertheless, it still adds come credibility to the claims based on ATR-IR. Both inherent and external factors will be discussed in this chapter, including the catalyst, reaction conditions, choice of solvent and the intrinsic nature of modifiers.

## 6.1 Effect of Ex-situ Thermal Treatment on the Performance of Catalyst

Prior to ATR-IR or reactivity evaluation experiment, catalyst needs to be pre-treated in a tube furnace at 350 $^\circ$C in Ar, $O_2$ and then $H_2$. Such procedure can significantly change the property of catalyst (table 6-1) and improve reaction performance (table 6-2).

*Table 6-1Calculated BET surface area, pore volume and pore diameter of Pt/SiO2 and Pt/Al2O3 before and after thermal pre-conditioning.*

|  | BET surface Area/m²*g | Pore Volume/cc*g | Pore diameter/nm |
|---|---|---|---|
| Pt/Al$_2$O$_3$ w/ Pre-conditioning | 142.910 | 0.457 | 14.016 |
| Pt/Al$_2$O$_3$ w/o Pre-conditioning | 157.370 | 0.492 | 14.089 |
| Pt/SiO$_2$ w/o Pre-conditioning | 364.766 | 1.448 | 20.538 |
| Pt/SiO$_2$ w/ Pre-conditioning | 247.565 | 1.024 | 16.852 |

*Table 6-2 Conversion and enantiomeric excess of hydrogenation of ethyl pyruvate with Cd as modifier in toluene. Reactions are performed with a hydrogen pressure of 10 bar for 4 minutes. Ratio of Pt/Cd/Et-Py is 3/0.4/750.*

| Catalyst | Conv/% | e.e/% | Configuration |
|---|---|---|---|
| Pt/Al$_2$O$_3$ not pre-conditioned | 57.7 | 30.6 | R |
| Pt/Al$_2$O$_3$ pre-conditioned | 86.2 | 45.6 | R |
| Pt/SiO$_2$ not pre-conditioned | 9.6 | 31.9 | R |
| Pt/SiO$_2$ pre-conditioned | 50.1 | 56.1 | R |

Thermal pre-conditioning dramatic decreases specific surface area of Pt/SiO$_2$ and its pore volume and diameter drop after the treatment. On the other hand, the surface area of alumina-supported Pt does become smaller after the same process, but only by a margin. This observation correlates with the change in reactivity of the two catalysts, as shown below.

Reactivity of Pt/SiO$_2$ modified by cinchonidine has been dramatically improved with sequential thermal pre-conditioning while Pt/Al$_2$O$_3$ only gets slightly better. Especially, the conversion of reaction catalyzed by Pt/SiO$_2$ without pre-conditioning is rather low. The thermal treatment might have changed the metal-support interaction of Pt/SiO$_2$ significantly and thus improved the overall performance. In conclusion, ex-situ thermal treatment in this case is necessary for both catalysts.

## 6.2 Nature of Surface Modifier

*Table 6-3 Hydrogenation of Et-Py, Catalyst: 50 mg Pt/Al$_2$O$_3$ @300K. Reaction time=20 min, P(H$_2$) =1 bar, Pt:modifier:Et-Py molar ratio=3:1:750. Solvent: acetic acid (6mL). Adapted with permission from reference 67, Copyright © 2017 by John Wiley Sons, Inc.*

| Modifier | Conversion (±1) [%] | e.e. (±1) [%] |
|---|---|---|
| No modifier | 15.8 | 0.2 |
| Quinoline | 12.3 | 0.3 |
| EtN | 13.1 | 0.9 |
| NMA | 23.2 | 0.7 |
| s-DNE | 25.8 | 0.4 |
| s-NEA | 12.3 | 24.4(S) |
| r-NEA | 12.5 | 29.0(R) |
| rac-NEA | 10.5 | 0.2 |
| Quinine | 54.5 | 68.5 (R) |
| Quinidine | 68.8 | 62.5 (S) |
| Cinchonine | 24.5 | 56.6(S) |
| Cinchonidine | 25.9 | 61.3(R) |

Results included in table 6-4 showing hydrogenation reaction with a variety of modifiers, confirm what has been reported in section 3.2. ATR-IR spectrum of s-NEA suggests strong adsorption on Pt surface and in actual hydrogenation reactions, it can promote enantioselectivity of the catalyst. Just as expected, r-NEA can do the same job, resulting in a preferred product but in an opposite configuration. Racemic mixture of NEAs will only lead to a racemic mixture of product compounds in both R- and S- configuration.

Non-chiral molecules such as quinoline and NMA does not show any improved selectivity over the case without any modifier. Though these molecules can adsorb on Pt surface per ATR-IR data, the lack of chiral center in their structure prevent them from being a viable option for surface modification. Meanwhile, compounds showing no adsorption in section 3.2 are not able to change the enantiomeric excess either since there is no interaction between these molecules and platinum surface in the first place.

## 6.3 Hydrogen Pressure and Reaction Time—Loss of Selectivity

Though hydrogenation of ethyl pyruvate does not require high $H_2$ partial pressure and the reaction takes place in liquid phase, partial pressure of $H_2$ still show influence on the reaction conversion as well as selectivity. As $H_2$ participates in the reaction as a reactant, higher pressure should shift the equilibrium to favor products. Table 6-4 and 6-5 shows the pressure dependence of enantioselectivity of hydrogenation of Et-Py with Cd and Cn being the modifier respectively.

*Table 6-4 Hydrogenation of Et-Py in toluene. Modifier: cinchonidine; Catalyst: Pt/SiO2 (25mg) Reaction time and temp: 4 minutes, 300K. Pt:Cd:Et-Py molar ratio=3:2:750. Reaction pressure is shown in table below*

| H$_2$ pressure/bar | Conv/% | e.e/% | Configuration |
|---|---|---|---|
| 1 | 25.5 | 39.6 | R |
| 2 | 78.8 | 66.8 | R |
| 4 | 82.3 | 67.6 | R |
| 6 | 80.1 | 62.4 | R |
| 8 | 84.2 | 61.7 | R |

*Table 6-5 Hydrogenation of Et-Py in toluene. Modifier: cinchonine; Catalyst: Pt/SiO2 (25mg) Reaction time and temp: 4 minutes, 300K. Pt:Cn:Et-Py molar ratio=3:2:750. Reaction pressure is shown in first column.*

| . H$_2$ pressure/bar | Conv/% | e.e/% | Configuration |
|---|---|---|---|
| 1 | 14.8 | 44.0 | S |
| 2 | 42.4 | 51.6 | S |
| 4 | 42.0 | 48.4 | S |
| 6 | 35.9 | 46.5 | S |
| 8 | 51.7 | 41.0 | S |

Le chatelier's principle is mostly true before H$_2$ pressure is raised to 6 bars. Though conversion still maintains the same level, enantioselectivity begins to see a moderate drop at 8 bars. This trend is seen in both Cd and Cn modified catalyst with Cd being a bit earlier at 6 bars. Modifiers might have gone through structural change under high H$_2$ pressure.

*Table 6-6 Hydrogenation of Et-Py in toluene. Modifier: cinchonidine; Catalyst: Pt/Al2O3 (25mg) Reaction temperature: 300K. H2 pressure: 20 bars. Pt:Cd:Et-Py molar ratio=3:1:750.*

| Reaction time/min | Conv/% | e.e/% | Configuration |
|---|---|---|---|
| 4 | 29.8 | 29.0 | R |
| 8 | 81.1 | 42.4 | R |
| 12 | 100 | 44.7 | R |
| 16 | 100 | 50.6 | R |
| 20 | 100 | 38.7 | R |

In an extreme case with even higher $H_2$ pressure (table 6-6), Et-Py is completely converted between 8 minutes to 12 minutes of reaction. However, decrease in selectivity is observed after 20 minutes of being on stream.

The loss of enantioselectivity can be explained by the hydrogenation of quinoline ring which then causes the destruction of cinchonidine or cinchonine on Pt surface. Quinoline is likely to be hydrogenated under elevated hydrogen coverage[23]. So extra care is needed when choosing the optimal reaction pressure and on-stream time.

However, hydrogenation of quinoline or the quinoline moiety of cinchona alkaloids modifiers is never see in the ATR-IR results included in this work. Since all ATR-IR experiments are performed under barometric pressure and it will probably take much longer time to hydrogenate quinoline, if possible.

## 6.4 Choice of Solvent

Solvent is another aspect that can dramatically change the adsorption of modifiers due to solvent-modifier interaction. This effect has been discussed in section 5.2 with three solvents—CCl$_4$, toluene and ethanol, where CCl$_4$ shows the weakest interaction with all modifiers while ethanol shows the strongest. In actual hydrogenation reactions, it involves additional interaction which is solvent—reactant on top of the modifier.

*Table 6-7 Hydrogenation of Et-Py in selected solvent as indicate in the table. Catalyst: Pt/Al2O3 (25mg) Reaction time and temperature: 20 minutes @300K. H2 pressure: 1 bar. Pt: modifier: Et-Py molar ration= 3:3:750*

| Solvent | Modifier | Conv/% | e.e/% | Configuration |
|---------|----------|--------|-------|---------------|
| Toluene | Cinchonidine | 28.0 | 27.4 | R |
| Toluene | Cinchonine | 29.5 | 21.6 | S |
| Ethanol | Cinchonidine | 75.8 | 19.7 | R |
| Ethanol | Cinchonine | 72.7 | 26.1 | S |
| CCl$_4$ | none | 3.0 | N/A | N/A |

It's believed that in ethanol, the initial reaction rate is faster than that occurring in toluene. As for selectivity, the two polar solvents used here are head to head[83]. CCl$_4$ is also tested as a reaction solvent but without modifier dissolved due to low solubility. Conversion in CCl$_4$ is extremely low, which might indicate that it's not a good solvent for Et-Py either. In this case, CCl$_4$ cannot even provide a homogeneous reaction environment for the reaction system, yet, it can make a good IR solvent due to a) it's low IR uptake; b) more modifier molecules tend to stay on metal surface rather than the solution phase.

## 6.5 Summary

The ultimate goal of geometry study via in-situ FT-IR spectroscopy is to gain knowledge on the mechanism of surface modification taking place on the solid/liquid interface and improve the enantioselectivity with current modifiers while explore expand the candidate pool for more chiral modifiers since there is no universal modifier that can fit all asymmetric hydrogenation reactions. In this work, in-situ ATR-IR and reaction are done separately, yet, the best way is to study the behavior of modifiers under reaction conditions because we've seen adsorption of these molecules can be influenced by solvation, concentration and other factors. The divergence of opinions regarding the adsorption of modifiers originates from difference in experimental setup—UHV or in solvent, in-situ or operando, modifier structure etc., there's always more for further investigation.

Figure 6-1 casts some light upon the future work. By tracking the change of peak intensity/area, reaction kinetics data can be measured just like using gas chromatograph. This figure only shows some preliminary data and more polishing is still necessary.

In the meantime, when we optimize the reaction conditions and look for better surface chiral modifiers, there are several factors that all need to be taken into account simultaneously (figure 6-2).
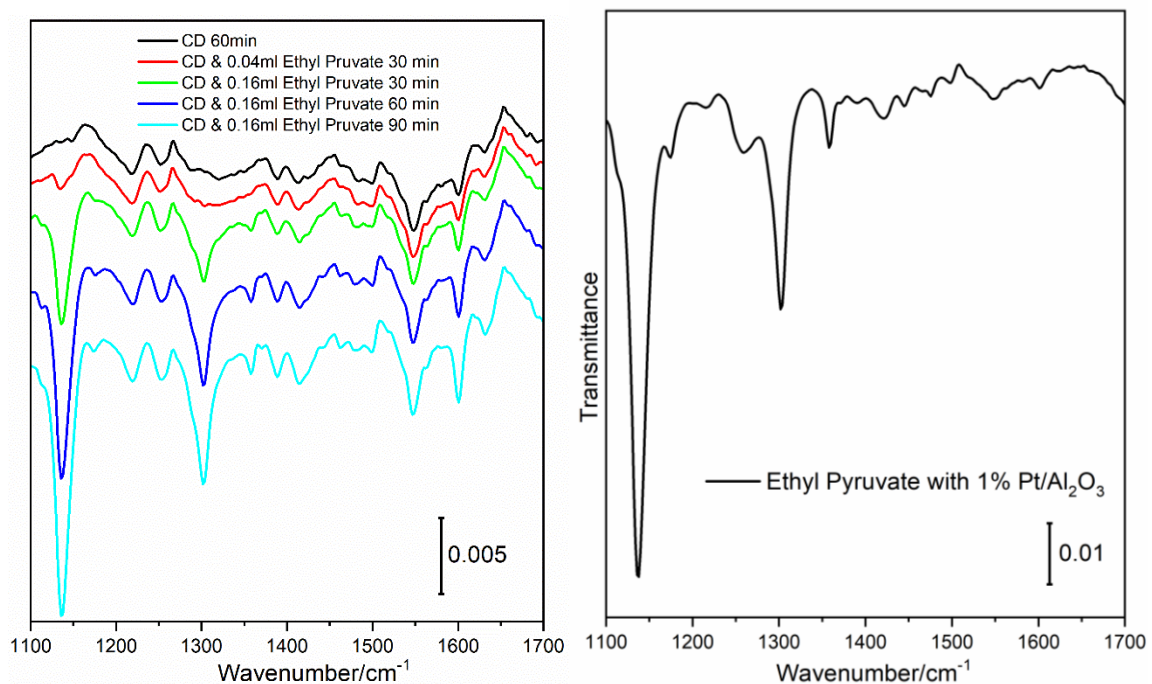
*Figure 6-1 ATR-IR spectra showing cinchonidine and Et-Py in CCl₄ at the same time. A proposed future work includes monitoring the reaction process with ATR-IR spectroscopy.*
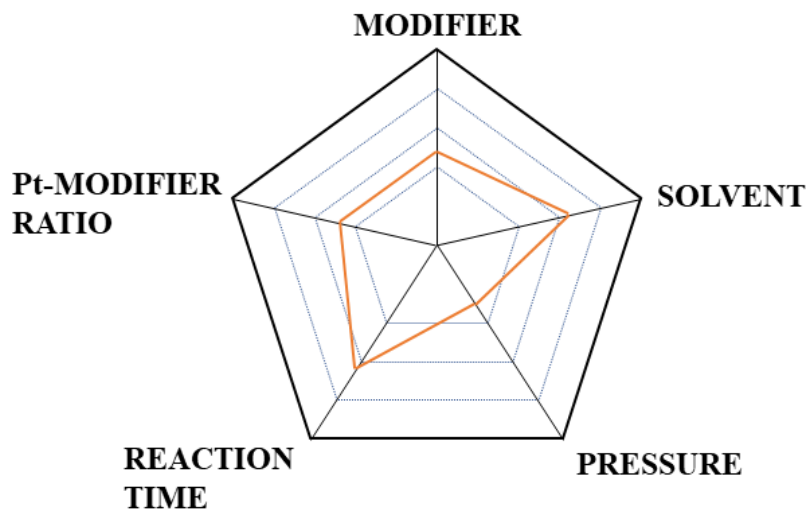


*Figure 6-2 Radar chart showing the factor that have direct impact on the chiral modification of Pt catalyst and hydrogenation reactions.*

To sum up, enantioselectivity is closely related to the adsorption of modifier on surface of the catalyst. Though the connection between IR studies and reactions can be established under certain circumstances, a combined operando study is probably a superior option to investigate the mechanism of adsorption and explore new modifiers.

# Chapter 7 Preliminary Data and Thoughts on Future Work

## 7.1 H-D Exchange Experiment—A NMR Investigation into the Adsorption of S-NEA

It's been suggested that s-NEA might undergo dissociative adsorption on Pt surfaces where the amine group is likely to dehydrogenate. To further examine the proton exchange happening in s-NEA solution. $D_2$ is introduced to the solution instead of $H_2$ bubbling for adsorption experiment. Then the $D_2$ saturated s-NEA solution is analyzed using NMR to see if there is any sign of H-D exchange.

The ATR-IR experiment is performed with $Pt/Al_2O_3$ (thermal treated as described previously) immersed in $CCl_4$ which has been saturated with $D_2$ before beginning of each experiment. During exposure to s-NEA in $CCl_4$ no $H_2$ is bubbled into the solvent. ATR-IR cell is then flushed with $D_2$ saturated $CCl_4$.

Second stage of this test involves $H_2$, the cell is filled with $H_2$ saturated $CCl_4$ solvent to see the H-D exchange, if exists, is reversible. At each stage, solution is collected from cell outlet for NMR analysis.
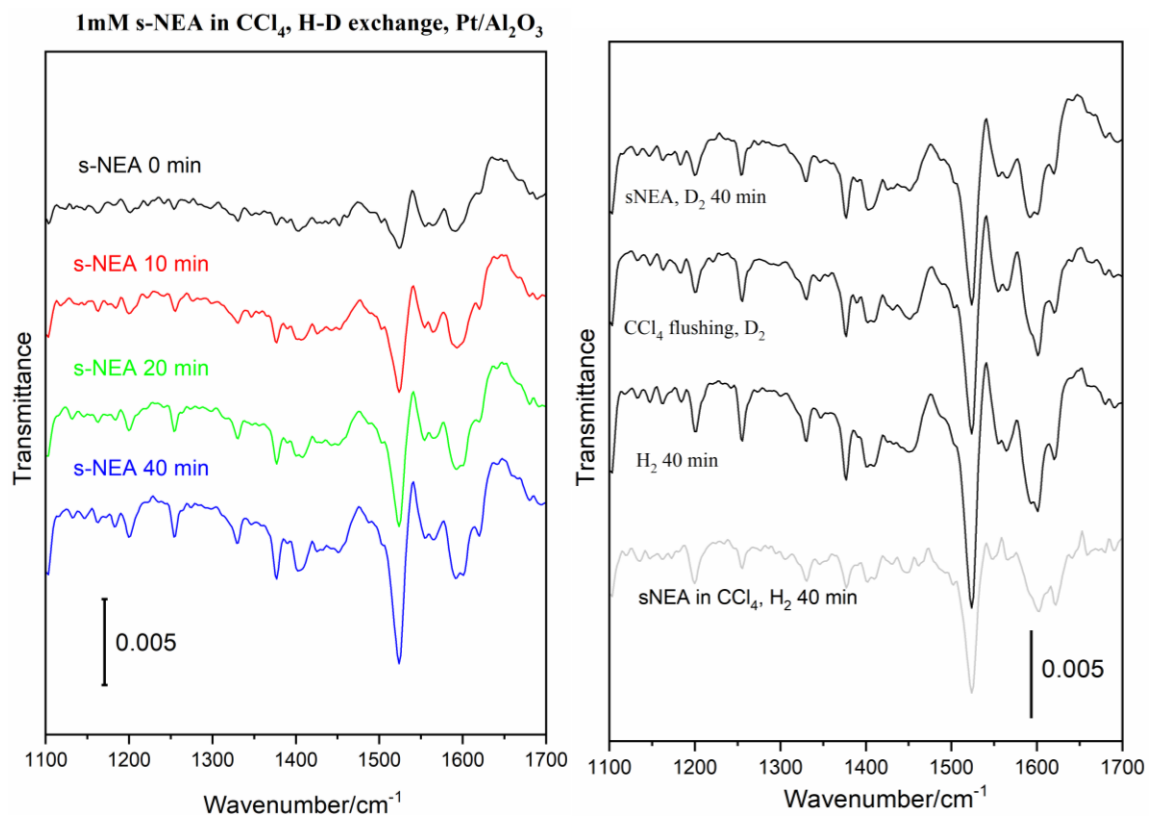
*Figure 7-1   ATR-IR spectra of H-D exchange experiment using 1mM s-NEA in $D_2$ -saturated $CCl_4$. $D_2$ assisted adsorption of s-NEA can be observed (left) even without $H_2$.  Right panel shows a comparison of $1^{st}$ and $2^{nd}$ stage of the H-D exchange experiment where ATR-IR cell is flushed with $H_2$ -saturated fresh solvent ($3^{rd}$ trace counting from top, right panel). A reference spectrum of s-NEA in $H_2$ saturated $CCl_4$ is included for comparison (bottom, right panel).*

ATR-IR spectra in figure 7-1 show no notable differences between $D_2$ and $H_2$ bubbling.

Considering the fact that the mass of $^2H$ and $^1H$ is so insignificant that it will not cause the

reduce mass of N-H to change by a large amount. As a result, ATR-IR cannot distinguish

the slight change, if there is any, in peak position of corresponding vibration mode.
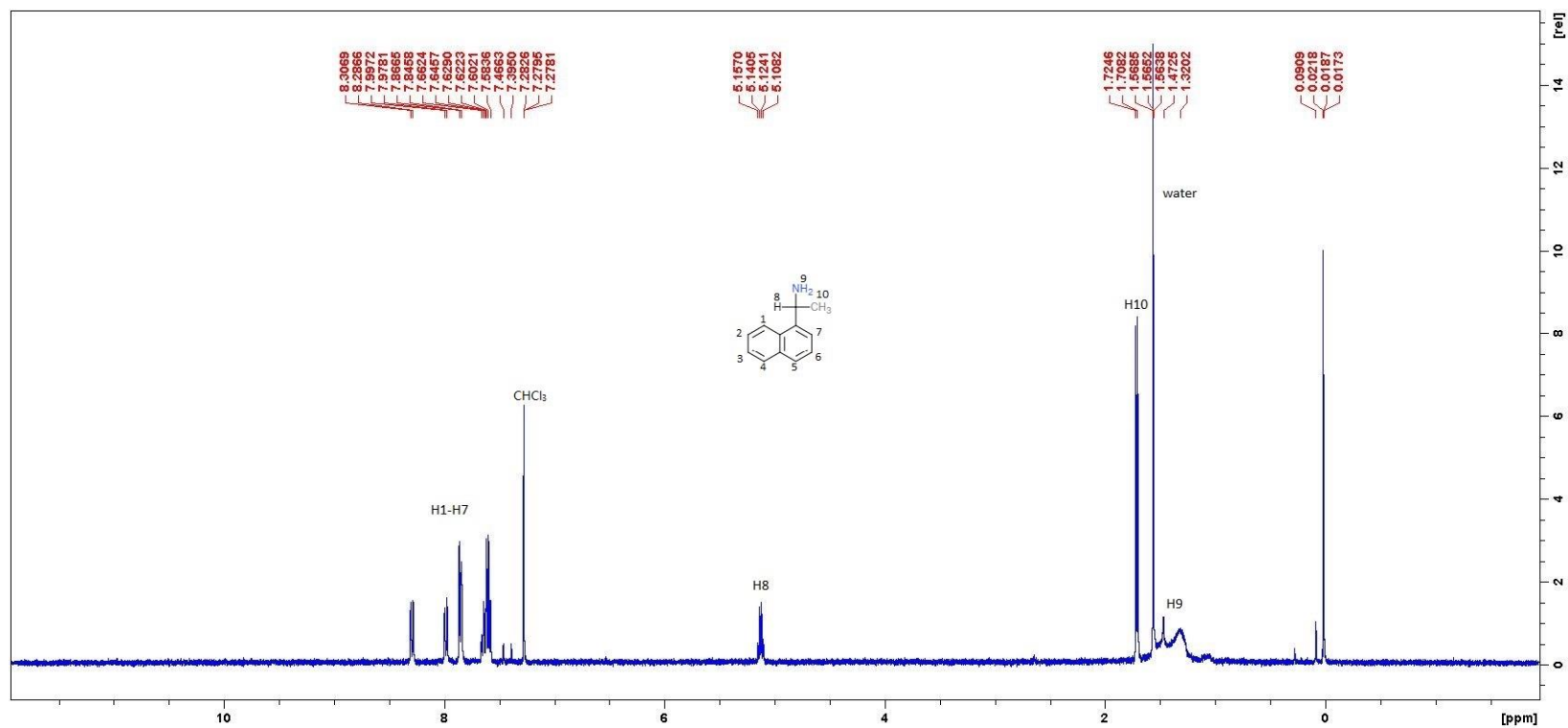
*Figure 7-2 NMR spectrum of original 1mM s-NEA dissolved in CCl₄ without further purification or separation. CDCl₃ is used as deuterated solvent for shimming and locking the magnetic field during NMR characterization. To avoid possible H-D exchange between s-NEA and deuterated solvent, 1mM s-NEA solution is sealed in a capillary tube to prevent physical contact. Experiment is performed on a Bruker Avance NEO 400.*
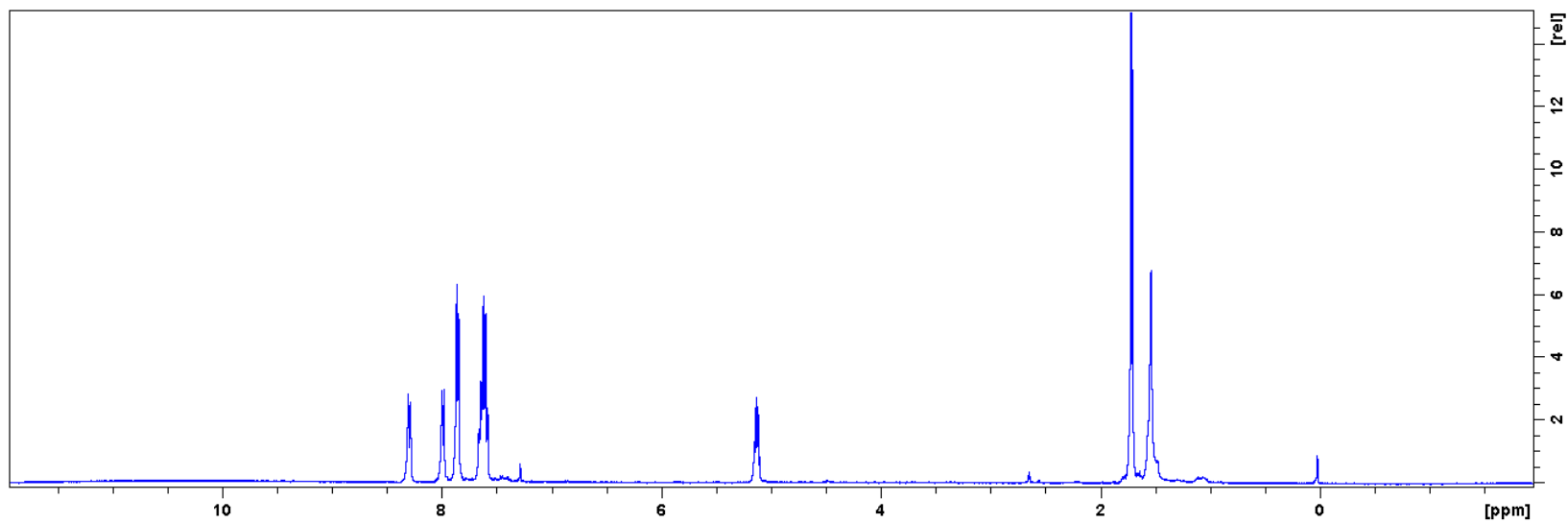
*Figure 7-3 NMR of 1mM s-NEA solution collected after the 1ˢᵗ stage of H-D exchange experiment described above. Again, to avoid H-D exchange with the solvent, s-NEA sample is transferred into a capillary tube before being placed in the NMR tube. CCl₄ solvent act as a spectator in NMR characterization since it does not have any ¹H so there is no need to evaporate the CCl₄ solvent. Experiment is performed on a Bruker Avance NEO 400.*

# ChemNMR $^1$H Estimation
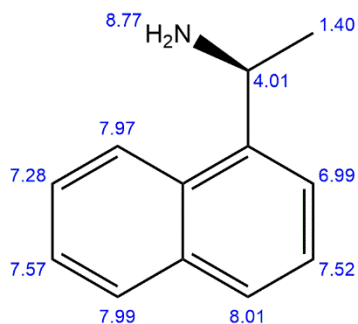


Estimation quality is indicated by color: good, medium, rough
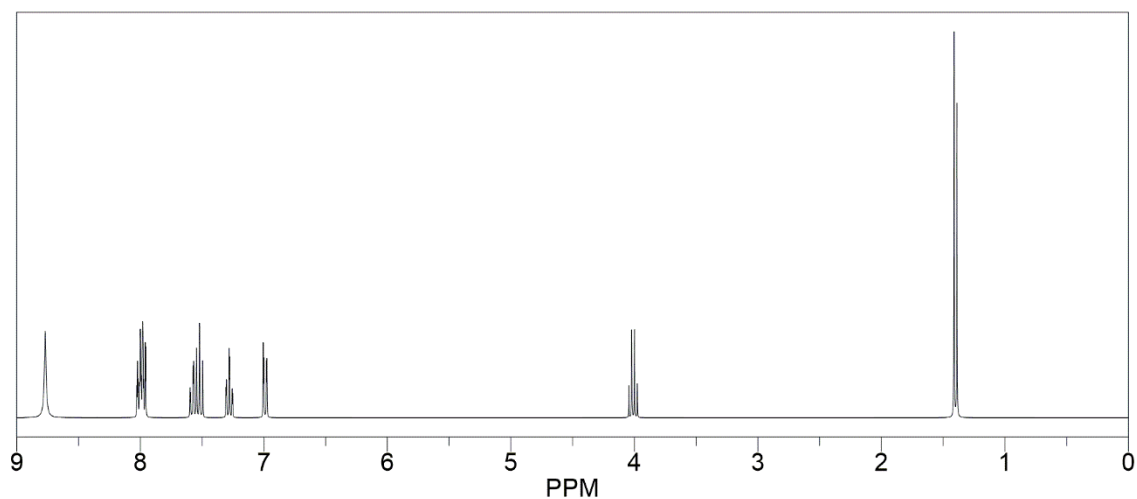


*Figure 7-4 ChemDraw Estimate of NMR spectrum of s-NEA (solvent: DSMO, 300MHz)*

NMR result is not promising by far as well. Figure 7-2 is the NMR spectrum of 1mM s-NEA dissolved in $CCl_4$ without involving Pt catalyst at all, which serves as the reference for figure 7-3, where $Pt/Al_2O_3$ is added to 1mM s-NEA $CCl_4$ solution that is saturated with $D_2$ instead of $H_2$. A theoretical estimate of NMR spectrum of s-NEA in DSMO is also added for better comparison (figure 7-4).

100

The failure to find signs of H-D exchange using NMR could come from several aspects:

First of all, concentration of s-NEA is already rather low (1mM) and after the 'addition' of CDCl$_3$, the impurities in deuterated solvent may overwhelm the signal of s-NEA or at least on the same level. In some experiments (not shown here) where s-NEA in lower concentration or more CDCl$_3$ is used, $^1$H peaks of s-NEA is barely observable. In this case, NMR is likely not a viable option without increasing the concentration of s-NEA.

Secondly, the H-D exchange is a dynamic process which happens rapidly, and it may have exceeded the time resolution of NMR with current experimental method. In addition, as mentioned earlier, increasing the concentration of s-NEA might help with S/N ratio, but this will possibly lead to a higher ratio of unturned s-NEA if the H-D exchange only happens on Pt surface.

Last but not the least, NMR is not a suitable characterization tool for mixtures or compound with uncertain structure. Adsorption of s-NEA is a complicated process on solid liquid interface and therefore, identifying the product that is only a fraction of all s-NEA molecules can be challenging.

## 7.2 Possible Changes Occurring to s-NEA on Pt surface

### 7.2.1 GC-MS Analysis of s-NEA After Adsorption Experiment

GC-MS (Gas chromatography–mass spectrometry) is an analysis technique that combines separation and identify the composition of mixture with relatively low boiling point. Unlike NMR, GC-MS can quickly recognize a certain compound from the mixture. GC-MS analysis is aimed to identify the product of s-NEA after possible dissociative adsorption under reaction conditions.
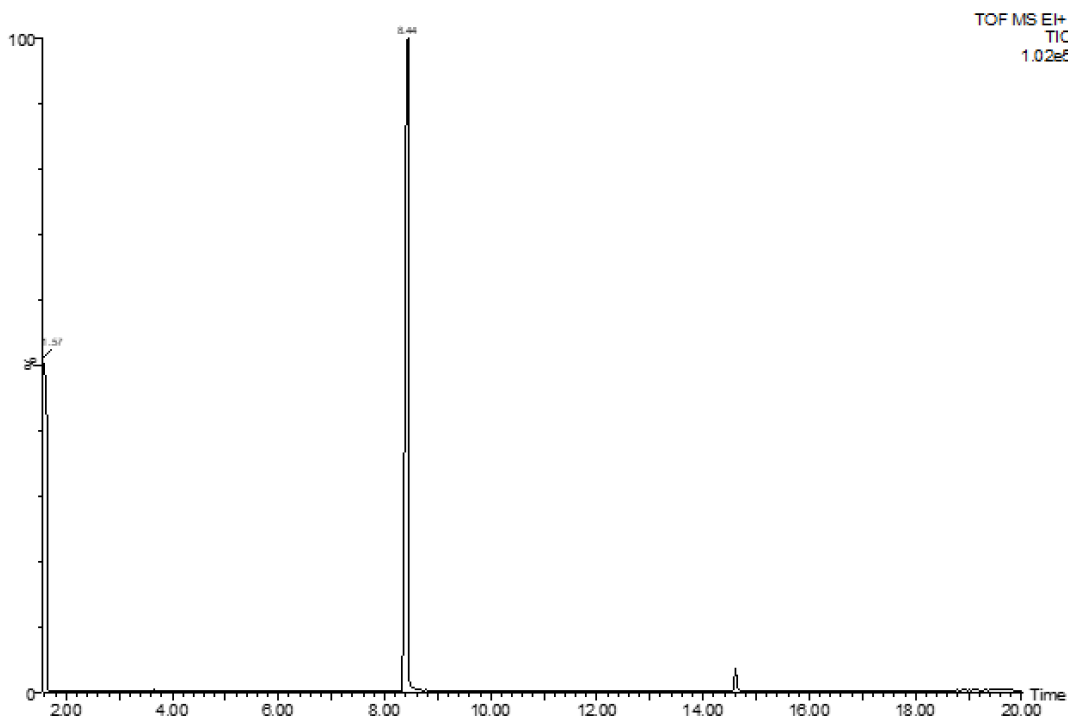


*Figure 7-5 1mM s-NEA CCl₄ solution analyzed with GCMS before H₂ bubbling and addition of any catalyst. This situation represents the most undisturbed s-NEA in CCl₄. GC data shows a single peak at 8.44 minutes*

05111801g 826 (8.444) AM (Cen,2, 80.00, Ar,5500.0,152.06,1.00); Cm (766:920)

TOF MS EI+
1.13e5
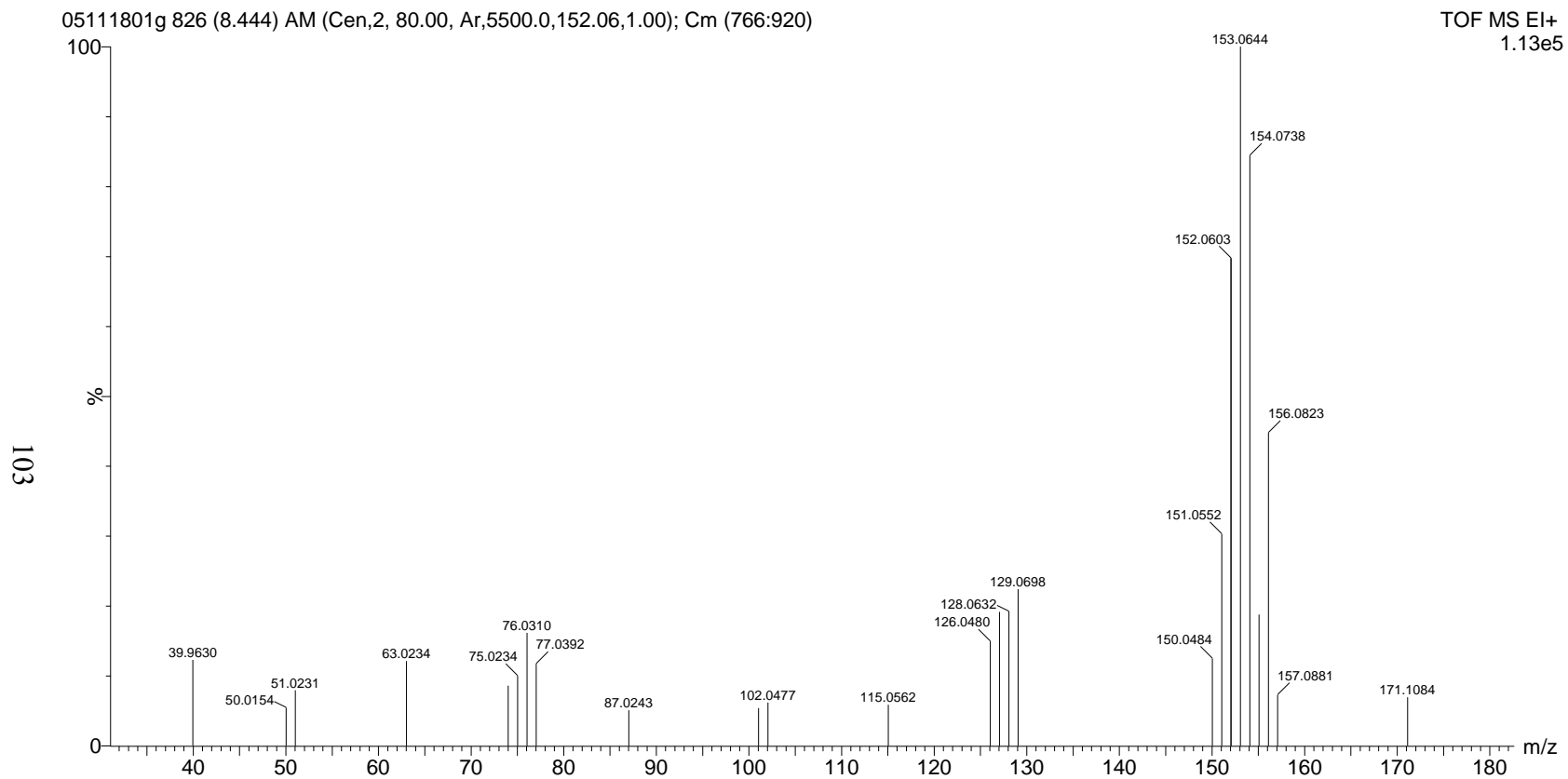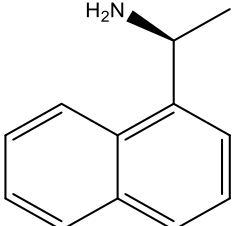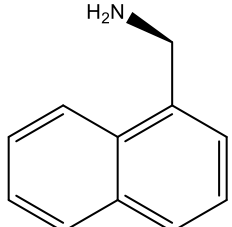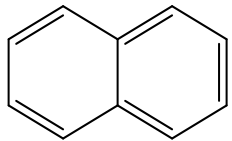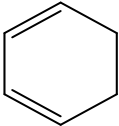


*Figure 7-6 Mass spectrum of the compound that appears at 8.44 minutes in the GC result in figure 7-5. The spectrum matches the standard result in NIST library for mass spectrum.*

*Table 7-1 Assignment of major peaks shown in figure 7-5 for s-NEA in CCl₄ without H₂ and any catalyst.*

| Fragment | Mass |
|----------|------|
| ![structure: 1-(1-naphthyl)ethylamine with H₂N] | 171.10 |
| ![structure: (1-naphthyl)methylamine with H₂N] | 156.08 |
| ![structure: naphthalene] | 128.06 |
| ![structure: six-membered ring] | 76.03 |

GC-MS data of s-NEA before addition of Pt catalyst (figure 7-5) and the introduction of H₂ is shown as above. These results set the baseline for all other fragments (figure 7-6) from s-NEA after adsorption experiment or hydrogenation reaction.
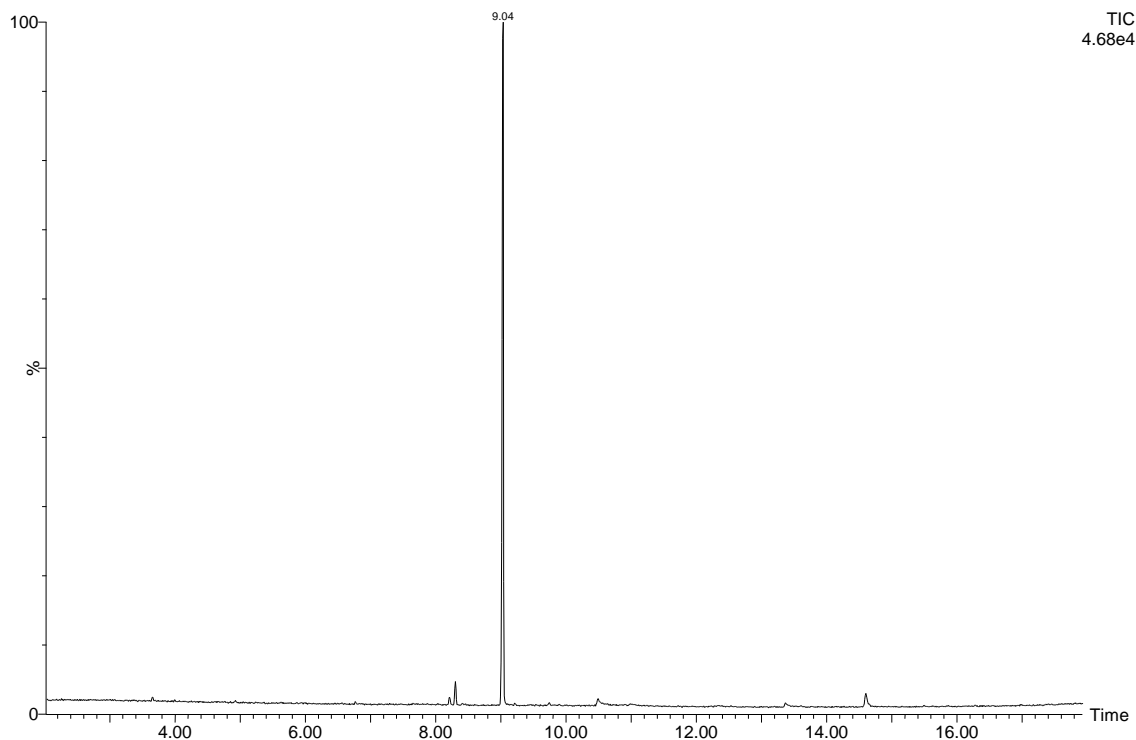
*Figure 7-7 25 mg Pt/Al$_2$O$_3$ is transferred into a flask filled with 30 ml of 1mM s-NEA CCl$_4$ solution. The slurry is stirred for 30 minutes with H$_2$ bubbling at room temperature under barometric pressure.*

In addition to the first peak which represents the s-NEA dissolved in NEA, the addition of Pt/Al$_2$O$_3$ catalyst actually added another GC peak at 9.04 minutes (figure 7-7). Both GC-MS test runs (figure 7-5 and 7-7) are performed using the same instrument method, hence there should not be any significant shift in peak position. This is highly likely to be another compound after the adsorption of s-NEA.

The fragment of the compound as observed at 9.04 minute is shown in figure 7-8, which depicts a fragment pattern from a completely different compound than s-NEA shown in figure 7-6.
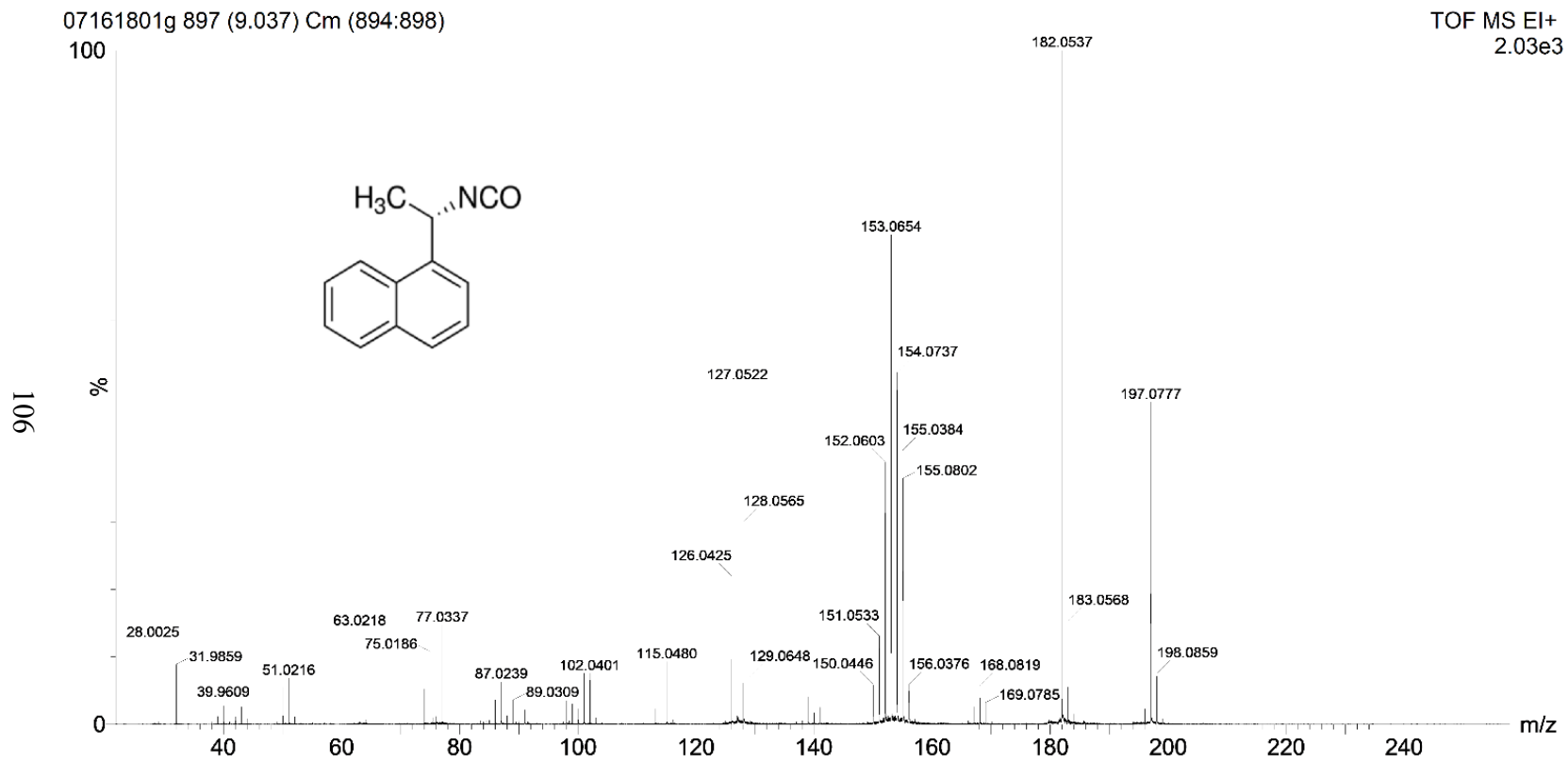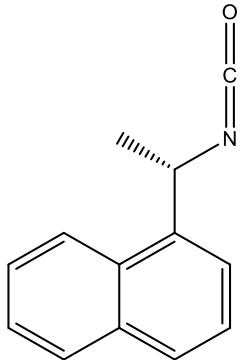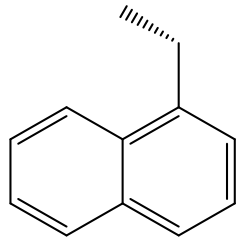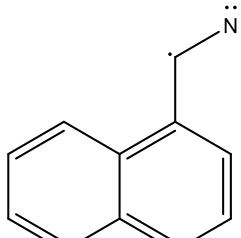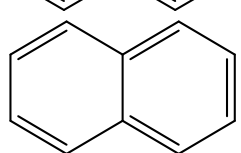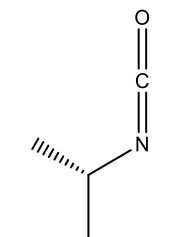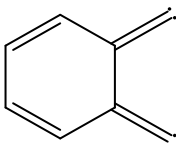
*Figure 7-8  Mass spectrum data of the additional peak at 9.04 minutes as shown in figure 7-7. Inset is a suggested compound that best matches the given fragment pattern.*

*Table 7-2 Fragment assignment of compound discovered after s-NEA adsorption experiment. Some smaller fragments are not listed due to their lack of characteristic.*

| Fragment | Mass |
|:---:|:---:|
|  | 197.08 |
|  | 156.09 |
|  | 154.06 |
|  | 128.06 |
|  | 85.06 |
|  | 101.03 |
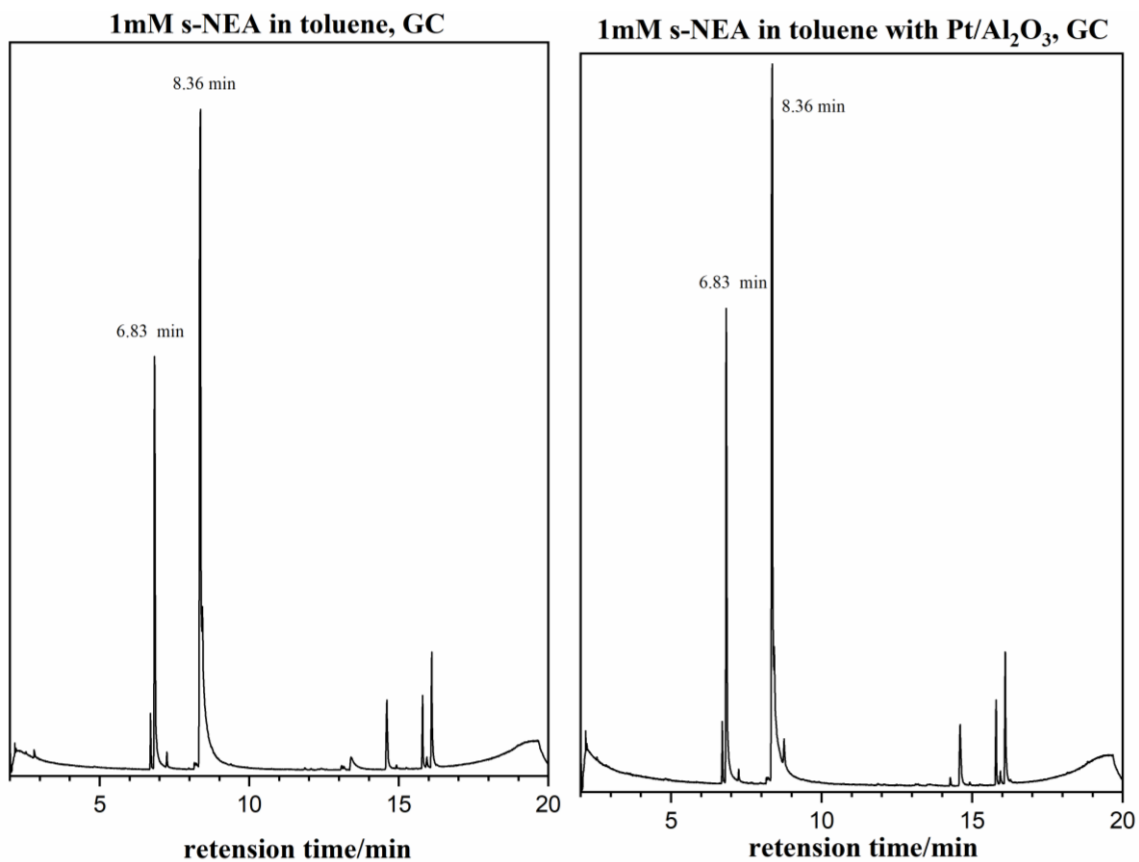
*Figure 7-9 Gas chromatograph of 1mM s-NEA in toluene before (left) and after (right) adsorption experiment. The solvent (toluene) contains a moderate amount of impurities but they don't cause any interference to the 8-9 minutes range.*

Solvent effect has been covered in section 5.2, where it is suggested that when s-NEA is more soluble in a solvent, the adsorption equilibrium in that specific solvent will shift toward the direction to favors the desorption of s-NEA from Pt surface thanks to stronger modifier-solvent interaction.
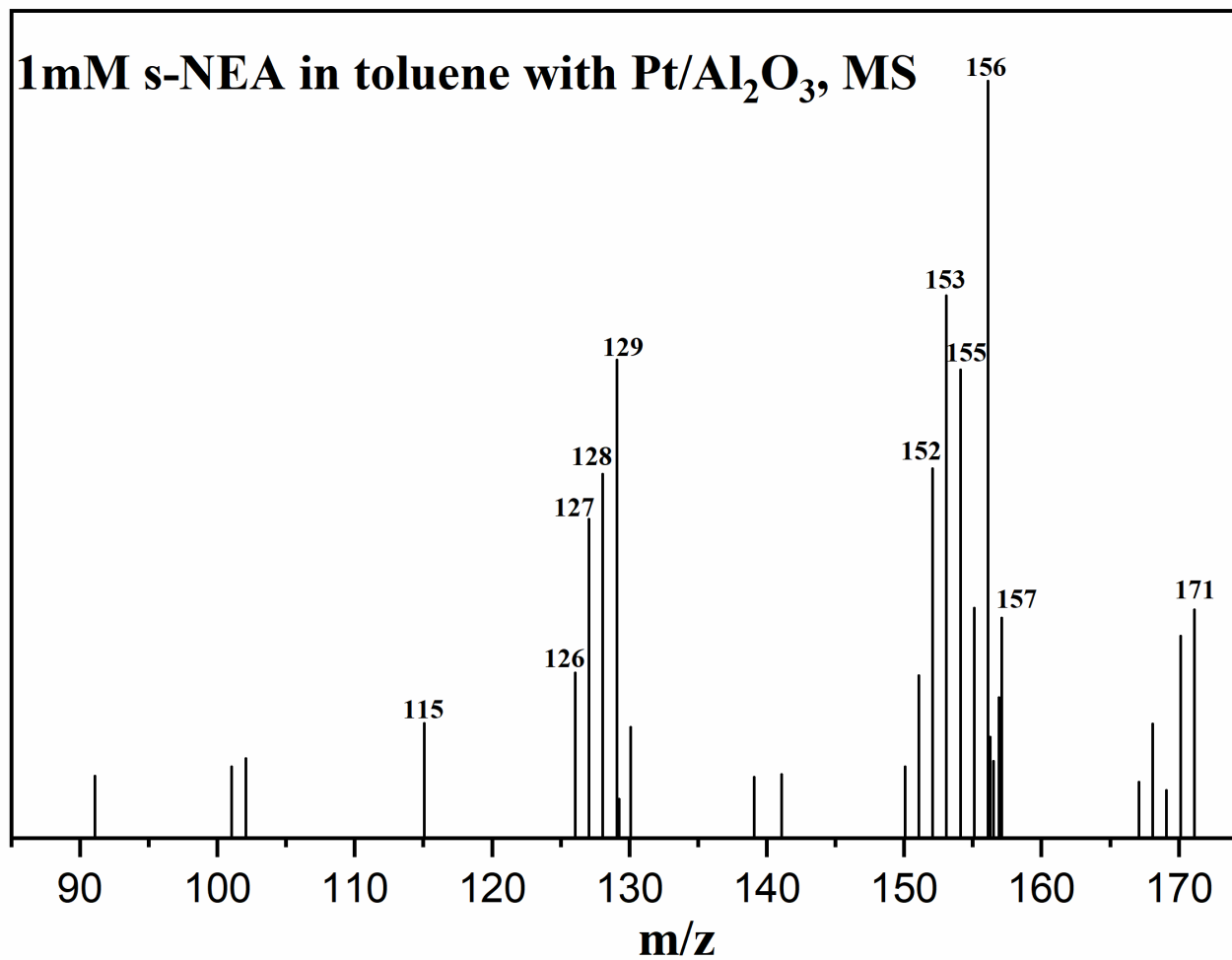
Figure 7-10  Mass spectrum representing the peak at 8.36 minutes in figure 7-9, both GC and MS results match s-NEA  results in CCl₄

The conversion from (S)-(−)-1-(1-Naphthyl) ethylamine to (S)-(+)-1-(1-Naphthyl) ethyl isocyanate found in CCl4 is barely observable in toluene. The right panel of figure 7-9 shows a tiny shoulder peak following the strong peak at 8.36 minutes. They are not completely separated, hence, it's hard to analyze MS data of that weak peak.

*7.2.2ATR-IR evidence for evolving of s-NEA—A Quick Look-back*
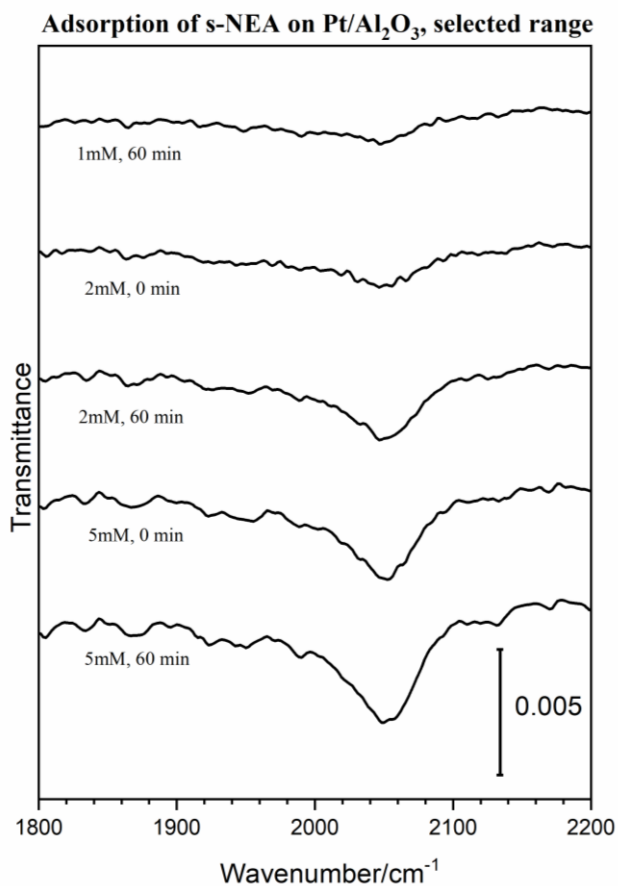


*Figure 7-11 Selected range of 1mM, 2mM, and 5mM s-NEA sequentially adsorbed on Pt/Al₂O₃ for certain period. Catalyst is exposed to 1mM for 60 minutes followed by 2mM and 5mM respectively*

Previously, 1800-2800 cm$^{-1}$ has been ignored because there is no signature peak of s-NEA expected within this range. However, there's a weak-middle strength peak sitting at around 2051 cm$^{-1}$, the intensity of grows stronger with the increase of s-NEA concentration as well as exposure time.

The arise of peak at 2051 cm$^{-1}$ is questionable. There are several possible explanations to this:

Firstly, CO adsorbed on Pt falls exactly within that range and actual position varies based on a lot of factors such as Pt particle size and CO coverage on platinum surface as well as solvation. However, in chapter one, the introduction to ATR-IR instrument, CO adsorbed on the same Pt/Al$_2$O$_3$ catalyst in CCl$_4$ is observed at a higher frequency, 2069 cm$^{-1}$. So, it might be CO from the decomposition of organic molecules dissolved in solution or on Pt surface but there's more to that.

Secondly, it might come from the -NCO group of the compound suggested by GC-MS data presented above. Yet, isocyanate is usually seen as a strong, broad peak within 2250-2270 cm$^{-1}$, much higher than the actual observed peak at 2050 cm$^{-1}$. It's worth noting that just like the case with CO, signature peak of -NCO group is likely to show up at a different frequency depending on the chemical environment it is exposed to as well. So, the adsorption and Pt-nitrogen interaction role may contribute to such shift.

Lastly, however, we cannot ignore the impurities from solvent or other reagents. The decomposition of organic molecules is likely to occur on Pt surface[84] and thus lead to the observed signature peak of C=O stretching.

### 7.3 Conclusion and Prospect

This chapter has covered some recent results regarding the attempt to investigate the transformation taking place on platinum during the adsorption of s-NEA in $CCl_4$ and toluene respectively.

The first section about H-D exchange experiment analyzed with NMR spectroscopy. Due to the lack of proper experiment design and some limitation of the instrumentation, no products for s-NEA H-D process has been identified. NMR experiment is succeeded by the GC-MS tests which is more specialized in identifying the composition of mixtures.

GC-MS results have revealed some preliminary data on the transformation happening to s-NEA on platinum surface in $CCl_4$ and it's likely to exist in toluene as well but not as obvious. Yet, there's still more effort needed to further look into the product related to s-NEA adsorption.

## References:

(1)     Gerlach, H. Chirality Forum Chirality: A Relational Geometric-Physical Property †. *Chirality* **2013**, *25*, 684–685.

(2)     Pasteur, L. . *Ann. Chem.* **1848**, *442*.

(3)     Le Bel, J. A. . *Bull. Soc. Chim. Fr. Ser.* **1874**, *2* (22), 237.

(4)     Cahn, R. S.; Ingold, C.; Prelog, V. Specification of Molecular Chirality. *Angew. Chemie Int. Ed. English* **1966**, *5* (4), 385–415.

(5)     STINSON, S. C. CHIRAL PHARMACEUTICALS. *Chem. Eng. News* **2001**, *79* (40), 79–97.

(6)     Heitbaum, M.; Glorius, F.; Escher, I. Asymmetric Heterogeneous Catalysis. *Angew. Chemie Int. Ed.* **2006**, *45* (29), 4732–4762.

(7)     Baiker, A. Chiral Catalysis on Solids. *Curr. Opin. Solid State Mater. Sci.* **1998**, *3* (1), 86–93.

(8)     Meemken, F.; Baiker, A. Recent Progress in Heterogeneous Asymmetric Hydrogenation of C═O and C═C Bonds on Supported Noble Metal Catalysts. *Chem. Rev.* **2017**, *117* (17), 11522–11569.

(9)     Zaera, F. Chirality in Adsorption on Solid Surfaces. *Chem. Soc. Rev.* **2017**, *46* (23), 7374–7398.

(10)    Hu, A.; Yee, G. T.; Lin, W. Magnetically Recoverable Chiral Catalysts Immobilized on Magnetite Nanoparticles for Asymmetric Hydrogenation of Aromatic Ketones. *J. Am. Chem. Soc.* **2005**, *127*, 12486–12487.

(11)  Annis, D. A.; Jacobsen, E. N. Polymer-Supported Chiral Co(Salen) Complexes: Synthetic Applications and Mechanistic Investigations in the Hydrolytic Kinetic Resolution of Terminal Epoxides. *J. Am. Chem. Soc.* **1999**, *121* (17), 4147–4154.

(12)  de Jesús Cázares-Marinero, J.; Przybylski, C.; Salmain, M. Proteins as Macromolecular Ligands for Metal-Catalysed Asymmetric Transfer Hydrogenation of Ketones in Aqueous Medium. *Eur. J. Inorg. Chem.* **2018**, *2018* (12), 1383–1393.

(13)  Schmidt, E.; Vargas, A.; Mallat, T.; Baiker, A. Shape-Selective Enantioselective Hydrogenation on Pt Nanoparticles. *J. Am. Chem. Soc.* **2009**, *131* (34), 12358–12367.

(14)  Blaser, H. U.; Jalett, H. P.; Monti, D. M.; Baiker, A.; Wehrli, J. T. Enantioselective Hydrogenation of Ethyl Pyruvate: Effect of Catalyst and Modifier Structure. *Stud. Surf. Sci. Catal.* **1991**, *67*, 147–155.

(15)  Lee, I.; Ma, Z.; Kaneko, S.; Zaera, F. 1-(1-Naphthyl)Ethylamine Adsorption on Platinum Surfaces: On the Mechanism of Chiral Modification in Catalysis. *J. Am. Chem. Soc.* **2008**, *130* (44), 14597–14604.

(16)  Blaser, H. U.; Jalett, H. P.; Lottenbach, W.; Studer, M. Heterogeneous Enantioselective Hydrogenation of Ethyl Pyruvate Catalyzed by Cinchona-Modified Pt Catalysts: Effect of Modifier Structure. *J. Am. Chem. Soc.* **2000**, *122* (51), 12675–12682.

(17)  Blaser, H. U.; Jalett, H. P.; Wiehl, J. Enantioselective Hydrogenation of α-Ketoesters with Cinchona-Modified Platinum Catalysts: Effect of Acidic and Basic Solvents and Additives. *J. Mol. Catal.* **1991**, *68* (2), 215–222.

(18)   ORITO, Y.; IMAI, S.; NIWA, S.; NGUYEN-GIA-HUNG, N.-G.-H. ChemInform Abstract: ASYMMETRIC HYDROGENATION OF METHYL BENZOYLFORMATE USING PLATINUM-CARBON CATALYSTS MODIFIED WITH CINCHONIDINE. *Chem. Informationsd.* **1979**, *10* (30), no-no.

(19)   Bürgi, T.; Baiker, A. Conformational Behavior of Cinchonidine in Different Solvents: A Combined NMR and Ab Initio Investigation. *J. Am. Chem. Soc.* **1998**, *120* (49), 12920–12926.

(20)   Ma, Z.; Zaera, F. Role of the Solvent in the Adsorption−Desorption Equilibrium of Cinchona Alkaloids between Solution and a Platinum Surface: Correlations among Solvent Polarity, Cinchona Solubility, and Catalytic Performance. *J. Phys. Chem. B* **2005**, *109* (1), 406–414.

(21)   Urakawa, A.; Meier, D. M.; Rüegger Heinz; Baiker, A. Conformational Behavior of Cinchonidine Revisited: A Combined Theoretical and Experimental Study. *J. Phys. Chem. A* **2008**, *112* (31), 7250–7255.

(22)   Olsen, R. A.; Borchardt, D.; Mink, L.; Agarwal, A.; Mueller, L. J.; Zaera, F. Effect of Protonation on the Conformation of Cinchonidine. *J. Am. Chem. Soc.* **2006**, *128* (49), 15594–15595.

(23)   Hahn, K. R.; Seitsonen, A. P.; Baiker, A. Chiral Modification of Platinum: Ab Initio Study of the Effect of Hydrogen Coadsorption on Stability and Geometry of Adsorbed Cinchona Alkaloids †. *Phys. Chem. Chem. Phys* **2015**, *17*, 27615.

(24)   Motobayashi, K.; Tomioka, R.; Uchida, T.; Osawa, M. Effect of Hydrogen on the Orientation of Cinchonidine Adsorbed on Platinum: An ATR-SEIRAS Study. *Chem. Lett.* **2015**, *44* (6), 770–772.

(25)   Ferri, D.; Bürgi, T. An in Situ Attenuated Total Reflection Infrared Study of a Chiral
       Catalytic Solid-Liquid Interface: Cinchonidine Adsorption on Pt. *J. Am. Chem. Soc.*
       **2001**, *123* (48), 12074–12084.

(26)   Bürgi, T.; Baiker, A. Heterogeneous Enantioselective Hydrogenation over Cinchona
       Alkaloid Modified Platinum: Mechanistic Insights into a Complex Reaction. *Acc.*
       *Chem. Res.* **2004**, *37* (11), 909–917.

(27)   Demers-Carpentier, V.; Goubert, G.; Masini, F.; Lafleur-Lambert, R.; Dong, Y.;
       Lavoie, S.; Mahieu, G.; Boukouvalas, J.; Gao, H.; Rasmussen, A. M. H.; et al. Direct
       Observation of Molecular Preorganization for Chirality Transfer on a Catalyst
       Surface. *Science (80-. ).* **2011**, *334* (6057), 776–780.

(28)   Dong, Y.; Svane, K.; Lemay, J.-C.; Groves, M. N.; McBreen, P. H. STM Study of
       Ketopantolactone/(R)-1-(1-Naphthyl)Ethylamine      Complexes      on      Pt(111):
       Comparison of Prochiral and Enantiomeric Ratios and Examination of the
       Contribution of CH⋯OC Bonding. *ACS Catal.* **2017**, *7* (3), 1757–1765.

(29)   Gordon, A. D.; Zaera, F. Adsorption of 1-(1-Naphthyl)Ethylamine from Solution
       onto Platinum Surfaces: Implications for the Chiral Modification of Heterogeneous
       Catalysts. *Angew. Chemie Int. Ed.* **2013**, *52* (12), 3453–3456.

(30)   Bañares, M. A. Operando Methodology: Combination of in Situ Spectroscopy and
       Simultaneous Activity Measurements under Catalytic Reaction Conditions. *Catal.*
       *Today* **2005**, *100* (1–2), 71–77.

(31)   Raval, R.; Parker, S. F.; Pemble, M. E.; Hollins, P.; Pritchard, J.; Chesters, M. A.
       FT-Rairs, Eels and Leed Studies of the Adsorption of Carbon Monoxide on Cu(111).
       *Surf. Sci.* **1988**, *203* (3), 353–377.

(32) Piccolo, L.; Loffreda, D.; Cadete Santos Aires, F. J.; Deranlot, C.; Jugnet, Y.; Sautet, P.; Bertolini, J. C. The Adsorption of CO on Au(1 1 1) at Elevated Pressures Studied by STM, RAIRS and DFT Calculations. *Surf. Sci.* **2004**, *566–568*, 995–1000.

(33) Greenler, R. G. Infrared Study of Adsorbed Molecules on Metal Surfaces by Reflection Techniques. *J. Chem. Phys.* **1966**, *44* (1), 310–315.

(34) Greenler, R. G. Reflection Method for Obtaining the Infrared Spectrum of a Thin Layer on a Metal Surface. *J. Chem. Phys.* **1969**, *50* (5), 1963–1968.

(35) Greenler, R. G. Design of a Reflection–absorption Experiment for Studying the Ir Spectrum of Molecules Adsorbed on a Metal Surface. *J. Vac. Sci. Technol.* **1975**, *12* (6), 1410–1417.

(36) Kubota, J.; Ma, Z.; Zaera, F. In Situ Characterization of Adsorbates in Solid−Liquid Interfaces by Reflection−Absorption Infrared Spectroscopy. *Langmuir* **2003**, *19* (8), 3371–3376.

(37) Ma, Z.; Zaera, F. Competitive Chemisorption between Pairs of Cinchona Alkaloids and Related Compounds from Solution onto Platinum Surfaces. *J. Am. Chem. Soc.* **2006**, *128* (51), 16414–16415.

(38) Mink, L.; Ma, Z.; Olsen, R. A.; James, J. N.; Sholl, D. S.; Mueller, L. J.; Zaera, F. The Physico-Chemical Properties of Cinchona Alkaloids Responsible for Their Unique Performance in Chiral Catalysis. *Top. Catal.* **2008**, *48* (1–4), 120–127.

(39) McQuillan, A. J. Probing Solid–Solution Interfacial Chemistry with ATR-IR Spectroscopy of Particle Films. *Adv. Mater.* **2001**, *13* (12–13), 1034–1038.

(40)  Meemken, F.; Müller, P.; Hungerbühler, K.; Baiker, A. Simultaneous Probing of Bulk Liquid Phase and Catalytic Gas-Liquid-Solid Interface under Working Conditions Using Attenuated Total Reflection Infrared Spectroscopy. *Rev. Sci. Instrum.* **2014**, *85* (8), 084101.

(41)  Maillard, F.; Savinova, E. R.; Stimming, U. CO Monolayer Oxidation on Pt Nanoparticles: Further Insights into the Particle Size Effects. *J. Electroanal. Chem.* **2007**, *599* (2), 221–232.

(42)  VANNICE, M. SMSI Effects on CO Adsorption and Hydrogenation on Pt Catalysts Part II. Influence of Support and Crystallite Size on the Kinetics of Methanation. *J. Catal.* **1983**, *82* (1), 213–222.

(43)  Ma, Z.; Kubota, J.; Zaera, F. The Influence of Dissolved Gases on the Adsorption of Cinchonidine from Solution onto Pt Surfaces: An in Situ Infrared Study. *J. Catal.* **2003**, *219* (2), 404–416.

(44)  Ferri, D.; Bürgi, T.; Baiker, A. Pt and Pt/Al 2 O 3 Thin Films for Investigation of Catalytic Solid−Liquid Interfaces by ATR-IR Spectroscopy: CO Adsorption, H 2 - Induced Reconstruction and Surface-Enhanced Absorption. *J. Phys. Chem. B* **2001**, *105* (16), 3187–3195.

(45)  Ferri, D.; Bürgi, T.; Baiker, A. Chiral Modification of Platinum Catalysts by Cinchonidine Adsorption Studied by in Situ ATR-IR Spectroscopy. *Chem. Commun.* **2001**, No. 13, 1172–1173.

(46)  Blaser, H. U.; Jalett, H. P.; Monti, D. M.; Wehrli, J. T. Enantioselective Hydrogenation of α-Keto Esters: Temperature-Programmed Reduction Study of Liquid-Phase Pt/Al2O3 Hydrogenation Catalysts. *Appl. Catal.* **1989**, *52* (1), 19–32.

(47) Lieske, H.; Lietz, G.; Spindler, H.; Völter, J. Reactions of Platinum in Oxygen- and Hydrogen-Treated Pt/γ-Al2O3 Catalysts: I. Temperature-Programmed Reduction, Adsorption, and Redispersion of Platinum. *J. Catal.* **1983**, *81* (1), 8–16.

(48) Studer, D. I. and M. Kinetic Modeling of the Ligand Accelerated Catalysis in the Enantioselective Hydrogenation of Ethyl Pyruvate: Influence of Solvents, Catalysts and Additives. *Stud. Surf. Sci. Catal.* **1997**, *108*, 175–182.

(49) Blaser, H.-U.; Jalett, H.-P.; Garland, M.; Studer, M.; Thies, H.; Wirth-Tijani, A. Kinetic Studies of the Enantioselective Hydrogenation of Ethyl Pyruvate Catalyzed by a Cinchona Modified Pt/Al2O3Catalyst. *J. Catal.* **1998**, *173* (2), 282–294.

(50) Loffreda, D.; Simon, D.; Sautet, P. Dependence of Stretching Frequency on Surface Coverage and Adsorbate–adsorbate Interactions: A Density-Functional Theory Approach of CO on Pd (111). *Surf. Sci.* **1999**, *425* (1), 68–80.

(51) Ortega, A.; Huffman, F. M.; Bradshaw, A. M. The Adsorption of CO on Pd(100) Studied by IR Reflection Absorption Spectroscopy. *Surf. Sci.* **1982**, *119* (1), 79–94.

(52) Rodríguez-García, L.; Hungerbühler, K.; Baiker, A.; Meemken, F. The Critical Role of Tilted Cinchona Surface Species for Enantioselective Hydrogenation. *ACS Catal.* **2017**, *7* (6), 3799–3809.

(53) Maeda, N.; Hungerb€, K.; Baiker, A. Asymmetric Hydrogenation on Chirally Modified Pt: Origin of Hydrogen in the NÀHÀO Interaction between Cinchonidine and Ketone. *J. Am. Chem. Soc* **2011**, *133*, 56.

(54) Vargas, A.; Bürgi, T.; Baiker, A. Adsorption of Cinchonidine on Platinum: A DFT Insight in the Mechanism of Enantioselective Hydrogenation of Activated Ketones. *J. Catal.* **2004**, *226* (1), 69–82.

(55)   Kubota, J.; Zaera, F. Adsorption Geometry of Modifiers as Key in Imparting Chirality to Platinum Catalysts. *J. Am. Chem. Soc.* **2001**, *123* (44), 11115–11116.

(56)   Chu, W.; LeBlanc, R. J.; Williams, C. T.; Kubota, J.; Zaera, F. Vibrational Band Assignments for the Chiral Modifier Cinchonidine: Implications for Surface Studies. *J. Phys. Chem. B* **2003**, *107* (51), 14365–14373.

(57)   Zeng, Y.; Masini, F.; Rasmussen, A. M. H.; Groves, M. N.; Albert, V.; Boukouvalas, J.; McBreen, P. H. The Most Stable Adsorption Geometries of Two Chiral Modifiers on Pt(111). *Surf. Sci.* **2018**, *676*, 17–22.

(58)   Goubert, G.; Dong, Y.; Groves, M. N.; Lemay, J.-C.; Hammer, B.; McBreen, P. H. Monitoring Interconversion between Stereochemical States in Single Chirality-Transfer Complexes on a Platinum Surface. *Nat. Chem.* **2017**, *9* (6), 531–536.

(59)   Demers-Carpentier, V.; Goubert, G.; Masini, F.; Lafleur-Lambert, R.; Dong, Y.; Lavoie, S.; Mahieu, G.; Boukouvalas, J.; Gao, H.; Rasmussen, A. M. H.; et al. Direct Observation of Molecular Preorganization for Chirality Transfer on a Catalyst Surface. *Science* **2011**, *334* (6057), 776–780.

(60)   Dong, Y.; Goubert, G.; Groves, M. N.; Lemay, J.-C.; Hammer, B.; McBreen, P. H. Structure and Dynamics of Individual Diastereomeric Complexes on Platinum: Surface Studies Related to Heterogeneous Enantioselective Catalysis. *Acc. Chem. Res.* **2017**, *50* (5), 1163–1170.

(61)   Sato, K.; Yılmaz, H.; Ijuin, A.; Hotta, Y.; Watari, K. Acetic Acid Mediated Interactions between Alumina Surfaces. *Appl. Surf. Sci.* **2012**, *258* (8), 4011–4015.

(62)   Bartók, M. Solvent and Support Effects in the Case of Acetic Acid and Alumina: Oxonium Cations in Asymmetric Hydrogenation of Ethyl Pyruvate over Dihydrocinchonidine Modified Platinum. *Catal. Commun.* **2001**, *2* (8), 269–272.

(63)  Böhmer, U.; Franke, F.; Morgenschweis, K.; Bieber, T.; Reschetilowski, W. Enantioselective Hydrogenation of Ethyl Pyruvate. *Catal. Today* **2000**, *60* (3–4), 167–173.

(64)  Balázsik, K.; Török, B.; Szakonyi, G.; Bartók, M. Homogeneous and Heterogeneous Asymmetric Reactions. Part X: Enantioselective Hydrogenations over K-10 Montmorillonite Supported Noble Metal Catalysts with Immobilized Modifier1Part IX: B. Török, J. Wölfling, Gy. Schneider, M. Bartók, Asymmetric Transfer H. *Appl. Catal. A Gen.* **1999**, *182* (1), 53–63.

(65)  Balázsik, K.; Török, B.; Szakonyi, G.; Bartók, M. Homogeneous and Heterogeneous Asymmetric Reactions. Part X: Enantioselective Hydrogenations over K-10 Montmorillonite Supported Noble Metal Catalysts with Immobilized Modifier1Part IX: B. Török, J. Wölfling, Gy. Schneider, M. Bartók, Asymmetric Transfer H. *Appl. Catal. A Gen.* **1999**, *182* (1), 53–63.

(66)  Xing, L.; Du, F.; Liang, J.-J.; Chen, Y.-S.; Zhou, Q.-L. Preparation of Pt/SWNTs for Heterogeneous Asymmetric Hydrogenation of Ethyl Pyruvate. *J. Mol. Catal. A Chem.* **2007**, *276* (1–2), 191–196.

(67)  Liu, J. J. Advanced Electron Microscopy of Metal-Support Interactions in Supported Metal Catalysts. *ChemCatChem* **2011**, *3* (6), 934–948.

(68)  Mudiyanselage, K.; Trenary, M. Adsorption and Thermal Decomposition of N-Methylaniline on Pt(111). *Surf. Sci.* **2009**, *603* (21), 3215–3221.

(69)  Heinz, T.; Wang, G.; Pfaltz, A.; Minder, B.; Schürch, M.; Mallat, T.; Baiker, A. 1-(1-Naphthyl)Ethylamine and Derivatives Thereof as Chiral Modifiers in the Enantioselective Hydrogenation of Ethyl Pyruvate over Pt–alumina. *J. Chem. Soc., Chem. Commun.* **1995**, *0* (14), 1421–1422.

(70)  Mallat, T.; Orglmeister, E.; Baiker, A. Asymmetric Catalysis at Chiral Metal Surfaces. *Chem. Rev.* **2007**, *107* (11), 4863–4890.

(71)  Dong, Y.; Svane, K.; Lemay, J.-C.; Groves, M. N.; McBreen, P. H. STM Study of Ketopantolactone/( R )-1-(1-Naphthyl)Ethylamine Complexes on Pt(111): Comparison of Prochiral and Enantiomeric Ratios and Examination of the Contribution of CH⋯OC Bonding. *ACS Catal.* **2017**, *7* (3), 1757–1765.

(72)  Svane, K.; Dong, Y.; Groves, M. N.; Demers-Carpentier, V.; Lemay, J.-C.; Ouellet, M.; Hammer, B.; McBreen, P. H. Single-Chiral-Catalytic-Surface-Sites: STM and DFT Study of Stereodirecting Complexes Formed between (R)-1-(1-Naphthyl)Ethylamine and Ketopantolactone on Pt(111). *Catal. Sci. Technol.* **2015**, *5* (2), 743–753.

(73)  Stuart, B. Infrared Spectroscopy. *Kirk-Othmer Encycl. Chem. Technol.* **2005**.

(74)  Chabal, Y. J. Surface Infrared Spectroscopy. *Surf. Sci. Rep.* **1988**, *8* (5–7), 211–357.

(75)  Venezia, A. .; Parola, V. L.; Pawelec, B.; Fierro, J. L. . Hydrogenation of Aromatics over Au-Pd/SiO2-Al2O3 Catalysts; Support Acidity Effect. *Appl. Catal. A Gen.* **2004**, *264* (1), 43–51.

(76)  Reichardt, C. *Solvents and Solvent Effects in Organic Chemistry, Third Edition (Christian Reichardt)*; 2005; Vol. 82.

(77)  Chu, W.; LeBlanc, R. J.; Williams, C. T. In-Situ Raman Investigation of Cinchonidine Adsorption on Polycrystalline Platinum in Ethanol. *Catal. Commun.* **2002**, *3* (12), 547–552.

(78)  Wei Chu, †; Rene J. LeBlanc,  and; Williams*, C. T.; and, J. K.; Zaera, F. Vibrational Band Assignments for the Chiral Modifier Cinchonidine: Implications for Surface Studies. **2003**.

(79)   Jun, Y.; Zhu, X.-Y. FTIR Spectroscopy of Buried Interfaces in Molecular Junctions. *J. AM. CHEM. SOC* **2004**, *126*, 51.

(80)   Stokes, R. H.; Robinson, R. A. Interactions in Aqueous Nonelectrolyte Solutions. I. Solute-Solvent Equilibria. *J. Phys. Chem.* **1966**, *70* (7), 2126–2131.

(81)   Fu, L.; Kung, H. H.; Sachtler, W. M. H. Particle Size Effect on Enantioselective Hydrogenation of Methylacetoacetate over Silica-Supported Nickel Catalyst. *J. Mol. Catal.* **1987**, *42* (1), 29–36.

(82)   Wehrli, J. T.; Baiker, A.; Monti, D. M.; Blaser, H. U. Particle Size Effect on Enantioselective Hydrogenation of Ethyl Pyruvate over Alumina-Supported Platinum Catalyst. *J. Mol. Catal.* **1989**, *49* (2), 195–203.

(83)   Blaser, H. U.; Garland, M.; Jallet, H. P. Enantioselective Hydrogenation of Ethyl Pyruvate: Kinetic Modeling of the Modification of Pt Catalysts by Cinchona Alkaloids. *J. Catal.* **1993**, *144* (2), 569–578.

(84)   Ma, Z.; Zaera, F. *In Situ Reflection-Absorption Infrared Spectroscopy at the Liquid-Solid Interface: Decomposition of Organic Molecules on Polycrystalline Platinum Substrates*.